A SPATIAL SYNOPTIC CLASSIFICATION APPROACH TO PROJECTED HEAT VULNERABILITY IN CALIFORNIA UNDER FUTURE CLIMATE CHANGE SCENARIOS

Prepared for the California Air Resources Board and the California Environmental Protection Agency

Agreement number 07-304

Principal Investigator
Scott Sheridan, Kent State University

Co-Principal Investigator
Laurence Kalkstein, University of Miami

State of California Air Resources Board
Research Division
PO Box 2815
Sacramento CA 95812

Prepared by:

Scott Sheridan, Cameron Lee, Michael Allen
Department of Geography
Kent State University
Kent, Ohio

Laurence Kalkstein
Department of Geography and Regional Studies
University of Miami
Coral Gables, Florida

February 17, 2011

DISCLAIMER

The statements and conclusions in this Report are those of the contractor and not necessarily those of the California Air Resources Board. The mention of commercial products, their source, or their use in connection with material reported herein is not to be construed as actual or implied endorsement of such products.

ACKNOWLEDGMENT

This Report was submitted in fulfillment of CARB contract number 07-304, "A Spatial Synoptic Classification Approach to Projected Heat Vulnerability in California under Future Climate Change Scenarios" by "Kent State University" under the sponsorship of the California Air Resources Board. Work was completed as of August 13, 2010.

TABLE OF CONTENTS

LIST OF FIGURES **v**

LIST OF TABLES **vii**

ABSTRACT **ix**

EXECUTIVE SUMMARY **x**

CHAPTER 1 – INTRODUCTION **1**

1.1 – Overview of the Project and its Significance 1

1.2 – Heat Effects on Human Health 2

1.3 – Future Factors in Human Vulnerability 4

1.4 – Other Studies on Climate Change and heat-related mortality 7

CHAPTER 2 – MATERIALS AND METHODS **9**

2.1 – Study Area 9

2.2 – Materials 9

2.3 – Methods 15

CHAPTER 3 – RESULTS **26**

3.1 – Summary of Circulation Patterns with CCSM3 Model 26

3.2 – Future Circulation Type Frequencies 46

3.3 – Present and Future Weather Type Frequencies 51

3.4 – Historical Weather Type-Mortality Relationships 62

3.5 – Future Heat Event Estimates 64

3.6 – Future Heat-Related Mortality Estimates 68

3.7 – Future Heat-Related Mortality Estimates with Acclimatization 82

CHAPTER 4 – DISCUSSION **90**

CHAPTER 5 – SUMMARY AND CONCLUSIONS **95**

CHAPTER 6 – RECOMMENDATIONS **98**

REFERENCES **100**

GLOSSARY **107**

APPENDIX A **110**

APPENDIX B **126**

APPENDIX C **139**

LIST OF FIGURES

Figure 1 – Study Regions and SSC Stations Used in this Study 10

Figure 2 – SRES Model Scenarios Used 15

Figure 3 – The Fifteen Data Sets Entered into the Six-Step Method 16

Figure 4 – Schematic of the Six-Step Method 17

Figure 5 – Patterns of 500mb Heights and Monthly Frequencies 27

Figure 6 – Patterns of 700mb Heights and Monthly Frequencies 34

Figure 7 – Patterns of 850mb Temperatures and Monthly Frequencies 41

Figure 8 – Monthly Frequency of Selected 500z patterns in 2050s and 2090s 48

Figure 9 – Monthly Frequency of Selected 700z patterns in 2050s and 2090s 49

Figure 10 – Monthly Frequency of Selected 850t patterns in 2050s and 2090s 50

Figure 11 – Monthly Frequency of Modeled DT & MT Weather Types at Fresno 56

Figure 12 – Monthly Frequency of Modeled DT & MT Weather Types at Miramar 57

Figure 13 – Monthly Frequency of Modeled DT & MT Weather Types at Mountain View 58

Figure 14 – Monthly Frequency of Modeled DT & MT Weather Types at El Toro 59

Figure 15 – Monthly Frequency of Modeled DT & MT Weather Types at Riverside 60

Figure 16 – Monthly Frequency of Modeled DT & MT Weather Types at Sacramento 61

Figure 17 – Total Projected Annual Future Mortality for Fresno 70

Figure 18 – Total Projected Annual Future Mortality for Los Angeles 71

Figure 19 – Total Projected Annual Future Mortality for Oakland 72

Figure 20 – Total Projected Annual Future Mortality for Orange County 73

Figure 21 – Total Projected Annual Future Mortality for Riverside 74

Figure 22 – Total Projected Annual Future Mortality for Sacramento 75

Figure 23 – Total Projected Annual Future Mortality for San Diego 76

Figure 24 – Total Projected Annual Future Mortality for San Francisco 77

Figure 25 – Total Projected Annual Future Mortality for San Jose 78

Figure A.1 – CGCM3 500z Patterns and Monthly Frequency 111

Figure A.2 – CGCM3 700z Patterns and Monthly Frequency 116

Figure A.3 – CGCM3 850t Patterns and Monthly Frequency 121

Figure C.1 – Mean Monthly Frequency of Non-Summer CCSM3 500z Patterns 139

Figure C.2 – Mean Monthly Frequency of Non-Summer CCSM3 700z Patterns 141

Figure C.3 – Mean Monthly Frequency of Non-Summer CCSM3 850t Patterns 143

LIST OF TABLES

Table 1 – The Nine Regions Utilized in this Research 9

Table 2 – SSC Weather Types 11

Table 3 – SSC Station Utilized in this Research and Regions they Represent 12

Table 4 – Mean Seasonal Conditions for DT and MT Weather Types at SSC Stations 12

Table 5 – Predictive Variables for the SSC Type 21

Table 6 – Weather Type Frequency for Each SSC Station (CCSM3) 54

Table 7 – Weather Type Frequency for Each SSC Station (CGCM3) 55

Table 8 – Regression Terms Defining the Weather Type to Mortality Relationships 63

Table 9 – Average Annual Heat Events and Oppressive Weather Type Days (CCSM3) 66

Table 10 – Average Annual Heat Events and Oppressive Weather Type Days (CGCM3) 67

Table 11 – Mean Heat Related Mortality Estimates by Population Projection 79

Table 12 – Comparison of Regular and Acclimatized Mortality Projections (DIS-2) 84

Table 13 – Comparison of Regular and Acclimatized Mortality Projections (DIS-4) 87

Table 14 – Summary of Heat-Related Mortality Estimates by MSA 97

Table 15 – Summary of Oppressive Air Mass Days and Heat Events by MSA 97

Table B.1 – Mean Monthly Frequency of CCSM3 500z Patterns (2050s) 127

Table B.2 – Mean Monthly Frequency of CCSM3 700z Patterns (2050s) 128

Table B.3 – Mean Monthly Frequency of CCSM3 850t Patterns (2050s) 129

Table B.4 – Mean Monthly Frequency of CCSM3 500z Patterns (2090s) 130

Table B.5 – Mean Monthly Frequency of CCSM3 700z Patterns (2090s) 131

Table B.6 – Mean Monthly Frequency of CCSM3 850t Patterns (2090s) 132

Table B.7 – Mean Monthly Frequency of CGCM3 500z Patterns (2050s) 133

Table B.8 – Mean Monthly Frequency of CGCM3 700z Patterns (2050s) 134

Table B.9 – Mean Monthly Frequency of CGCM3 850t Patterns (2050s) 135

Table B.10 – Mean Monthly Frequency of CGCM3 500z Patterns (2090s) 136

Table B.11 – Mean Monthly Frequency of CGCM3 700z Patterns (2090s) 137

Table B.12 – Mean Monthly Frequency of CGCM3 850t Patterns (2090s) 138

ABSTRACT

Excessive heat significantly impacts the health of Californians during irregular but intense heat events. Through the 21st century, a significant increase in impact is likely, as the state experiences a changing climate as well as an aging population. To assess this impact, future heat-related mortality estimates were derived for nine metropolitan areas in the state for the remainder of the century. First, oppressive weather events were predicted for future years by first correlating past surface weather types with circulation patterns, and then predicting them in the future using projections of future atmospheric circulation at three levels. Second, we estimated heat-related mortality by initially determining historical weather-type mortality relationships for each metropolitan area. These were then projected into the future based on predicted weather types. Estimates account for several levels of uncertainty: for each metropolitan area, mortality values are produced for five different climate model-scenarios, three different population estimates (along with a no-growth model), and two different levels of acclimatization (along with no acclimatization). Results show a significant increase in heat events over the 21st century, with oppressive weather types potentially more than doubling in frequency, and with heat events of two weeks or longer becoming up to ten times more common at coastal locations. Major urban centers could have a greater than tenfold increase in heat-related mortality in the over 65 age group by the 2090s.

EXECUTIVE SUMMARY

Background. California currently experiences a number of excessive heat events each summer, which are associated with elevated rates of human mortality and morbidity. Over the coming century, climate change is likely to alter the frequency and intensity of these events, and demographic changes are expected to increase significantly the number of people vulnerable to these events. Given the mission of CARB, "To promote and protect public health, welfare and ecological resources," this work is highly relevant as it represents a significant advance in our efforts to determine the effect of future climate change on public health and welfare in the state of California.

Methods. This project developed consistent and robust estimates of changes in heat-related mortality through the 2090s for nine major urban regions in California. Future projections of shifts of weather patterns affecting California were developed from general circulation models. Using a new technique, these weather patterns were then used to derive the surface weather type. To do this, first the historical connections between surface weather type and atmospheric circulation patterns were derived, and then through logistic regression models, future weather type were inferred for each day. To assess future heat related mortality, for each metropolitan area we developed historical relationships between weather type and mortality in the past, accounting for additional factors such as seasonality and the length of a heat wave. These relationships can then be used to drive future projections of heat-related mortality by utilizing future weather type predictions.

Our future predictions are more robust since we account for several levels of uncertainty. First, two climate models were used. With one model, two emissions scenarios were used; for the other, three were used; this yields a total of five 'model-scenarios' of the future climate. To assess uncertainty in demographic change, three population scenarios for the future were assessed, along with a 'no-growth' model that assumes that population is constant. The no-growth model enables an assessment of the relative changes in mortality due to climate changes versus demographic ones. Last, as it is likely that some acclimatization to the warmer climate will occur, we assessed two partial acclimatization scenarios, along with a no-acclimatization scenario.

Results. Over the course of the 21st century, a dramatic increase in the frequency of offensive weather types is observed in every month, exacerbated in the higher emissions scenarios and deeper into the century. These results translate into a substantial rise in prolonged heat events. By the 2090s, heat events that last two weeks or more are projected to occur about once a year at each station, while the occurrence of 10-day or greater heat events is projected

to increase nearly tenfold in some locations under the higher emissions scenarios. The broadened future seasonality and the increase in the frequency of offensive weather types along with the increased frequency of consecutive day heat events will have a substantial effect on mortality.

Our results suggest that presently an average of 508 additional heat-related deaths occur per year across the nine regions (using no acclimatization), with totals ranging from 15 in Fresno to 165 in Los Angeles. Collectively, heat related mortality is projected to increase significantly, though the magnitude varies by population projection and emissions scenario. In the medium population growth projections (with no acclimatization), by the 2090s annual mortality could rise by more than a factor of 9, to an annual total of 4684-8757 deaths per year depending upon GCM scenario. For a no-population growth case, the annual projected heat-related mortality increases to 1074-2051 deaths per year. Thus, most of this increase is due in large part to a rising and aging population, although the increase in mortality due specifically to a warming climate is projected to be from 1.9 times (San Francisco) to 7.5 times (San Diego) greater than current levels by the 2090s. Acclimatization, which is difficult to estimate, has the potential to reduce these values by around 20 percent, so that under the medium population growth scenario, across all nine regions a total of 3526-7371 annual deaths are projected, with the variability again according to GCM scenario.

Conclusions. Our results show that over the course of the 21st century, the state of California may experience a significant public health challenge due to the impacts of heat. This is primarily because heat events will be more numerous and longer lasting, and the most vulnerable subset of the population is the most rapidly growing. This challenge may require significant changes to the infrastructure, including emergency medical services as well as outreach. The effectiveness of adaptive measures, such as heat-health warning systems, and the development of mitigation plans, should be assessed in the context of future decades.

1. INTRODUCTION

1.1 – Overview of the Project and its Significance

California currently experiences a number of oppressive heat events each summer. These events are correlated with reduced air quality, prolonged and extreme heat, and elevated rates of human mortality and morbidity. Over the coming century, climate change is likely to alter the frequency and intensity of these events, and demographic change is expected to increase markedly the number of people vulnerable to these events. These changes are expected to significantly affect public health across the state, particularly in urban areas where temperatures are already elevated due to the urban heat island effect.

The goal of this project is to develop consistent, robust estimates of projected changes in heat-related mortality over the next century for nine major urban regions in California, based on historical observed relationships between large-scale weather patterns and region-specific mortality rates. These observed relationships currently form part of the basis for operational Heat Watch-Warning Systems (HWWS) present in the Bay Area and part of the Central Valley. Application of the Spatial Synoptic Classification (SSC, which places each day into a "weather type"), on which the HWWSs are based, to future climate conditions provide a direct connection between projected climate change impacts and existing adaptation methods.

Future heat-related mortality is estimated across nine urban regions of the state: San Francisco, Oakland, San Jose, Los Angeles, Orange County, Riverside, Sacramento, Fresno, and San Diego. Together, these regions comprise nearly 80 percent of California's population. Future projections of shifts in weather systems affecting each of these cities were developed based on two different atmosphere-ocean general circulation models (AOGCMs). Three future emissions scenarios, a higher, mid-high, and lower, were examined, in order to cover a range of possible emissions futures. Similarly, three sets of population projections were separately assessed, to account for uncertainty in California's future growth.

With 30 years of mortality data, a robust relationship between human mortality and weather types was derived for three age groups (under 65, 65-74, over 74) separately, as it has been shown that heat vulnerability increases significantly with age. These age-specific responses for both regular and hot summers were then incorporated within the projections of California's population through 2100. Given these projections, we then utilized GCM output to infer future SSC types, based on the algorithms developed. These SSC types were then related to heat vulnerability utilizing the relationships developed. Population projections were then incorporated to convert the levels of vulnerability from rates into estimates of heat mortality.

In this final report, we present estimates of heat-related mortality across nine urban regions of California through 2100 for five different model-scenarios, three population growth scenarios, and with no acclimatization, as well as two theoretical levels of acclimatization. We also estimated the number of heat events of different duration and seasonality. Given the mission of CARB, "To promote and protect public health, welfare and ecological resources," this work is highly relevant as it represents a significant advance in our efforts to determine the effect of future climate change on public health and welfare in the state of California.

This study is unique in two key ways. First, rather than basing our analyses on surface predictions generated from downscaled AOGCM output, we have associated AOGCM projections of mesoscale, mid-tropospheric patterns with their likelihood of manifesting oppressive SSC weather types at the surface, a procedure new to future heat-health projections. As AOGCMs are better able to predict general atmospheric patterns than localized weather variables, capitalizing on the relationships we derive enables us to more effectively and appropriately utilize model output in predicting future health impacts. Second, existing studies have not adequately accounted for the significant demographic shifts that are virtually certain to occur in the 21st century. These demographic changes, resulting in a population much older than what currently exists, will exhibit a much greater collective vulnerability than the current population.

1.2 – Heat Effects on Human Health

Heat is generally recognized as the deadliest atmospheric hazard in the developed world (e.g., CDC 2004). In addition to its direct impacts, sustained extreme heat events exacerbate pre-existing cardiovascular, respiratory, and other chronic health conditions (e.g., Ellis and Nelson 1978; Kalkstein and Valimont 1987). During the summer of 1980, as many as 10,000 deaths in the U.S. may have been associated with oppressive heat (National Climatic Data Center 2007), while the summer heat wave of 2003 claimed over 15,000 lives in France and 40,000 throughout Europe (Valleron and Boumendil 2004). Though some research has suggested an overall decrease in heat vulnerability in recent decades (Davis et al. 2002), especially as air-conditioning has become more commonplace (Smoyer 1998), there is still a clear vulnerability to heat (Sheridan et al. 2009), and dramatic mortality episodes have occurred in the U.S. within recent years (Klinenberg 2002), most notably in Chicago and other northern cities in July 1995.

The human impacts of heat exposure have been widely studied and summarized in the literature (e.g., Kovats and Hajat 2008, Basu 2009). Most commonly, the human response to thermal extremes is assessed by comparing human mortality rates with an ambient thermal

metric such as temperature or a heat index. Typically the relationship between the two variables is described as a U-, V-, or J-shaped curve; thus, mortality increases both above and below an 'optimal temperature' at which mean mortality is at a minimum. In the middle latitudes, mean mortality is typically on average around 10 to 20 percent higher in the cold season than in the warm season (Keatinge et al. 2000); however, in most cases, the mortality-temperature relationship has a greater slope on the warmer side than the colder side (e.g. Keatinge et al. 2000, Curreiro et al. 2002), suggesting that human vulnerability in warmer temperatures has a stronger temperature dependence. Many epidemiological studies have attempted to assess the interaction between high ambient temperature and atmospheric pollution, although collectively the results are mixed and inconclusive (Basu 2009).

Significant research has also evaluated which subsets of the population are most vulnerable to the heat (e.g., Bouchama et al. 2007), and has identified both physical factors (e.g., age, inability to leave home, cardiovascular problems) as well as social factors (e.g., socioeconomic status, level of social interaction) and behaviors (e.g., use of fans or air conditioning) as risk factors that influence vulnerability. Fundamentally, it has been recognized that heat-related mortality is largely preventable (O'Neill et al. 2009). Accordingly, many locations, mostly across the developed world, have initiated HWWS over the past 15 years (e.g., Sheridan and Kalkstein 2004). While based on varied methodologies, these HWWS aim to assess whether forecast weather conditions over the coming days resemble those in the past that have led to increased mortality. As part of these HWWS, mitigation activities are then initiated to reduce human vulnerability, such as the opening of cooling centers, providing additional water to the public, and discouraging outdoor labor and exercise. These mitigation activities have been shown to save lives (Ebi et al. 2004).

Research specific to the state of California has been somewhat limited. Though a heat-health relationship broadly in line with other middle latitude locations has been identified (e.g. Basu et al. 2008, Anderson and Bell 2009, Sheridan et al. 2009), heat vulnerability appears to be greater than across the southern US, while not as great as across the midwestern and, northeastern US. The recent heat wave of July 2006 across the state was relatively uncommon in affecting nearly the entire state simultaneously, as well as having record maximum and minimum temperatures simultaneously (Gershunov et al. 2009). Two recent papers have analyzed the impacts of the 2006 event. Ostro et al. (2009) evaluated the total increase in mortality during this event, and suggested that the 'official' heat toll of 147 deaths is an underestimate by a factor of 1.5-3. Moreover, their research suggested that the temperature-mortality relationship was more acute in the 2006 event than overall, suggesting that there is an added 'heat wave effect', that is, that the relationship between heat and mortality is non-linear, so that the population responds more significantly to a longer sequence of oppressive weather (Hajat et al. 2006,

Anderson and Bell 2009). Knowlton et al. (2009) examined hospitalizations and emergency room visits during the 2006 event, and discovered significant increases statewide; interestingly, the largest relative increases were found in the Central Coast region, which had lower absolute temperatures than most other regions, suggesting that acclimatization to local climate is significant.

1.3 – Future Factors in Human Vulnerability

Moving into the future, there are several factors that may significantly affect human vulnerability to future heat events. Luber (2008) is among those that broadly divides these factors into three categories: climate change, demographic change, and the urban heat island.

Climate change. The IPCC (Meehl et al., 2007) projects that globally, temperatures by the end of the 21st century when compared with the end of the 20th century are expected to be from 1.1°C to 2.9°C higher using a relatively environmentally friendly scenario, and from 2.4°C to 6.4°C higher using a business as usual scenario. These mean increases show large spatial variability, with larger increases in general observed over land, as well as over more poleward latitudes. Research has also suggested changes in atmospheric circulation, with future climate change projecting onto the dominant modes of atmospheric variability such as the Arctic (AO) and North Atlantic (NAO) Oscillations that already affect climate over North America (Stone et al., 2001; Gillett et al., 2003), as well as El Niño/Southern Oscillation (ENSO)-like patterns (Boer et al., 2004).

Specific modeling of excessive heat events in the future has been less studied; aside from global changes in the radiative balance, and circulation changes, other regional considerations such as soil moisture may play a role (Clark et al., 2006). A key question is the role of climate variability, and the relative roles of changes in the mean and variance of future temperature patterns. Schär et al. (2004) address this directly, in their analysis of the 2003 European heat event in the context of future climate scenarios, showing a nearly 100% increase in climate variability in future GCM scenarios relative to control runs, and a spatial pattern of temperature variability change which is entirely different from that of the mean temperature increase. Ballester et al. (2010) reach a different conclusion, suggesting future heat events will increase in proportion with the mean temperature increase. Nevertheless, several studies (Stott et al. 2004; Beniston, 2004; Beniston, 2007; Kysely 2009) suggest that with circulation changes associated with climate change, heat waves similar to the 2003 event be commonplace by the end of the 21st century.

Several studies have also examined future changes in heat events over North America. As part of a global analysis of weather extremes, Tebaldi et al. (2006) and Meehl and Tebaldi (2004) show a significant increase in the frequency and intensity of heat events in the future, with three-day events more than 3°C warmer than present across interior California. Clark et al. (2006) show a large amount of variability in predicted heat events, with the largest increases across the northern US, but with increases over California between 2°C and 8°C. In the precursor to the present study (Hayhoe et al., 2004), heat extremes for five cities in California were analyzed. By the 2090s, average heat-wave intensity inland increases at nearly double the rate of coastal cities under either scenario. As the total number of heat-wave days is approximately equal across all locations, this indicates much hotter heat waves for inland cities. This conclusion is also supported by their higher growth rate of extreme heat waves, which make up 23 to 54 percent (B1) and 56 to 84 percent (A1FI) of all heat waves by the 2090s.

Demographic change. While there is still significant uncertainty in the manifestation of climate change, there is less uncertainty with demographic change. Simply, the population of much of the developed world, including California, is collectively aging at an unprecedented rate. This aging is expected to continue into the 21st century. Though the US population as a whole is projected by the Census Bureau (Census, 2010) to increase by around 41 percent from 2010 to 2050, the population of those 65 and older is expected to more than double from 40 to over 88 million (and comprise 20 percent of the US population); those over 85 will triple to more than 19 million. As the elderly are most susceptible to the heat, these changes strongly point to a population much more heat vulnerable than present.

Urban heat island. Due to significant land use change, infrastructure development, as well as the energy utilized in heating and cooling, urban areas are significantly warmer than their rural surroundings, by values generally up to 6°C (Brazel et al., 2007). Around 95 percent of California's population is considered "urban", above the near 80 percent average for the US as a whole (Census, 2010). Two recent studies have discovered significant correlation between heat island magnitude and heat vulnerability on a sub-city level: Johnson et al. (2009) for Philadelphia and Harlan et al. (2006) for Phoenix. Given the significant urbanization across California, and the drain on energy resources that heat events have placed in the past, leading to blackouts and brownouts (Caruba, 2008), there is significant potential for continued urbanization to further burden human health.

There are two sources of uncertainty with regard to future heat-related mortality estimates: mortality displacement (or harvesting) and acclimatization (or adaptation). Mortality displacement refers to the fact that short-term mortality increases during a heat event have been observed to be offset somewhat by short-term mortality decreases following the event

(Hajat et al. 2005). In other words, a percentage of apparent heat-related deaths were deaths that would have occurred soon afterwards anyway. This effect has been estimated from near zero (meaning that no displacement occurs) to near total (meaning that every short-term increase in mortality is associated with a near-term decrease following the heat event), depending upon location or heat event magnitude and strength (e.g. Hajat et al. 2005, Kysely et al. 2009).

Adaptation is another uncertainty. Just as heat-mortality relationships in the present day are place-specific due to the local population acclimatizing, it is expected that the population in a future, warmer world could at least partially acclimatize to a changed climate (Kinney et al. 2008). Acclimatization can occur through multiple mechanisms. First, there is physiological adaptation; as heat-related deaths are more common in areas in which excessive heat is rare (Kinney et al. 2008) and threshold temperatures – the point above which mortality is observed to rise – vary by climate (e.g. Curreiro et al. 2002), a population with a slowly warming background climate may at least partially acclimatize. In addition, people may adapt through behavioral mechanisms, such as relying more significantly on air conditioning (e.g. O'Neill 2003), changes to an urban structure to reduce the heat burden, or simply by changing the structure of their activities. While these are all different mechanisms with different time frames of implementation, one difficulty in examining their efficacy is that it is difficult to utilize the historical record of the heat-health relationship to distinguish between these effects (Gosling et al. 2009), as for example, places with lower heat-related mortality both have warmer climates and greater incidence of air conditioning.

Thus, while acclimatization as a confounder of the heat-health relationship is easy to conceptualize, it has been difficult to address quantitatively in existing research (Gosling et al. 2009, Kinney et al. 2008). As a result, there are several different approaches that have been taken. An *analog city* method assumes that if a city's climate changes in the future to that of a warmer city, then its heat-mortality relationship in the future will be similar to the warmer city's (e.g. Knowlton et al. 2007). An *analog summer* method assumes that a population within a given city responds less strongly to weather conditions in hot summers than in relatively cool summers, and thus future mortality estimates can be based on the historical relationship only during the hottest summers, as those would be most similar to future summers. Last, there are fixed-value methods, in which the heat-mortality relationship is adjusted by a fixed value, e.g. 2°C, representing a certain amount of acclimatization (e.g. Gosling et al. 2009).
To date these methods, while producing broadly similar results in terms of percentage changes (discussed further in Section 1.4), cannot readily be verified as being appropriate. Analog cities may not be appropriate where urban structure is dissimilar across the cities being compared, and in locations such as California where the unique climate yields no true analog cities. Analog

summers may not be appropriate as they would not necessarily be representative of long-term climate drifts, only climate variability between warmer and cooler summers. And, fixed value mechanisms are generally not based on some physiological reasoning but rather are approximations, and also assume that the heat-mortality relationship can simply be shifted on a temperature scale. Among all of these methods, there are further inherent uncertainties such as the fact that trends in the heat-health relationship are not linear (e.g. Sheridan et al. 2009, Davis et al. 2002), uncertainty about the variability of the heat-health relationship if climate variability changes (Kinney et al. 2008), as well as the uncertainties in the modeling of adaptive mechanisms such as air conditioning, which will eventually reach saturation while perhaps relying on a tenuous electricity grid (O'Neill et al. 2003).

1.4 – Other Studies on Climate Change and Heat-Related Mortality

Fewer works have tried to estimate heat-related mortality in the future, although the number of studies has increased significantly over the last decade. A number of works have attempted general assessments to evaluate the offset between heat-related mortality increases and cold-related mortality decreases, with conflicting results (e.g., Donaldson et al., 2001; Nicholls, 2009; Doyon et al., 2008) suggesting the offset may be place-specific or that the methodology used plays a critical role. Gosling et al. (2009) also tested model performance in their estimates of heat-related mortality for six cities in the US and Europe. The results varied widely, and suggested strongly that model bias, if unaccounted for, can lead to a significant miscalculation in mortality estimates.

Among the research that has specifically focused on quantifying mortality from heat impacts, in Hayhoe et al. (2010), the Spatial Synoptic Classification was used to project future heat events for Chicago; 1995-like heat events increased in frequency to from 0.5 (B1 emissions scenario) to 2.8 (A1FI) events per year by the end of the 21st century. Correspondingly, annual heat-related mortality rates were expected to increase by a factor of 3.5 (B1) to over 9 (A1FI) over present day levels. One study, which utilized the 2003 European heat wave as an analog for climate change in major U.S. cities, showed that such conditions would increase heat-related mortality by up to five times typical summer mortality rates (Kalkstein et al., 2008).

Through the 2050s, Knowlton et al. (2007) showed a significant increase in heat-related mortality across the greater New York metropolitan area, from 47% to 95% depending on scenario used. Analog-city acclimatization reduced heat mortality in the future by 25%. Their work also analyzed the area on the county level, and showed much greater increases in the urban areas than the rural periphery. Dessai (2003) in a similar time frame, showed heat-related mortality in Lisbon increasing from 5.4 to 6 deaths/100,000 in the historical record to

7.3 to 35.6, with the large range in uncertainty due to model choice. Hayhoe et al. (2004) showed an increase in annual heat-related mortality in Los Angeles from 165/year to 394 to 1429/year by 2070-2099; this increase in mortality was reduced by 20% if acclimatization was included.

There has been recent work suggesting that wider use of HWWSs will help mitigate increases of heat-related mortality in a globally-warmed world. In one study for 40 U.S. cities, it is suggested that recent declines in heat-related mortality are largely due to the more widespread use of more sophisticated heat mitigation techniques, including the increased integration of synoptic-based HWWSs (Kalkstein et al., 2010). A similar study shows that nationalization of such systems in a globally warmed world will help ameliorate some of the increases that might be expected from the increased frequency of extreme heat events (Greene et al., in press). Thus, there may be ways to mitigate the mortality numbers for California that are described within this project.

2. MATERIALS AND METHODS

2.1 – Study Area

The study area for this project includes nine urbanized regions in California (Table 1; Figure 1). These regions in the 2000 census included 26,791,319 Californians, nearly 80 percent of the state total population. They generally coincide with the US Census defined Combined Statistical Areas (CSA), although the two largest CSAs are subdivided for analysis due to their size and climatic variability. Riverside is a metropolitan statistical area (MSA), and Los Angeles and Orange are both metropolitan divisions of the greater Los Angeles CSA; Oakland and San Francisco are both divisions of the greater San Francisco CSA. As historical mortality data is not extensively available below the county level, no subdivisions below this level were made.

2.2 – Materials

For this project, a number of data sets were necessary: population and weather data for both historical periods and future projections, along with historical mortality data. Each of these data sets along with the initial methods utilized to prepare the data for analysis is described below.

2.2.1 – Historical and Future Population Data

Historical population data for the state of California have been obtained from the Census (2010) on a county level for the years 1970, 1980, 1990, and 2000. Data are stratified by age groups (in bins of no greater than 5 years), sex, and race.

Table 1 – The nine regions utilized in this research.

Region	Largest City	Counties	Population (2000)
Fresno	Fresno	Fresno, Madera	922,516
Los Angeles	Los Angeles	Los Angeles	9,519,338
Oakland	Oakland	Alameda, Contra Costa	2,392,557
Orange	Santa Ana	Orange	2,846,289
Riverside	Riverside	Riverside, San Bernardino	3,254,821
Sacramento	Sacramento	El Dorado, Placer, Sacramento	1,628,197
San Diego	San Diego	San Diego	2,813,833
San Francisco	San Francisco	Marin, San Francisco, San Mateo	1,731,183
San Jose	San Jose	Santa Clara	1,682,585

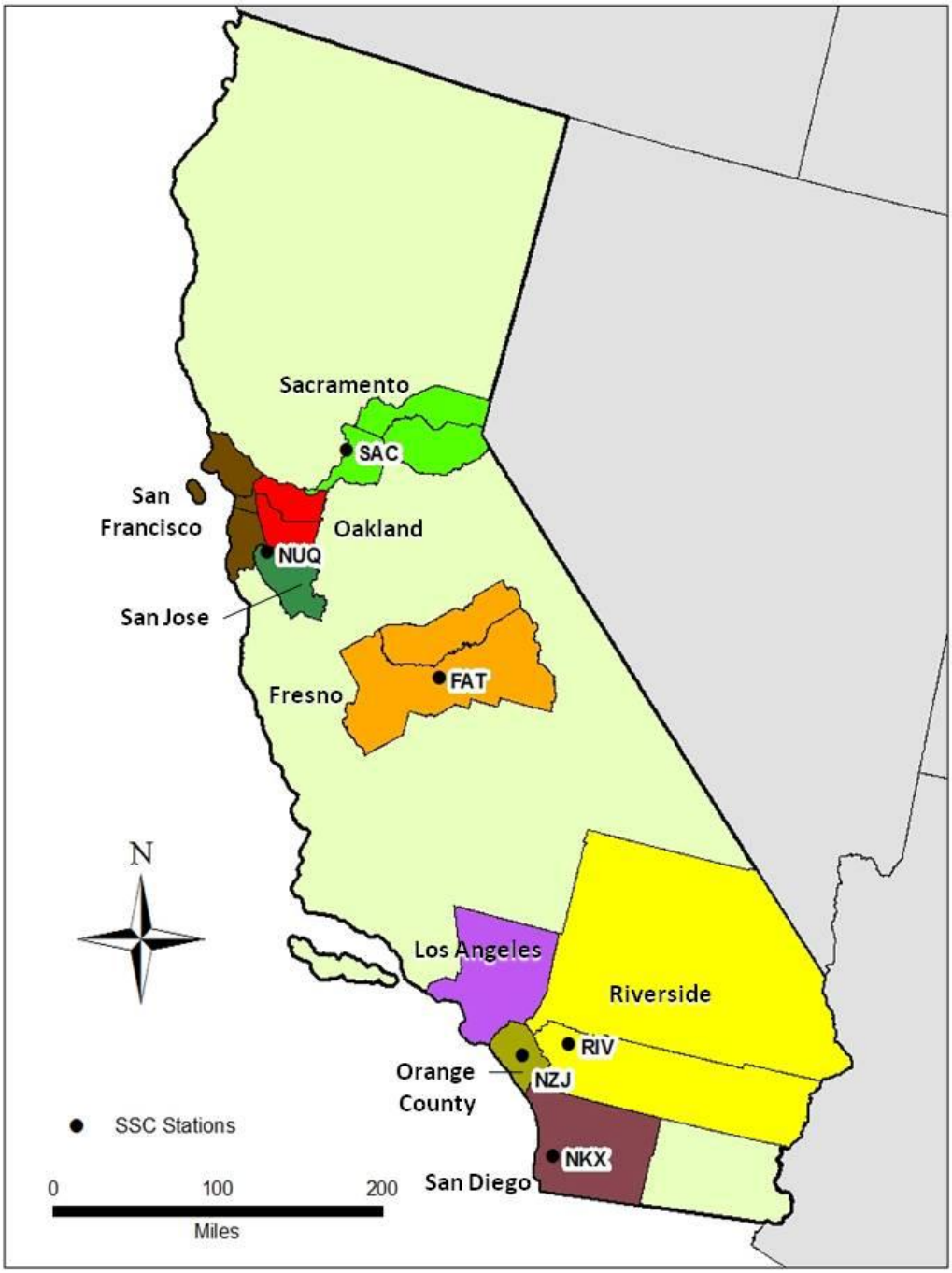

Figure 1 – Study regions (colored counties) and SSC stations (black dots with three letter identifiers) used in this study.

Population projections were provided by the California Department of Finance (2007) for five-year intervals from 2000 to 2100. Population values were provided on a county level, and were stratified by age (in bins of 5 years), race, and sex. Three sets of these population projections were used in this research, termed the *low*, *medium*, and *high* projections, addressing uncertainties in demographic changes and migration. The projections thus vary widely in later years, with the California state population ranging from 47.8 million people in 2100 in the low projection to 147.7 million in the high projection.

For use in this research, population values for both the historical and future periods were calculated for each of the nine regions in Table 1 for three age groups: under 65, 65 to 74, and over 74. As population baselines were needed on an annual basis, annual values are derived by linear interpolation between the years provided.

2.2.2 – Historical Mortality Data

Historical mortality data covering the period 1975 to 2004 were acquired from the National Center for Health Statistics. Mortality data for each death in California are available with information on county, date, age, sex, race, and cause of death. For each of the nine regions, mortality totals by day in the historical period were summed up for each of the three age groups.

2.2.3 – Historical Surface Weather Type Data

Table 2 – SSC weather types

Abbreviation	Weather Type
DM	Dry Moderate
DP	Dry Polar
DT	**Dry Tropical**
MM	Moist Moderate
MP	Moist Polar
MT	**Moist Tropical**

The Spatial Synoptic Classification (SSC) is a station-based weather-type classification scheme (Sheridan, 2002), where each day is classified into one of six weather types (Table 2) or a transition (TR). These weather types are based on local values of temperature, dew point, sea-level pressure, wind speed and direction, and cloud cover four times daily (2:00 am, 8:00 am, 2:00 pm, 8:00 pm PDT). Complete details of the procedures that comprise weather-type classification with the SSC can be found in Sheridan (2002).

Table 3 – SSC stations utilized in this research and the regions for which they were utilized.

Station Name	Code	Years	Regions
El Toro (Irvine)	NZJ	1975-1997	Los Angeles, Orange
Fresno	FAT	1975-2002	Fresno
Miramar (San Diego)	NKX	1975-2002	San Diego
Moffett Field (Mountain View)	NUQ	1975-1999	Oakland, San Francisco, San Jose
Riverside	RIV	1975-2002	Riverside
Sacramento	SAC	1975-2002	Sacramento

For this research, extensive preliminary testing was done to evaluate the most appropriate SSC stations to use with each region (Table 3). The SSC surface weather type must be adequately predicted by upper-atmospheric circulation patterns in order for future projections to be appropriate. Several airport weather stations, such as Los Angeles (LAX), San Francisco (SFO), and San Diego (SAN), are located directly adjacent to the coastline, and surface weather type can be significantly affected by a sea breeze that is difficult to predict using larger-scale atmospheric circulation. Further, weather conditions at these airport locations are not indicative of the region as a whole. Thus, for Los Angeles and Orange, the El Toro Marine Corps Air Station (MCAS) in Irvine was used; for San Diego, Miramar MCAS was used; and for the three Bay Area regions, Moffett Field in Mountain View was used. As shown in the results, weather types at all of these stations could successfully be predicted from larger scale circulation patterns.

Table 4 – Mean conditions for Dry Tropical and Moist Tropical weather types in April, June, and August, for the cities used in this study. 2pm and 2am values are temperature and dew point (°C), respectively, while Freq refers to the mean monthly frequency of occurrence, as a percentage of all days.

		April			June			August		
Station		2pm	2am	Freq	2pm	2am	Freq	2pm	2am	Freq
El Toro	**DT**	**29/4**	**15/3**	**10%**	**34/11**	**20/10**	**4%**	**35/15**	**22/14**	**5%**
	MT	23/12	14/11	17%	27/17	18/16	6%	29/19	21/17	20%
Fresno	**DT**	**28/5**	**15/7**	**19%**	**34/10**	**22/10**	**41%**	**36/12**	**24/13**	**42%**
	MT	21/10	15/11	1%	30/14	23/15	1%	29/15	25/14	1%
Miramar	**DT**	**27/3**	**13/3**	**7%**	**33/9**	**19/10**	**3%**	**33/14**	**21/14**	**2%**
	MT	23/13	14/11	20%	27/16	18/15	9%	29/18	20/18	23%
Mountain View	**DT**	**25/4**	**14/5**	**14%**	**31/9**	**18/10**	**8%**	**32/10**	**20/12**	**2%**
	MT	21/10	14/9	14%	26/14	18/13	6%	28/16	21/16	1%
Riverside	**DT**	**29/1**	**12/3**	**20%**	**35/7**	**18/9**	**25%**	**36/10**	**21/11**	**39%**
	MT	24/11	14/10	7%	32/15	18/14	9%	34/16	21/15	17%
Sacramento	**DT**	**25/4**	**12/3**	**12%**	**34/10**	**19/10**	**23%**	**35/12**	**20/11**	**24%**
	MT	25/12	15/12	2%	32/14	21/12	<1%	31/13	24/11	<1%

To correspond with the work of two of the authors (Sheridan and Kalkstein 2004), two weather types in particular, Dry Tropical (DT) and Moist Tropical (MT)), have most often been associated with increases in human mortality. As discussed further below, the frequency of these two weather types was predicted for future scenarios; a sample of historical mean conditions of these two weather types is presented in Table 4.

2.2.4 – Historical Atmospheric Circulation and Temperature Data

One of the most common historical weather data sets available is the NCEP/NCAR reanalysis (NNR) data set (Kalnay et al., 1996). This data set includes many variables for the global domain across many layers of the atmosphere from 1957 to the present. Though the data are derived from both actual observations as well as short-term model simulations, and have some inherent biases, the data set is generally considered to be an appropriate representation of 'observed' historical conditions, particularly for large scale atmospheric phenomena.

In this research, data from the NNR data set were taken at a once daily resolution (at 1200 UTC – 4 AM PST) from September 1, 1957 through August 31, 2002 for the 500mb and 700mb geopotential height fields (500z and 700z respectively) and the 850mb temperature field (850t). These variables are commonly used in synoptic classifications (Sheridan and Lee, 2010; Vrac et al., 2007) and are considered among the more reliable variables in the NNR data set (Kalnay et al., 1996). These fields are also considered appropriate for the evaluation of surface heat events; as the geopotential height field at the 500mb level is useful for looking at the overall trough and ridge pattern over the study area, indicative of larger scale advection and subsidence in the atmosphere; the 700mb geopotential heights are strongly correlated to surface temperatures (Knapp, 1992); and the 850mb temperatures are a good approximation of surface temperature as well. Due to the unique approach used in this research, there was no *a priori* assumption as to which of the levels would most accurately correspond to surface weather types better than others, and thus, all three fields were included in the analysis.

Data were interpolated from a 2.5° by 2.5° grid to a 5° by 5° resolution from 46°N to 26°N latitude and from 108°W to 128°W longitude – roughly spanning from Northern Oregon south into Baja California and from the Nevada/Utah border west into the Pacific Ocean. Due to the large amount of spatial autocorrelation of geopotential height and temperature data, the coarser grid is not likely to affect the results of a synoptic scale classification of circulation patterns. Additionally, previous synoptic research has shown better results with a more coarse resolution (Demuzere et al. 2009; Saunders and Byrne, 1999), Several different domains were

tested, and this domain was chosen as it most adequately represented surface conditions; larger domains included the Rocky Mountains which contain noise irrelevant to California climate conditions, and smaller domains could not adequately resolve larger scale circulation patterns.

2.2.5 – Future Atmospheric Circulation and Temperature Data

Future atmospheric circulation and temperature data have been acquired from two general circulation models (GCMs). As GCMs each have inherent biases (e.g. Sheridan and Lee, 2010), two models were chosen to provide a greater robustness to the modeled results. Both GCMs are recent updates to long-developed models, and model the atmosphere, land surface, sea ice, and oceans through dozens of levels of the atmosphere. The first GCM used is the Community Climate System Model 3 (CCSM3), which is able to model stable climates for thousands of years under future scenarios (Collins et al., 2006). The second model is from the Canadian Centre for Climate Modeling and Analysis (CCCma) and is the third generation Coupled Global Climate Model, or the CGCM3 (Environment Canada, 2009a, 2009b).

Similarly, future projections of climate change must account for uncertainty in a number of socioeconomic factors, such as economic development, the pace of globalization, and population growth; these all affect future greenhouse-gas emissions levels, and hence atmospheric concentration. The IPCC (2001) has created six different scenarios in its Special Reports on Emissions Scenarios (SRES) to account for the range of future emissions variability (Figure 2). Three of these six are analyzed in this research. **A1FI** represents a rapid, globalized economic development, with population reaching a plateau in mid-century (9 billion), falling to 7 billion by 2100. This FI subset of the A1 scenario also assumes that fossil fuels will remain as the most significant source of energy during the 21st century. In contrast, the **A2** scenario is manifest in continued technological development, albeit somewhat less than A1FI due to less globalization, and hence greater regional differentiation of economic development. Population does not decline, but continues to climb, reaching 15 billion by 2100. The **B1** scenario is similar to the A1FI in that there is significant push towards globalization, although in this case, there is more significant environmental and social consciousness, leading to a greater amount of sustainable development. Population levels plateau in mid-century, as in the A1FI scenario. Colloquially, A1FI is termed the “business as usual” scenario, and B1 is considered the most “environmentally friendly” of the three.

For CCSM3, all three scenarios were used, while for CGCM3, only A2 and B1 were available. Thus, five total model-scenarios were analyzed. Projections were acquired through 2099 in all scenarios with CCSM3, and in two windows from 2045-2064 and 2081-2100 for CGCM3.

Historical model runs, produced to verify the ability of GCMs to simulate present-day climate and climate variability, were also acquired. The 20th Century run of the CCSM3 GCM was taken from the same 1957-2002 time period as the NNR data, while the CGCM3 GCM historical time period spanned only from 1961 to 2000. GCM data were interpolated to the same resolution (5° by 5°) over the same domain (46°N to 26°N latitude and from 108°W to 128°W), and for the same variables at the three pressure height levels (500z, 700z, 850t).

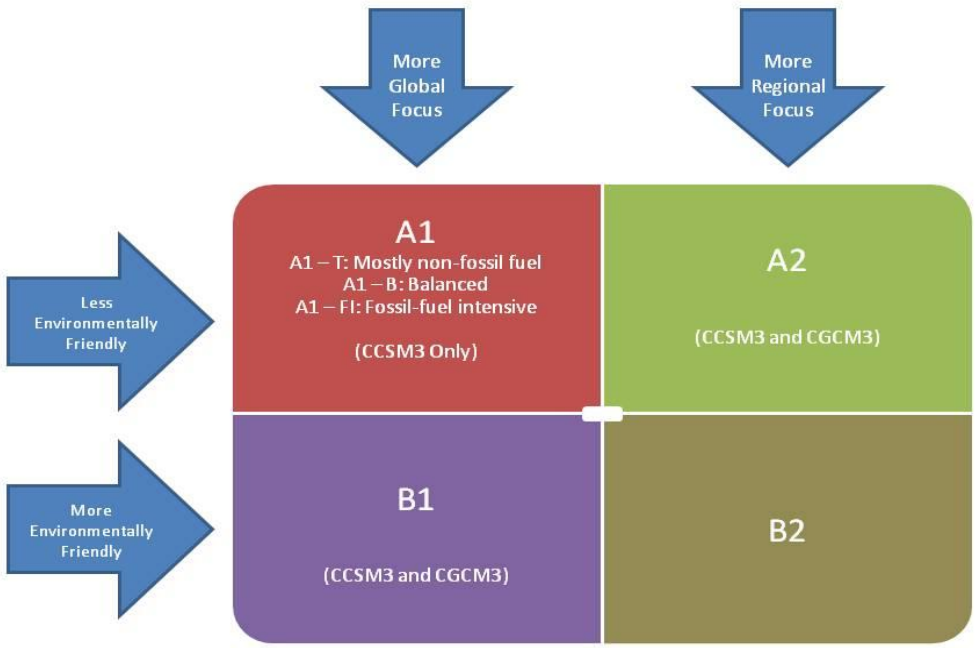

Figure 2 – SRES model scenarios used. Color schemes for each scenario will remain the same throughout the report (adapted from Lee, 2010).

2.3 Methods

2.3.1 – Principal component analysis, cluster analysis, and circulation type determination – the 'Six-step' method

Based upon previous research and after a number of permutations using trial and error, better correlations between the patterns created with the NNR data set and those created with a GCM's 20th Century (hereafter referred to as GCM20c) data set were ultimately found only after 'debiasing' the GCM data; that is, removing the mean model bias. This method has been successfully used in other literature (e.g., Hope, 2006; Lee, 2010). For each grid point, the mean monthly difference between the GCM20c and the NNR data set in the historical period

was removed from the GCM historical data set. The same difference was then subtracted from the relevant future scenarios. In order to 'debias' the data sets, the NNR, GCM20c and GCM-Future data sets were combined into the same spreadsheet, but were kept separate by adding a delineating variable that classifies each case into one of the three. These combined 'debiased' data sets were used for all further analysis. Fifteen total data sets exist – one for each of the three levels, and one for each of the five model scenarios (Figure 3).

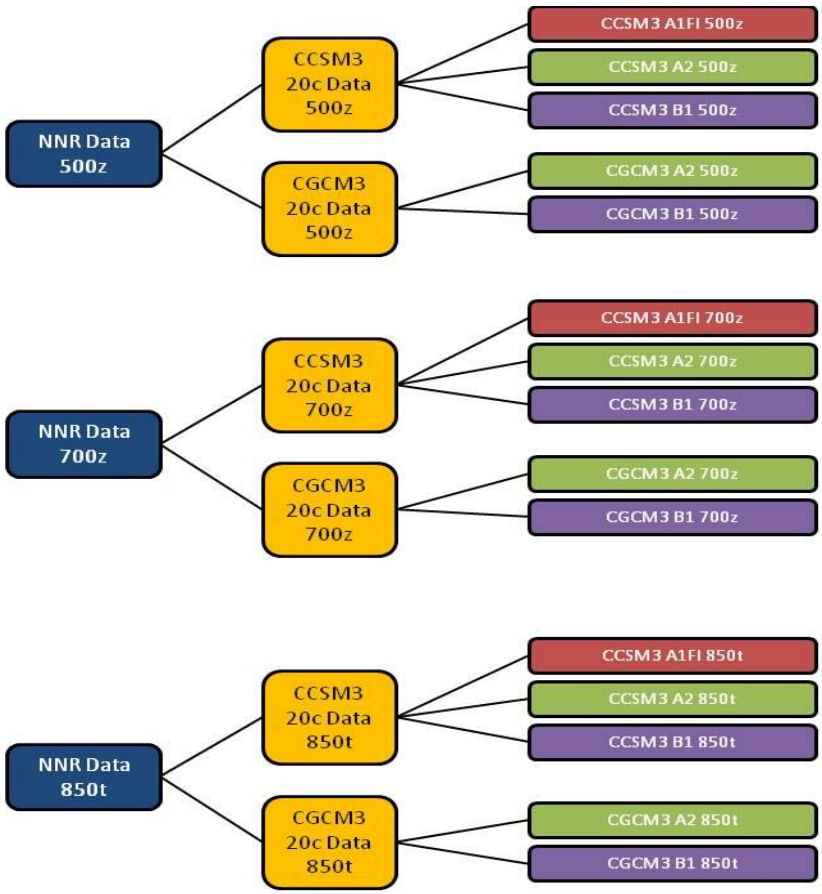

Figure 3 –The fifteen data sets entered into the six-step method

Originally, it was planned to use all 12 calendar months in this research. However, as synoptic variability is greatest in winter months, year-round classifications tend to create more winter patterns at the expense of summer patterns. Hence, a 9-month warm season (March through November) was delineated, and the classification was performed only on these months.

The patterns were classified using a novel six-part process (Lee, 2010; Figure 4). This process is iterated once for each of the 15 combined (5 model-scenarios x 3 levels of atmosphere)

debiased data sets (Figure 3). The process described below is an example of one iteration with one of the data sets (i.e. the NNR/GCM20c/CCSM3 – A1FI 500z data set).

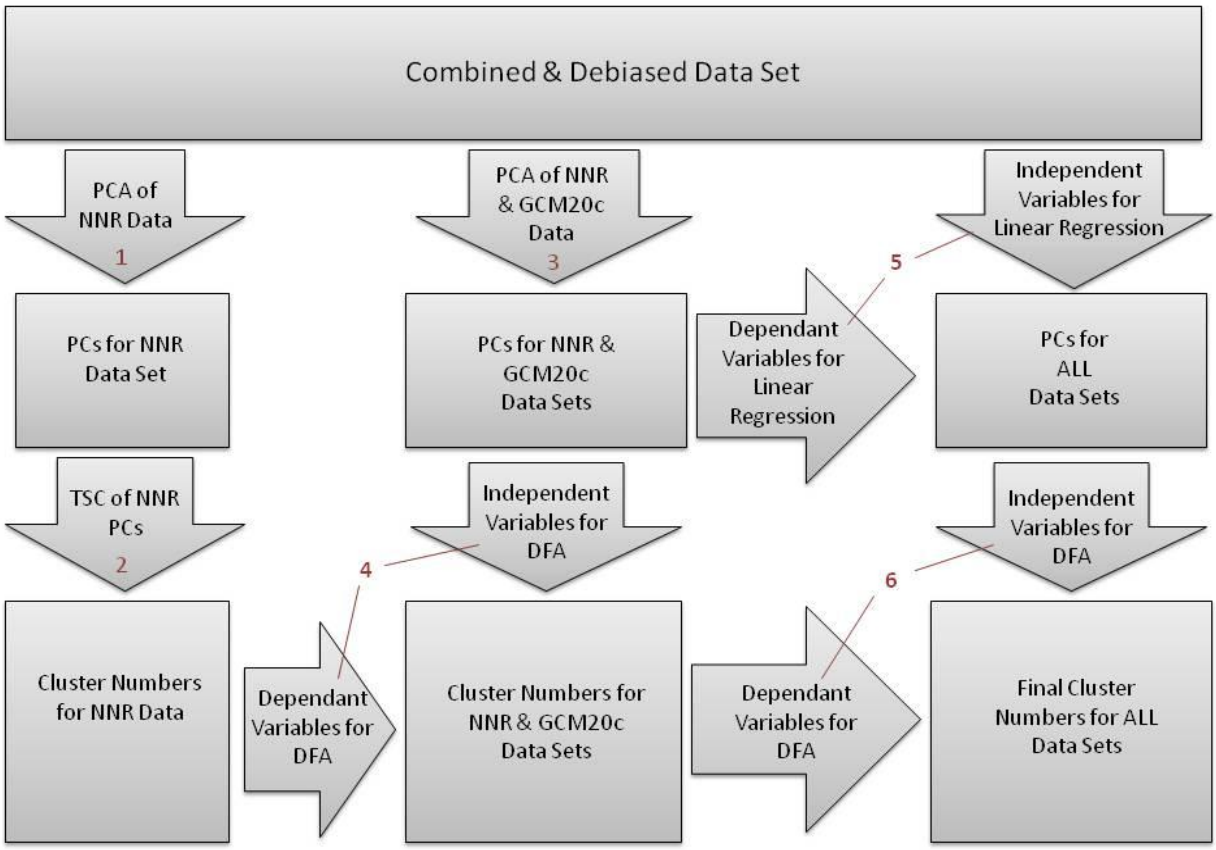

Figure 4 – Schematic of the "six-step" method utilized in this research to derive future atmospheric circulation types. Red numbers in figure correspond to steps in text.

Part 1 *– Principal Components Analysis with NNR Data Set*

The first step in the pattern creation process is to perform a principal components analysis (PCA) on just the data in the NNR data set. In SPSS, each of the 25 grid points' 500z values were entered as variables. In addition to reducing total data volume, PCA in this instance creates completely uncorrelated variables for use in a cluster analysis in subsequent steps. Due to the tendency of climate data to be naturally autocorrelated – both spatially and temporally – this is a necessary precursor to cluster analysis in order to eliminate the possibility that some variables will be over-represented once entered into the clustering algorithm. The PCA creates principal component (PCs) scores that are added to the data set as variables. Although the total number of PCs to retain for further analysis is ultimately a subjective decision, this research uses the standard in synoptic climatology – which keeps only the PCs with eigenvalues greater than one (Yarnal, 1993). Several other permutations were tested in preliminary research, as

Cuell and Bonsal (2009) have noted that the number of PCs retained may have a significant impact upon final clusters. However, among the permutations evaluated, the resulting classifications yielded no distinctly superior patterns that better captured the variability of the variable being clustered, and hence we chose the conventional rule.

Part 2 *– Two Step Cluster Analysis with PC Scores*

The second step was to perform a Two-Step cluster analysis (TSC) on the PC scores saved as new variables from the previous step. In SPSS, the PCs were entered as standardized continuous variables, the number of groups was specified at 10, and the group membership variable was saved into the data set. All other settings in SPSS were left in their defaults: the log-likelihood was used as the distance measure; and Schwarz's Bayesian Criterion was used as the clustering criterion.

Again, ultimately, the number of clusters to retain is a subjective decision. Due to the nature of the atmosphere, within any classification, a certain amount of variability is going to exist within each group. The goal of any cluster analysis is to minimize the total variance within each cluster and maximize the variance between clusters (Yarnal, 1993); however the utility of the classification must also be kept in mind as well. While permutations with fewer and more clusters were also tried, it was found that the 10-cluster classification was the best at resolving the actual atmospheric patterns important to heat events in the area of interest.

Part 3 *– PCA of NNR and GCM20c Data Sets*

After selecting all but the GCM-Future data, the third part of the process was to perform a second PCA on the 25 grid point variables of 500z values. All settings were identical to the settings described in part 1 above, and the PC scores were retained as new variables in the data set. PCA was used in this step instead of linear regression (used in step 5 below) in order to capture the variability of the GCM, instead of basing PC scores on just the variability that exists within the NNR data set.

Part 4 *– Discriminant Function Analysis of PC Scores*

The fourth part of the process was to perform a discriminant function analysis (DFA). DFA utilizes a subset of data for which group membership is already known in order to classify the rest of the data set into similar groups based upon the relationship of a shared set of variables to the group number (Wilks, 2006). In this research, the patterns of circulation had already been created (in Step 2 above) for a potion of the data. In order to classify additional data into similar groups, DFA was the most logical method to use. The relationship between the group numbers created in the TSC for the NNR data set (step 2) and the PCs created in step 3 were used to classify the rest of the data set (GCM20c). In SPSS, the PCs created in part three are the

dependant variables, and the TSC group number is selected as the grouping variable with the range set at 1 to 10. The stepwise method was used, and the F-score of Wilks' lambda (entry at 3.84, removal at 2.71) was the criterion used for inclusion. The classification was set to be based on the group sizes of the TSC groups rather than all groups being equal, and the group membership variable were saved into the data set. After completion of the DFA, the NNR and the GCM20c data were classified into groups.

Part 5 *– Linear Regression to Predict PC Scores for GCM Future Data*

The fifth part of the process was to perform a series of linear regressions on all three data sets (NNR, GCM20c and GCM Future data) in order to predict the PC scores for GCM future data. This linear regression was used instead of PCA in order create patterns from future data based upon the patterns that were already created. A separate linear regression was performed for each of the principal components retained from part 3. The PC was entered into the linear regression as the dependent variable to be predicted, and the 25 500z values were entered as the independent variables. The stepwise method of regression was used with the entry significance level set at 0.05 and removal at 0.10, and the unstandardized predicted values were saved as variables into the data set. Again, this regression was repeated for each of the PCs retained from part 3.

Part 6 *– DFA with all Data*

A second DFA was performed on the entire data set in the sixth and final part of the process, creating the final clusters that represent the different patterns of atmospheric circulation. The same process used in part four above was repeated here in part six, except that the grouping variable in this step was the DFA cluster number that was created in part four above, and the dependant variables were the saved PCs (or the unstandardized predicted values) created in part five. Again, the group membership variable was saved into the data set – this time representing the final group to which each day belongs. Ultimately, the use of DFA here creates circulation patterns in the GCM-Future data set that are as similar as possible in shape to the patterns created in the NNR and GCM20c data sets.

In order to better visualize the atmospheric circulation patterns created from this process, the mean 500z value at each of the 25 grid points was mapped for each cluster. This entire six-part process was then repeated for each of the other 14 combined debiased data sets.

As mentioned throughout the methodology, a number of different permutations were attempted. After varying the months to include, the PCs to retain, the final number of clusters, and the domain size, the decisions outlined above reflect the patterns that most accurately encompass both the range and the variability of the patterns of the three variables throughout

the entire region and time period, and are the most successful at reproducing SSC weather types in later steps.

2.3.2 – Using multinomial logistic regression to predict SSC weather-type

After the atmospheric circulation patterns were created, for each of the five model scenarios the next task was to predict the daily SSC type for the GCM-Future data based upon the relationship of the atmospheric circulation patterns to SSC type in the historical NNR data set. Thus, the DFA cluster numbers for each of the three levels (500z, 700z, and 850t) were combined into the same data set, creating a total of five working data sets – one for each model scenario. A new data set that represents each of the six SSC stations used in this study was then created for each of these five data sets – creating a total of 30 data sets – one for each of the five model scenarios at each of the six SSC stations.

Additional variables were then added to each data set (Table 5): the actual historical SSC-type number (DM=1, DP=2, DT=3, MM=4, MP=5, MT=6) for each station (in the NNR portion of the data set only); the 850t values at 36°N, 123°W and 36°N, 118°W; either an inland or a coastal variable that represents the time of the year (a sinusoidal curve) depending on station location; one day lags and one day leads of the atmospheric circulation patterns; and one day lags of each of the three PCs at each of the three levels.

A custom multinomial logistic regression was then used in order to predict the SSC type for both the GCM20c portion of the data and the GCM Future portion of the data. Multinomial logistic regression (MLR) is able to use both continuous and categorical independent variables in order to predict the value of a categorical dependant variable. The custom MLR included different variables (Table 5) depending on whether a SSC station was considered a coastal station (within 80km of the coast) or an inland station (farther than 80km from the coast). Sacramento (SAC) and Fresno (FAT) were the only two stations that used the Inland MLR method, while Mountain View (NUQ), El Toro (NZJ), Miramar (NKX), and Riverside (RIV) used the Coastal MLR method. For each of the 30 data sets, either the Inland or the Coastal MLR method (described below) was used to determine future SSC types.

<u>Inland MLR Method</u>

For each station the SSC type number was used as the dependant variable to be predicted. As previously noted, two types of independent variables can be used – categorical and continuous. Thus, in SPSS, the following independent categorical variables were entered as factors into the

Inland MLR equation: the 850t DFA cluster number, the one day lag of 850t DFA cluster number, and the one day lead of the 850t DFA cluster number.

Table 5 – Predictive variables for the SSC type (dependent variable). 'X' in right two columns denotes their inclusion for coastal and inland cities.

Variable Name	Description of Variable(s)	Used in:	
		Coastal	Inland
CATEGORICAL VARIABLES			
700_DFA	The DFA cluster number for 700z	X	
850_DFA	The DFA cluster number for 850t	X	X
700_DFA_LAG	The one day lag of the DFA cluster number for 700z	X	
850_DFA_LAG	The one day lag of the DFA cluster number for 850t	X	X
700_DFA_LEAD	The one day lead of the DFA cluster number for 700z	X	
850_DFA_LEAD	The one day lead of the DFA cluster number for 850t	X	X
MONTH	The month of the case	X	
CONTINUOUS VARIABLES			
500_PC1	The three PCs created in Step 5 of the Six-Step Process for 500z	X	
500_PC2		X	
500_PC3		X	
700_PC1	The three PCs created in Step 5 of the Six-Step Process for 700z	X	
700_PC2		X	
700_PC3		X	
850_PC1	The three PCs created in Step 5 of the Six-Step Process for 850t	X	X
850_PC2		X	X
850_PC3		X	X
500_PC1_LAG	The one-day lag of the three PCs for 500z	X	
500_PC2_LAG		X	
500_PC3_LAG		X	
700_PC1_LAG	The one-day lag of the three PCs for 700z	X	
700_PC2_LAG		X	
700_PC3_LAG		X	
850_PC1_LAG	The one-day lag of the three PCs for 850t	X	X
850_PC2_LAG		X	X
850_PC3_LAG		X	X
36_123	The 850t value at 36°N, 123°W	X	X
36_118	The 850t value at 36°N, 118°W	X	X
COASTAL_CURVE	The sinusoidal curve of seasonality of coastal SSC stations	X	
INLAND_CURVE	The sinusoidal curve of seasonality of inland SSC stations		X

In addition to the categorical variables, several continuous variables were added into the equation as covariates: the three 850t PCs; the one day lag of the three 850t PCs; the 850mb temperature at 36°N, 123°W; and the 850mb temperature at 36°N, 118°W. To account for different seasonal cycles in weather conditions (with peak temperatures occurring later in the year climatologically at coastal stations than inland stations), two seasonally oscillating variables (one for coastal cities and one for inland cities) were created that contained the sine of the season cycle as reflected in the SSC; with a value of 1 for the warmest weather-type day, and -1 for the coldest weather-type day. The inland sinusoidal curve was thus incorporated as well. The 'main effects' of each of these variables were added into the equation.

To emphasize the combined effect of two variables, the MLR was customized to include 'interaction terms' in the equation. Five interaction terms were added: 1) the 850t DFA number and the one day lag of the 850t DFA number; 2) the 850t DFA number and the one day lead of the 850t DFA number; 3) the 850t DFA number and the inland sinusoidal curve; 4) the 850t DFA number and the 850t value at 36°N, 123°W; and 5) the 850t DFA number and the 850t value at 36°N, 118°W.

Coastal MLR Method

After using the aforementioned *Inland MLR Method* for stations located close to the coast, it was discovered – using trial and error – that the SSC type for these stations was more dependent on the 700mb geopotential height pattern than the 850mb temperature pattern. Thus, while the dependent variable remained the same as in the *Inland MLR method* (the SSC type number for the station), in SPSS, the following independent categorical variables were entered as factors into the *Coastal MLR* equation: the 700z DFA cluster number, the 850t DFA cluster number, the one day lag of the 700z cluster number, the one-day lead of the 700z cluster number, the one day lag of the 850t cluster number, the one day lead of the 850t cluster number, and the month.

The following continuous variables were added as covariates into this same equation: the three 500z PCs, the three 700z PCs, the three 850t PCs, the one day lags of each of these nine PCs, the two 850t temperatures mentioned above, and the coastal sinusoidal curve representing the time of the year. With the exception of the month, the 'main effects' of all of the aforementioned terms are added to the equation.

The interaction terms used in this equation are: 1) the 700z DFA number with the 700z DFA one day lag; 2) the 700z DFA number with the 700z DFA one day lead; 3) the 700z DFA number with the month; 4) the 700z DFA number with the 850t at 36°N, 123°W; and 5) the 700z DFA number with the 850t at 36°N, 118°W.

In both the Inland and the Coastal MLR method, as opposed to using the stepwise method, *all* independent variables were used as 'forced entry' terms into the equation. All other settings were left in their default setting, and the predicted category was saved as a variable into the data set – this variable representing the predicted daily SSC type for every day in both the GCM20c and the GCM Future portions of the data set.

2.3.3 – Historical mortality data: standardization and the determination of heat-mortality relationships

The daily mortality totals for each of the nine regions for each of the three age categories were first standardized to account for demographic changes over the 1975-2004 baseline period. Rates were calculated in terms of deaths per 100,000 for each of the categories. From these rates, anomalous mortality rates were calculated, through standard procedures (e.g. Sheridan and Kalkstein, 2004) to account for both the season cycle (through an 11-day running mean mortality rate over the period of analysis) and long-term trends (through a 3-year running mean mortality rate). From this standardization, mean anomalous mortality rates from baseline ('expected') mortality are available for each day, each region, and each age group.

In order to develop the historical relationship between human mortality and weather, potential independent variables were developed to predict anomalous mortality (dependent variable). These independent variables fall into three categories: weather-type related, seasonality related, and temperature related.

Previous research has shown that the two tropical weather-types, DT and MT, are associated with the most significant increase in mortality. To correspond with the authors' heat-health watch warning systems, the synoptic weather type was utilized as an important component in determining heat vulnerability, and thus formed the basis of regression equations that were derived for each region/age group (Sheridan and Kalkstein, 2004). The SSC station used for each region is listed in Table 3. As possible independent variables in the regression equations, four variables were derived from the SSC weather-type information, including:

- A *Day in Sequence* (DIS) variable, which counts the number of consecutive days in which DT or MT occurs. Research has shown an added 'heat wave effect' in human vulnerability to hot weather (e.g.; Hajat et al., 2006).
- Along the same line, a *binary lag DIS* variable was set to 1 if the prior day was DT or MT.
- Two individual binary variables for DT and MT, set to 1 if the weather type occurred on the given day.

As there is significant seasonal variability in the heat-health relationship (e.g. Sheridan and Kalkstein, 2010), due to acclimatization and/or changes in the size of the pool of susceptible people, two variables were created to account for the season cycle. A *time of season* (TOS) variable was calculated; in each year, January 1st is assigned 1, and December 31st is 365. The relevant sinusoidal curve (coastal or inland) discussed above was also incorporated.

As there is within-weather type variability in atmospheric conditions, two continuous variables – the NNR 850mb temperatures at the two most relevant grid points for the state of California (36°N, 123°W and 36°N, 118°W) – were included as potential variables. While surface temperatures are available historically, these variables were chosen specifically to correspond with available GCM data that is well predicted.

Once all potential independent variables were calculated, regression equations were determined based on a stepwise entry method, using a p=0.15 threshold value. A separate regression equation was produced for each age category for each region. The final output model's coefficients were utilized for the regression equation to predict future mortality.

2.3.4 – Predicting future heat-related mortality

Once projections of the future daily SSC type were made, the regression equations discussed above – representing the relationship between SSC type and mortality in a city – were used to project the impacts of climate change on heat-related mortality in these cities. Mortality predictions were calculated only on days for which an oppressive weather-type was present. Furthermore, only oppressive weather type days with forecasts for increased mortality were included in the calculation. Not every oppressive weather-type day possesses increased mortality; some may be borderline low situations, barely making the oppressive category. Others may be a single day event or may occur late in the season when even oppressive days show little sensitivity as related to mortality variation. The projections discussed below are in terms of the summed change in heat-related mortality predictions derived from these calculations.

2.3.5 – Predicting heat-related mortality that accounts for acclimatization

For this project, we employed a new acclimatization method based on the results of recent research. Given the unique climate of California's urban areas, an analog city method would not be appropriate. Our previous research (Hayhoe et al. 2004) showed varying levels of acclimatization from using the analog city method that were difficult to explain. As our initial research in this project yielded similar results, we decided to use a different method.

Because of the added 'heat wave effect' and short-term mortality displacement discussed previously, in this research, we rendered acclimatization and short-term displacement by adjusting the day-in-sequence. Specifically, we defined a moderate amount of acclimatization as neglecting all heat-related mortality that occurs in the first 1 day of a given string of oppressive weather type days (hereafter, DIS-2, or day in sequence of 2 or greater is counted); for a higher level of acclimatization, we also define heat-related mortality as omitting the first 3 days (DIS-4). We believe that this method captures a measure of the potential for adaptation to short-term heat events, where physiological and behavioral adaptations may be more significant, yet still evaluate the impact of longer-term heat events, where physiological and behavioral adaptations may be less valuable, and thus the mortality response is more significant.

3. RESULTS

3.1 – Summary of circulation patterns with the CCSM3 model

The maps and discussion in section 3.1 are based on the CCSM3 model output. For CGCM3, as discussed above, the same process was undertaken, although the resulting clusters are slightly different. As the ultimate use of these clusters is to derive surface weather type, only CCSM3 is discussed here, and the CGCM3 maps can be found in Appendix A.

3.1.1 – 500-mb height clusters (500z)

At the 500mb level, patterns 5, 8 and 9 each exhibited a strong summer seasonality – together accounting for over 98% of July and August days and 46.1% of days overall (Figure 5). Featuring a strong ridge over the Desert Southwest, pattern 8 is the warmest of the summer patterns at the 500z level, occurring over half the time in July and August before dropping off markedly from September through November. Overall, pattern 8 was the most frequent of any 500z pattern, occurring an average of 18.8% of warm season days.

Although pattern 9 also peaked in July and August, it occurred nearly equally in June and September as well (at about 25% of the days in each month), but only about 30% of the time in the heart of summer. This pattern features a more zonal flow than pattern 8, with the highest geopotential heights (which are generally associated with the highest upper-atmospheric temperatures) only in the extreme southern tip of California, and occurs 14.4% of the days overall.

Pattern 5 is more meridional than the previous two patterns, with the highest geopotential heights being well south and east of California. Pattern 5 peaked in June, occurring on 31% of the days in the month, before dropping off substantially in July, but remaining steady thereafter into October (occurring 13% to 18% of the time in those four months). Throughout the entire warm season, pattern 5 was the third most frequent pattern, occurring 13.2% of the time.

Most of the other seven patterns peaked in the spring before declining or disappearing entirely in the summer months and reoccurring in September and October. Among the coolest of all the 500mb level patterns is pattern 7, which features a trough just west of California. This pattern peaked in March and then declined in frequency steadily thereafter into June and was the least frequent pattern throughout the warm season, occurring only 4.2% of the time.

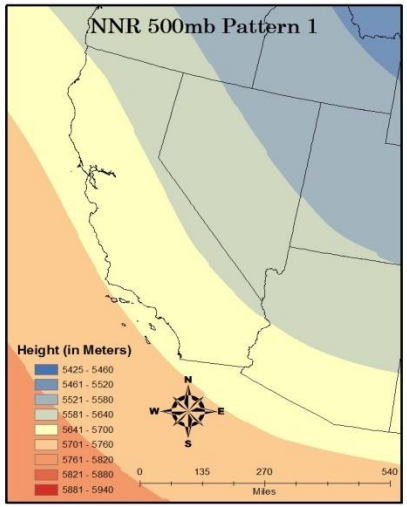

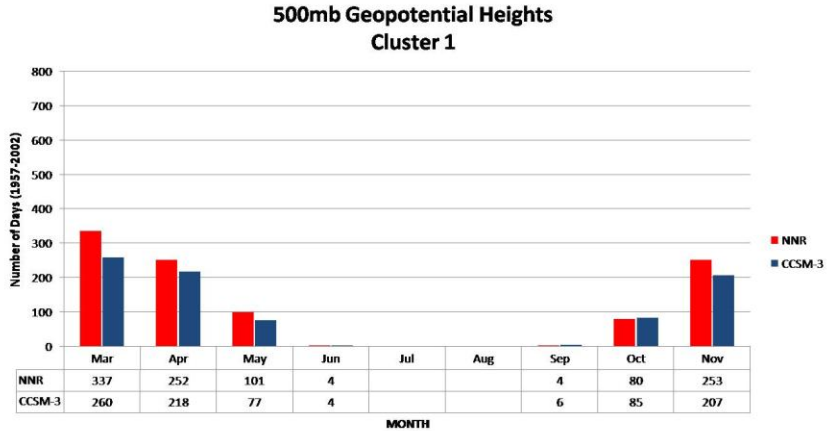

	Mar	Apr	May	Jun	Jul	Aug	Sep	Oct	Nov
NNR	337	252	101	4			4	80	253
CCSM-3	260	218	77	4			6	85	207

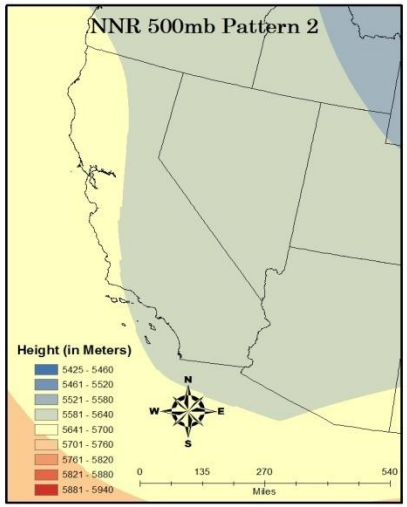

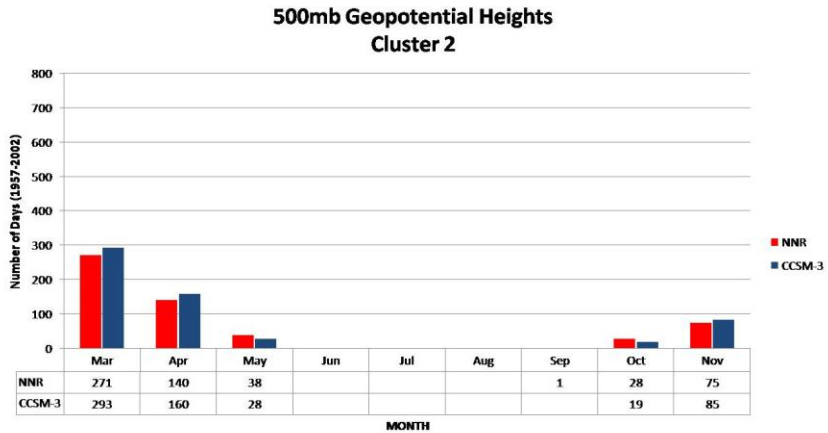

	Mar	Apr	May	Jun	Jul	Aug	Sep	Oct	Nov
NNR	271	140	38				1	28	75
CCSM-3	293	160	28					19	85

Figure 5 – Patterns of 500mb geopotential heights (left) and monthly frequency of each pattern (right) from 1957-2002. Continued on the following page.

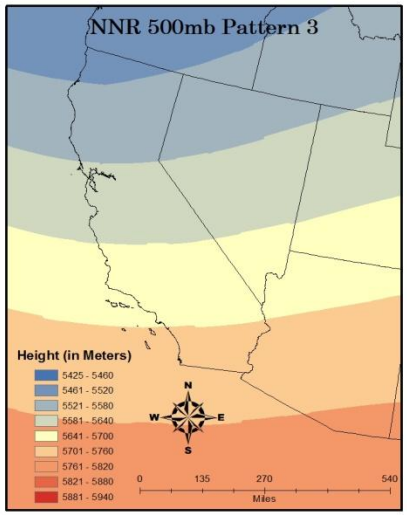

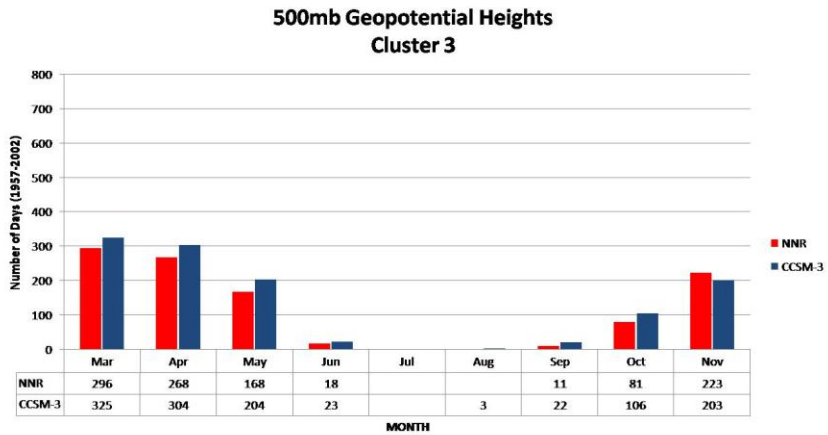

	Mar	Apr	May	Jun	Jul	Aug	Sep	Oct	Nov
NNR	296	268	168	18			11	81	223
CCSM-3	325	304	204	23		3	22	106	203

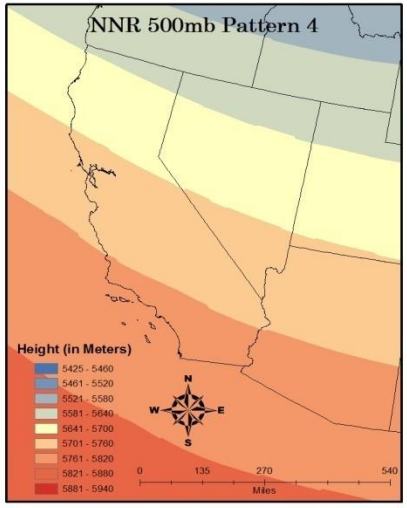

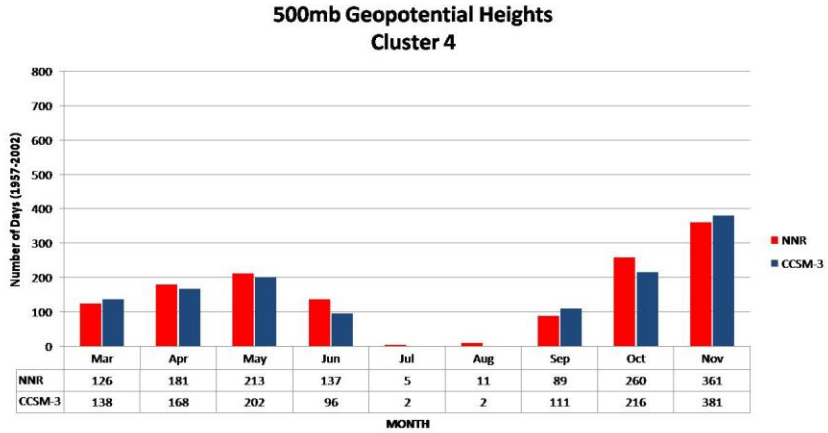

	Mar	Apr	May	Jun	Jul	Aug	Sep	Oct	Nov
NNR	126	181	213	137	5	11	89	260	361
CCSM-3	138	168	202	96	2	2	111	216	381

Figure 5 – Continued.

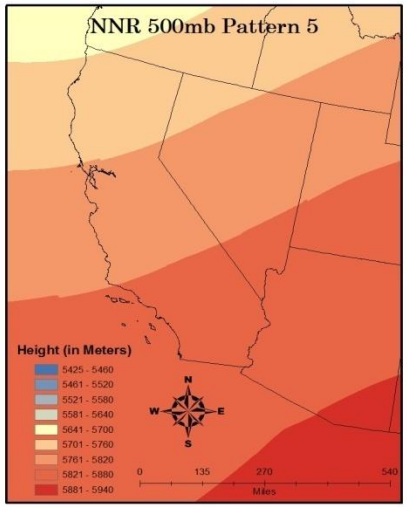

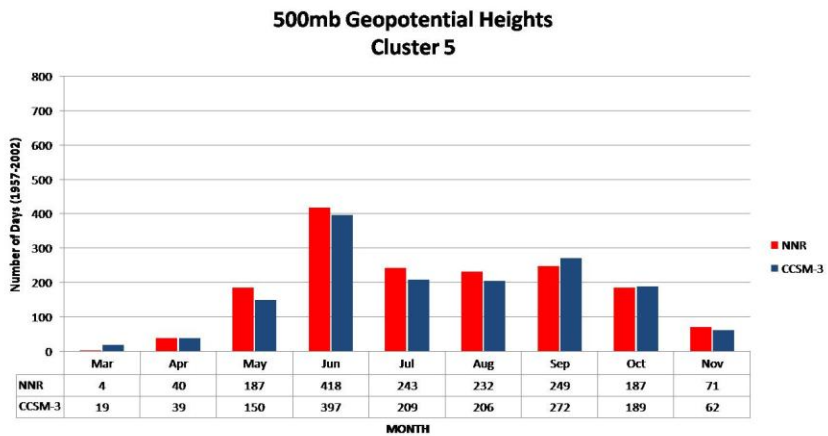

	Mar	Apr	May	Jun	Jul	Aug	Sep	Oct	Nov
NNR	4	40	187	418	243	232	249	187	71
CCSM-3	19	39	150	397	209	206	272	189	62

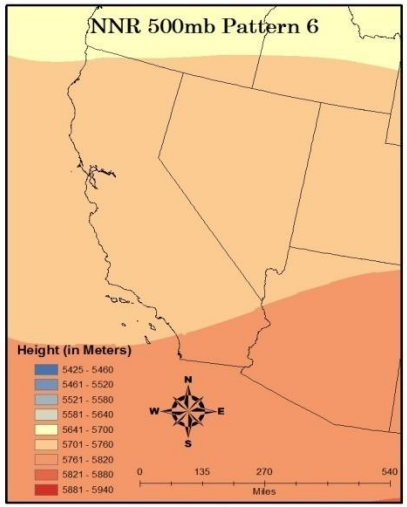

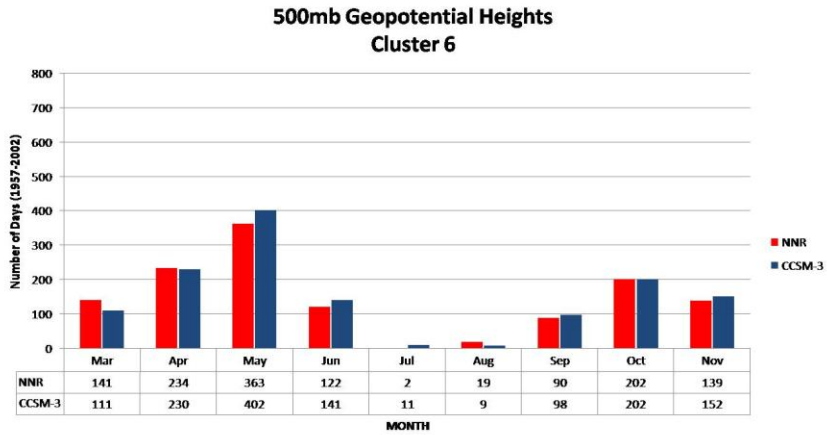

	Mar	Apr	May	Jun	Jul	Aug	Sep	Oct	Nov
NNR	141	234	363	122	2	19	90	202	139
CCSM-3	111	230	402	141	11	9	98	202	152

Figure 5 – Continued.

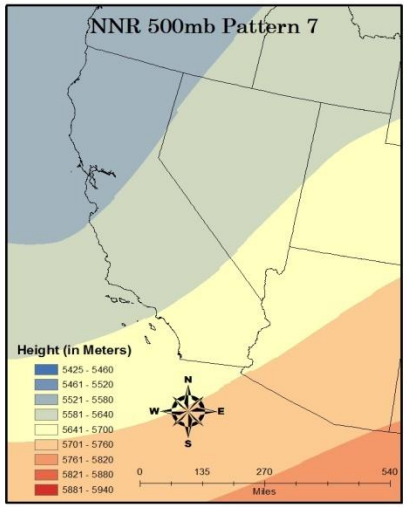

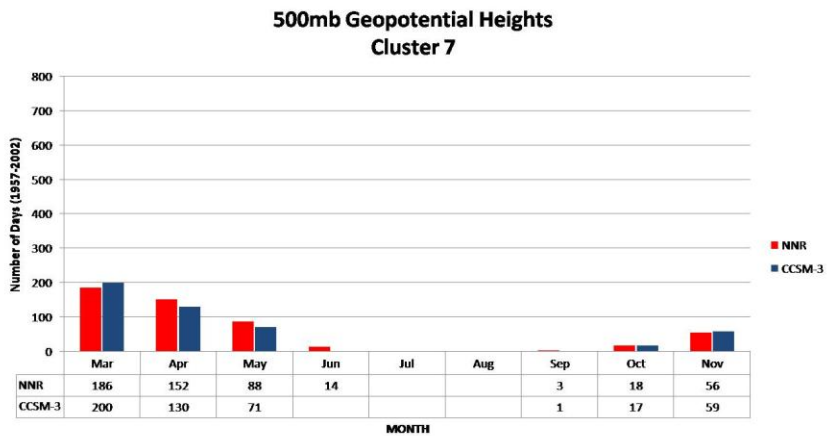

	Mar	Apr	May	Jun	Jul	Aug	Sep	Oct	Nov
NNR	186	152	88	14			3	18	56
CCSM-3	200	130	71				1	17	59

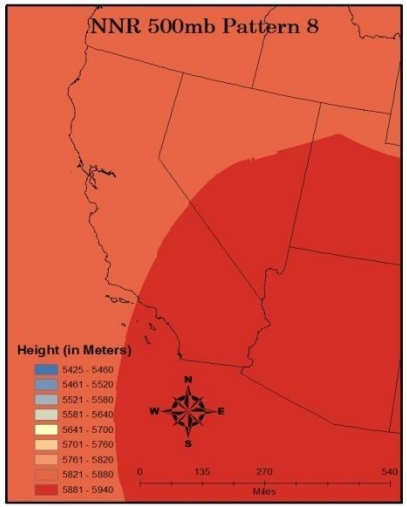

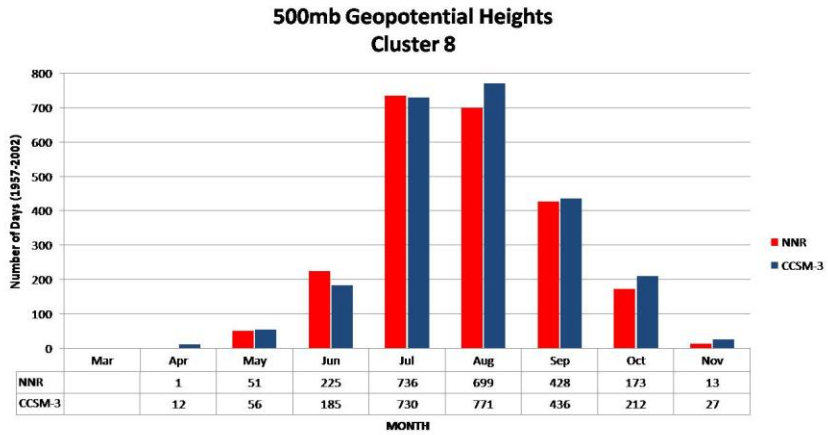

	Mar	Apr	May	Jun	Jul	Aug	Sep	Oct	Nov
NNR		1	51	225	736	699	428	173	13
CCSM-3		12	56	185	730	771	436	212	27

Figure 5 – Continued.

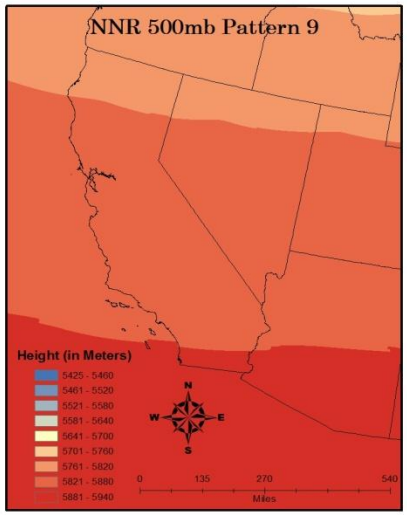

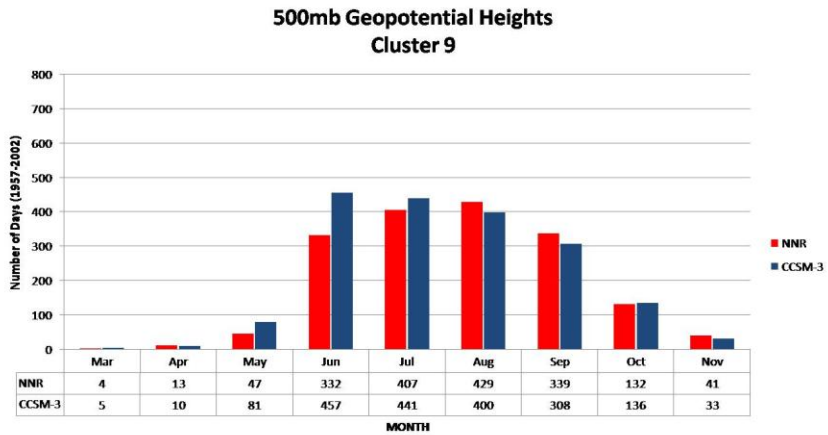

	Mar	Apr	May	Jun	Jul	Aug	Sep	Oct	Nov
NNR	4	13	47	332	407	429	339	132	41
CCSM-3	5	10	81	457	441	400	308	136	33

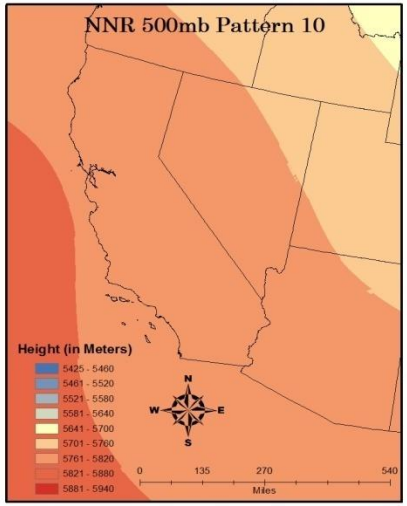

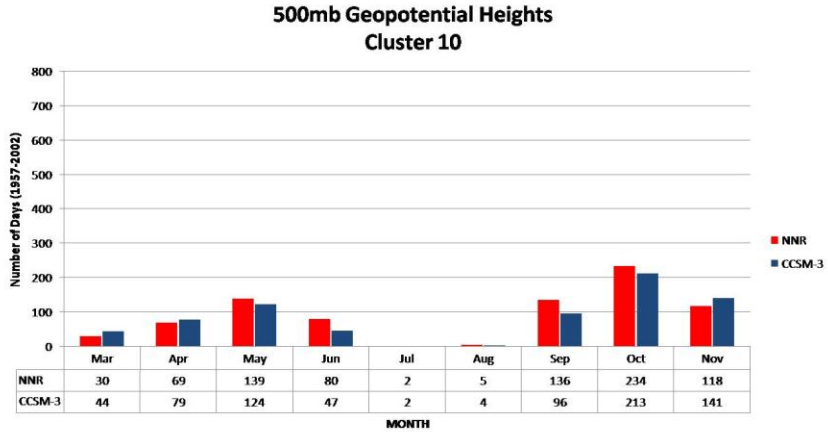

	Mar	Apr	May	Jun	Jul	Aug	Sep	Oct	Nov
NNR	30	69	139	80	2	5	136	234	118
CCSM-3	44	79	124	47	2	4	96	213	141

Figure 5 – Continued.

3.1.2 – 700-mb height clusters (700z)

Three patterns dominated the summer scene at the 700z level (Figure 6). It is not surprising that a majority of patterns occur outside the summer season; the cool season weather is always more variable than warm season weather, yielding a higher number of patterns.

Pattern 1 was clearly the most frequent in summer at this level, occurring over 56% of time in July and August – more than double pattern 3 or 4 which also occurred most frequently in the warm season. Much like pattern 8 at 500z, pattern 1 at 700z is highlighted by a strong ridge over the Desert Southwest that extends into much of Southern California. After its summer peak, pattern 1 still occurred nearly 30% of September days and about 15% of October days as well. Overall, the pattern occurred over 20% of the time during the warm season.

Pattern 3 can occur any time of year, but was most frequent during the warm season, when it occurred over 14% of the time. However it was much more frequent than pattern 1 in the shoulder months of the warm season. Pattern 3 features a trough just off the coast of California, likely bringing more moderate temperatures to much of the state compared to pattern 1, which is associated with hotter conditions. Pattern 3 peaked in June, but remained relatively frequent from May through October.

Similar in shape to pattern 3, although generally more zonal, pattern 4 at the 700z level is highlighted by a more pronounced summer seasonality – occurring much more frequently from June through August than it does in spring or autumn. Overall, pattern 4 occurred less than 10% of the time during the warm season. Overall, patterns 1, 3, and 4 accounted for nearly 95% of July and August days, and over 44% of all days in the time period.

Among the remaining seven patterns at the 700z level, only patterns 2 and 5 exhibited a strong spring and autumn seasonality. Occurring nearly 12% of total days over the warm season, pattern 2 features a tilted trough running from the northeast through the southwest portions of the study area. Pattern 2 had dual peaks in May and October – occurring over 20% of the time in both months – and rarely in summer. California sits just downstream of a trough off the coast in pattern 5. This pattern is also highlighted by a dual peak seasonality, in May and September, and occurred on about 11% of days during the nine-month season.

The remaining 700z patterns all featured similar seasonalities, peaking in the fringe months of the warm season (March and November) and occurring rarely or never over the summer. Of these patterns, only pattern 10 occurred on more than 10% of days during the warm season,

while pattern 8 occurred on only 2.3% of days – the least of any 700z pattern – never occurring more than 8% of the time in any single month. Not surprisingly, most of the cooler season patterns demonstrated a more non-zonal flow than the summer patterns.

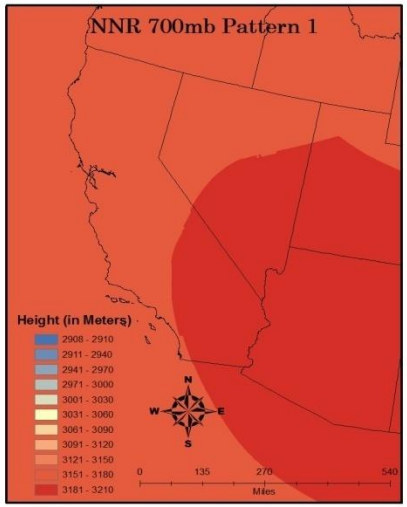

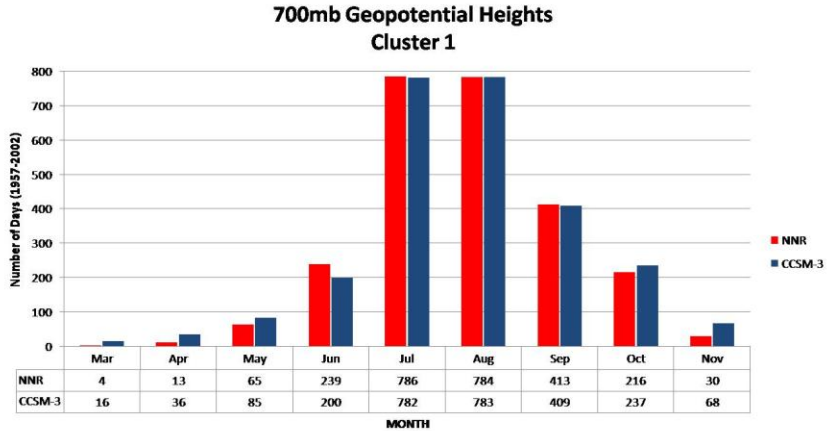

	Mar	Apr	May	Jun	Jul	Aug	Sep	Oct	Nov
NNR	4	13	65	239	786	784	413	216	30
CCSM-3	16	36	85	200	782	783	409	237	68

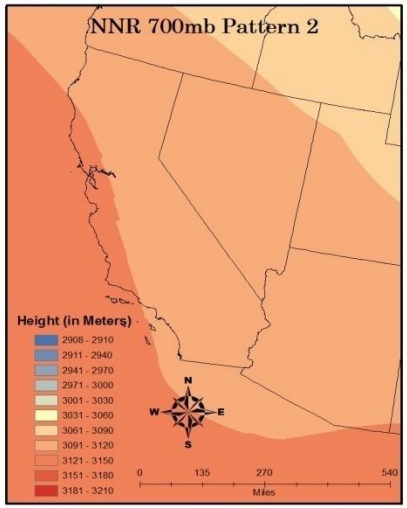

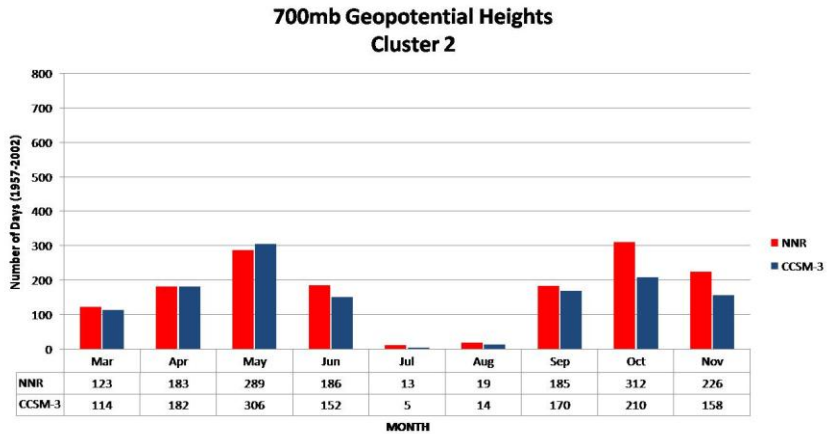

	Mar	Apr	May	Jun	Jul	Aug	Sep	Oct	Nov
NNR	123	183	289	186	13	19	185	312	226
CCSM-3	114	182	306	152	5	14	170	210	158

Figure 6 – Patterns of 700mb geopotential heights (left) and monthly frequency of each pattern (right) from 1957-2002. Continued on the following page.

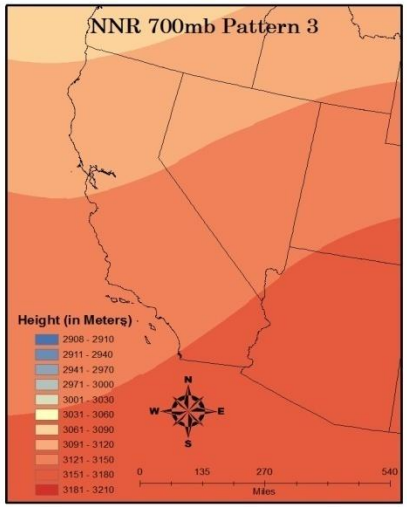

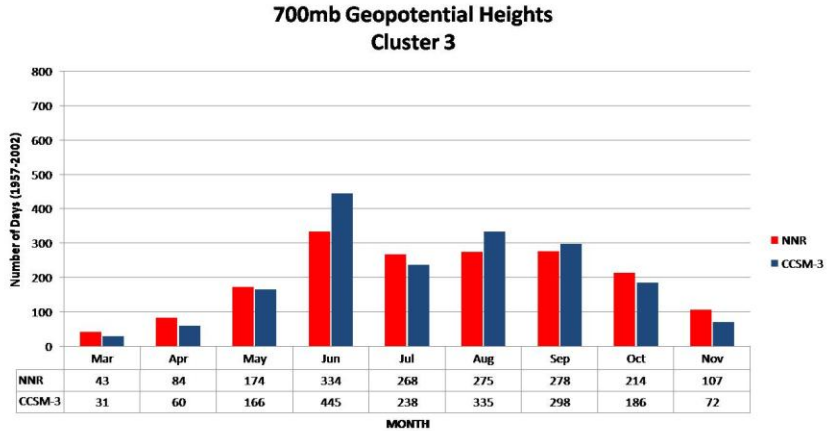

	Mar	Apr	May	Jun	Jul	Aug	Sep	Oct	Nov
NNR	43	84	174	334	268	275	278	214	107
CCSM-3	31	60	166	445	238	335	298	186	72

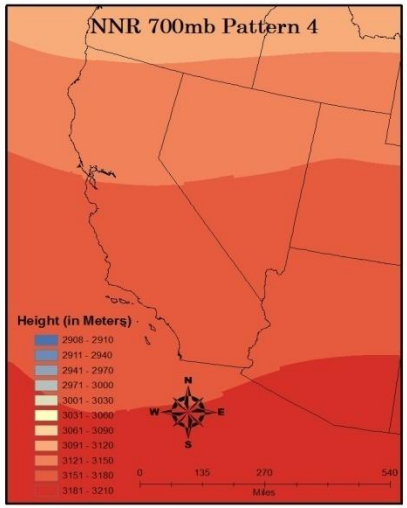

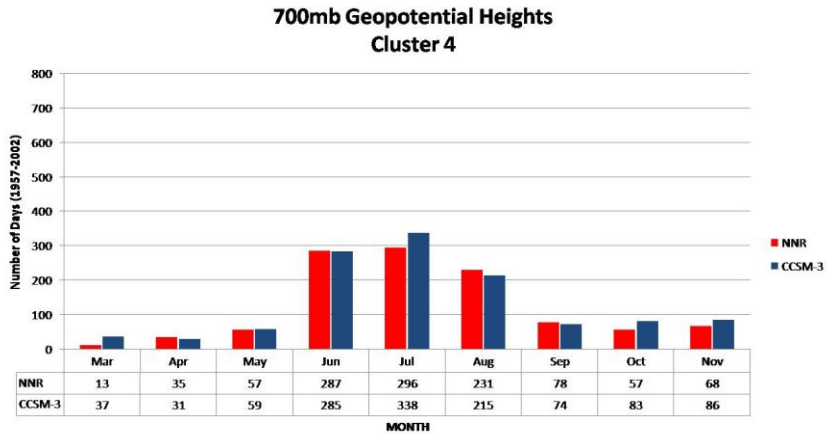

	Mar	Apr	May	Jun	Jul	Aug	Sep	Oct	Nov
NNR	13	35	57	287	296	231	78	57	68
CCSM-3	37	31	59	285	338	215	74	83	86

Figure 6 – Continued.

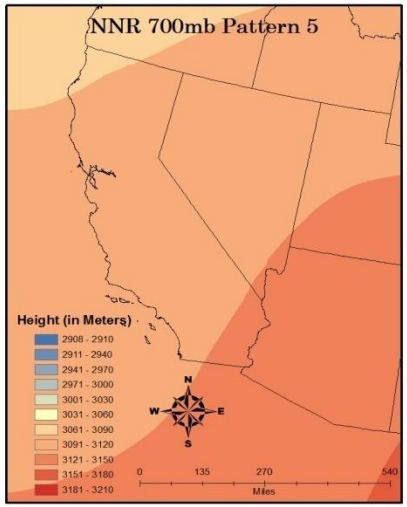

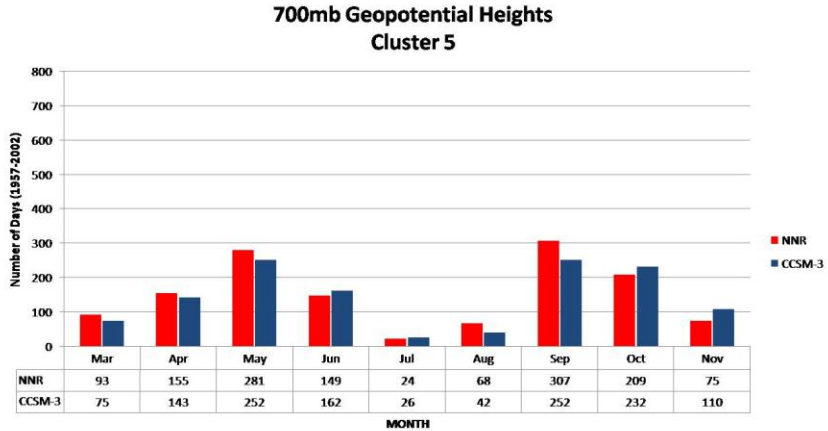

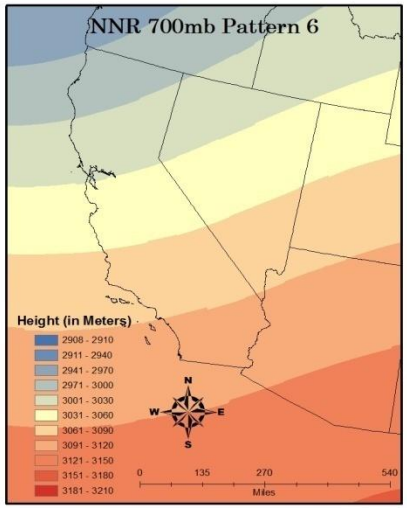

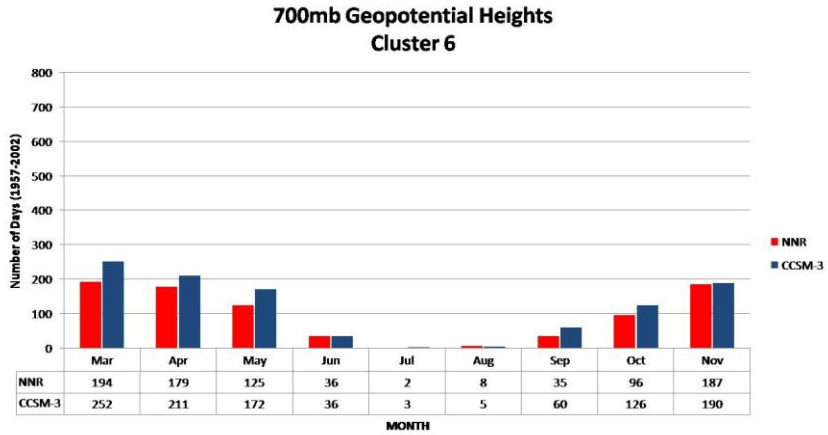

Figure 6 – Continued.

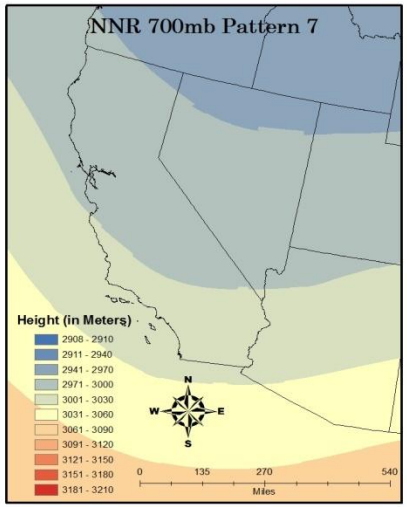

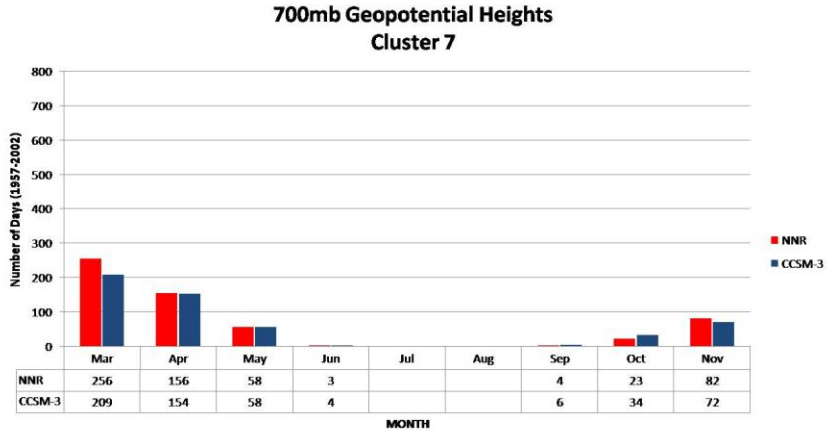

	Mar	Apr	May	Jun	Jul	Aug	Sep	Oct	Nov
NNR	256	156	58	3			4	23	82
CCSM-3	209	154	58	4			6	34	72

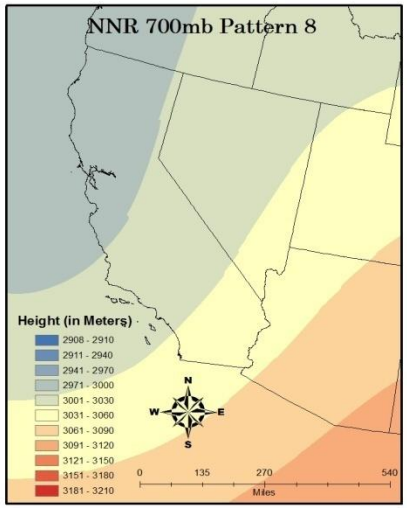

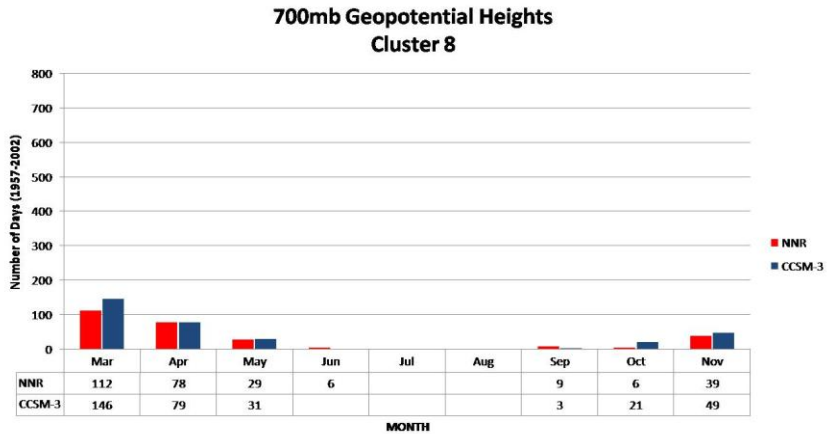

	Mar	Apr	May	Jun	Jul	Aug	Sep	Oct	Nov
NNR	112	78	29	6			9	6	39
CCSM-3	146	79	31				3	21	49

Figure 6 – Continued.

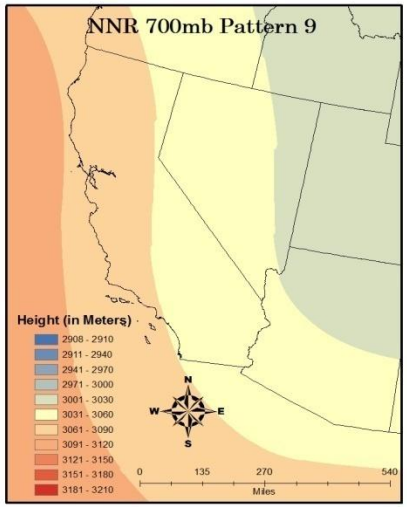

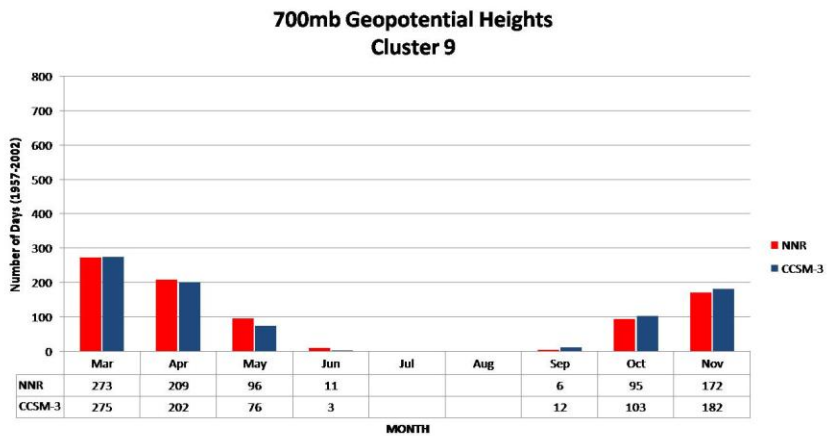

	Mar	Apr	May	Jun	Jul	Aug	Sep	Oct	Nov
NNR	273	209	96	11			6	95	172
CCSM-3	275	202	76	3			12	103	182

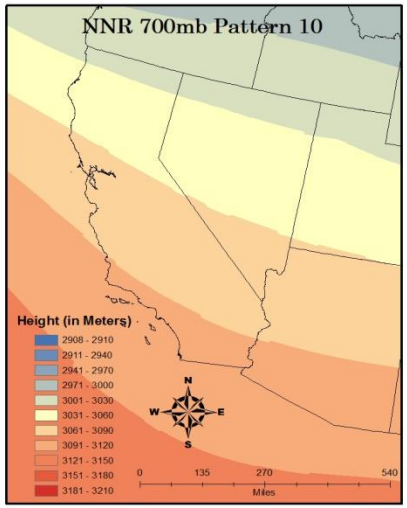

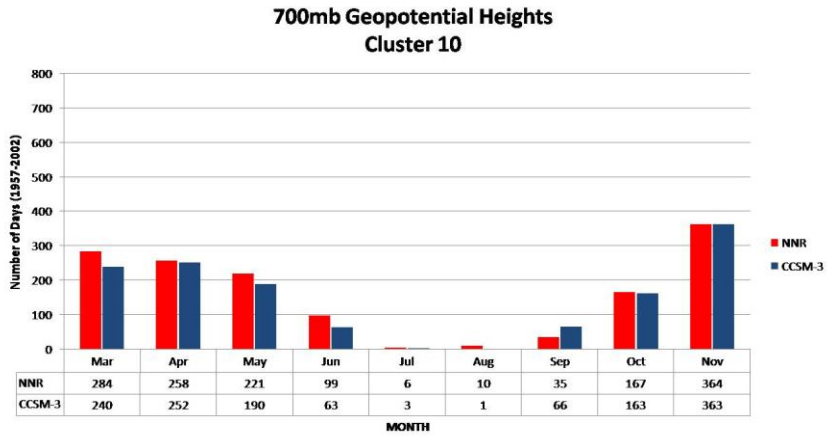

	Mar	Apr	May	Jun	Jul	Aug	Sep	Oct	Nov
NNR	284	258	221	99	6	10	35	167	364
CCSM-3	240	252	190	63	3	1	66	163	363

Figure 6 – Continued.

3.1.3 – 850-mb temperature clusters (850t)

In contrast to the two previous levels using geopotential height data, the 850mb level temperature patterns showed a bit more breadth in their seasonality with six different patterns occurring at least 10% of the entire warm season (Figure 7). Four different 850t patterns occur at least 10% of days in July and August. Of those four, pattern 10 occurred the most often in those months at nearly 44% of the time. Much like the warmer patterns at the other two levels, pattern 10 features a strong ridge over Arizona and New Mexico, extending westward into extreme southeastern California before heights begin falling moving northwestward through the state. Flanking the heart of summer, pattern 10 also occurred over 18% of the time in June and September before dropping off substantially in frequency deeper into both the spring and autumn. Overall this pattern occurred 14.8% of the warm season.

Pattern 8 was the next most frequent summer pattern, occurring over 22% of the time in July and August; and 11.3% of all days. Pattern 8 is shaped similarly to pattern 10 with the warmest temperatures in the Desert Southwest, although these temperatures do not reach as far west as in pattern 10, and comparatively, decline more rapidly towards the northwest. Pattern 8 has an early summer peak, occurring most often in June and July before declining steadily through October.

Although the warmest temperatures in pattern 7 reach the farthest west of any 850t pattern, overall these temperatures are not as hot compared to the previous two 850t patterns. Overall, pattern 7 occurred about 16% of the time in July and August before actually peaking in September and dropping off again in October. Throughout the nine-month time period, pattern 7 occurred less than 8% of the time.

Pattern 4 was the only other pattern to occur often in summer. Although it did occur on 13.6% of July and August days, this pattern tended to concentrate in late-spring and early-autumn with dual peaks in June and September. Highlighted by a deep thermal trough running just west of the coastline, pattern 4 is much cooler than the previous three summer-oriented patterns and occurred fairly steadily from May through October – peaking in September. Together these four 850t patterns (patterns 10, 8, 7 and 4) combine to account for over 96% of July and August days.

Of the remaining six patterns, most shared a shoulder month seasonality, peaking in March and again in November, suggesting that they might represent winter patterns that occasionally occur in late autumn and early spring. Exceptions to this seasonality at the 850t level were

patterns 3 and 9. Pattern 3 peaked in May and June before tailing off in frequency over the summer and then re-emerging in the early autumn. Overall, pattern 3 occurred 11% of the warm-season and is highlighted by sharp temperature gradients from west to east and a thermal high over New Mexico. Comparatively, pattern 9 was a distinctly autumn-dominant pattern, occurring in September (12.7%), October (30.5%) and November (11.9%) more often than it did in any other month. Featuring a more zonal temperature gradient across California, pattern 9 occurred 9.5% of the time overall.

Not unexpectedly, closer to the surface, gradients increase within these categories. Thus, the 850mb conditions varied more greatly than those at higher altitudes. They also better represent the true cores of summer heat conditions since they represent situations that exist more closely to the population.

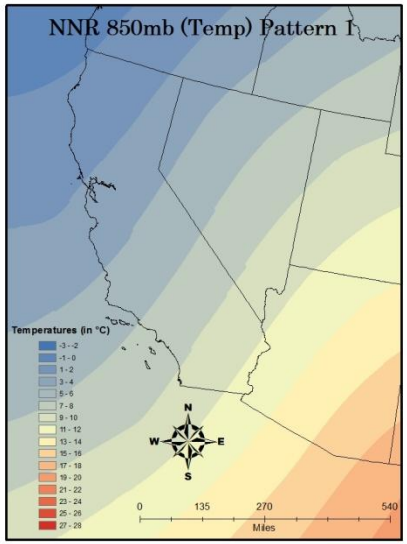

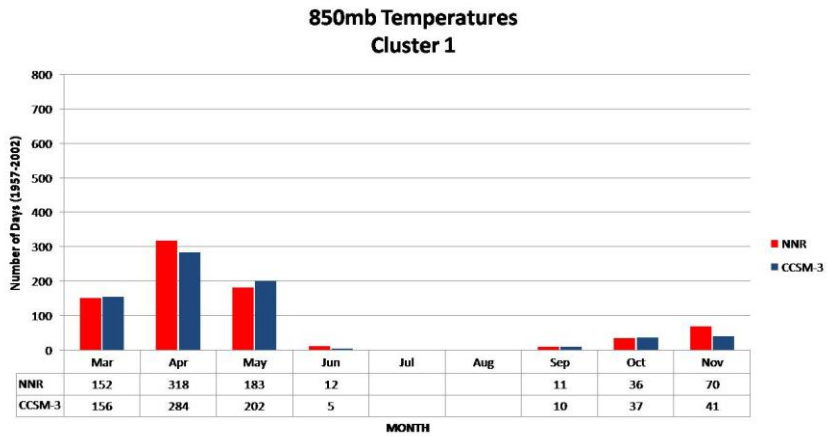

	Mar	Apr	May	Jun	Jul	Aug	Sep	Oct	Nov
NNR	152	318	183	12			11	36	70
CCSM-3	156	284	202	5			10	37	41

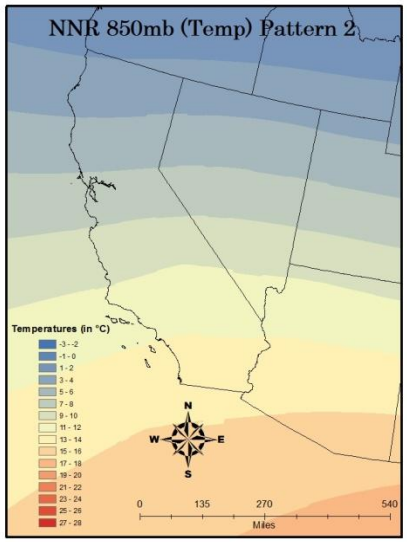

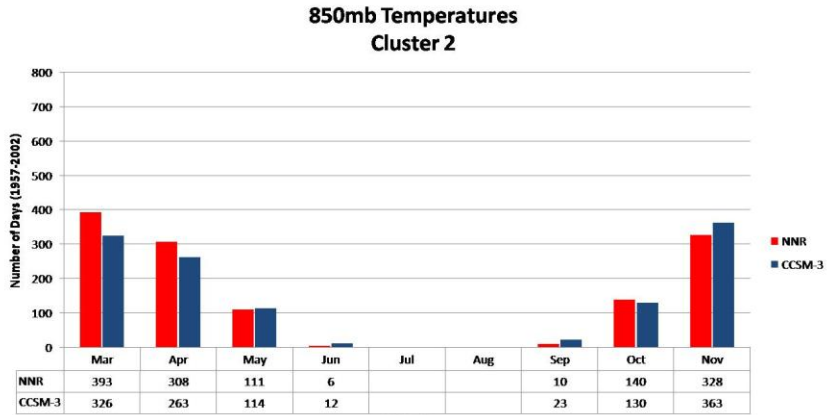

	Mar	Apr	May	Jun	Jul	Aug	Sep	Oct	Nov
NNR	393	308	111	6			10	140	328
CCSM-3	326	263	114	12			23	130	363

Figure 7 – Patterns of 850mb temperatures (left) and monthly frequency of each pattern (right) from 1957-2002. Continued on the following page.

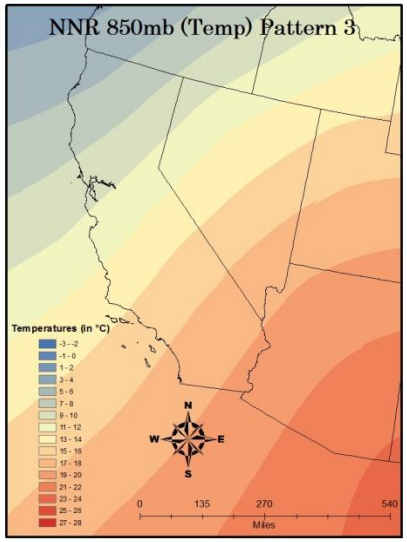

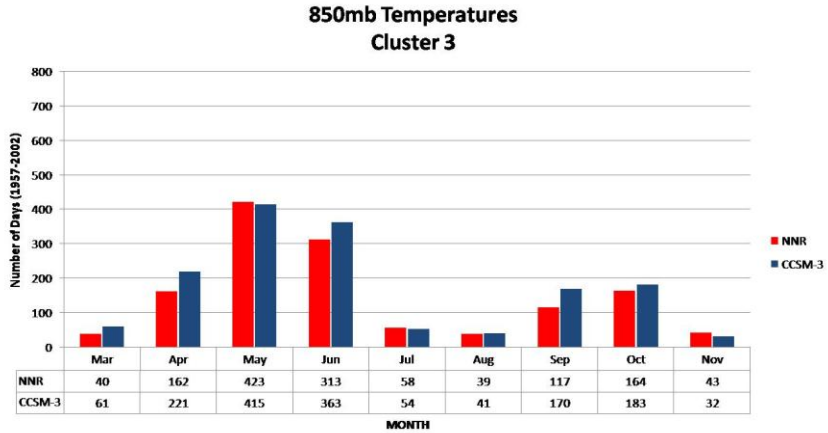

	Mar	Apr	May	Jun	Jul	Aug	Sep	Oct	Nov
NNR	40	162	423	313	58	39	117	164	43
CCSM-3	61	221	415	363	54	41	170	183	32

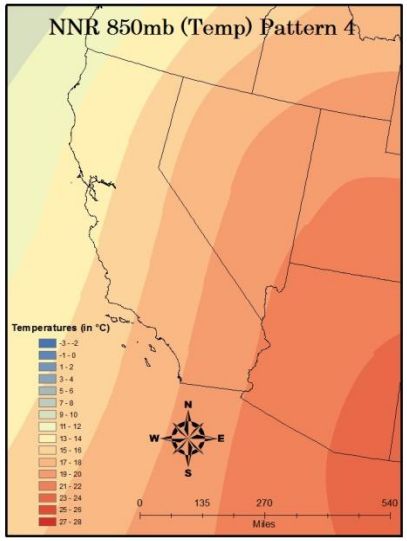

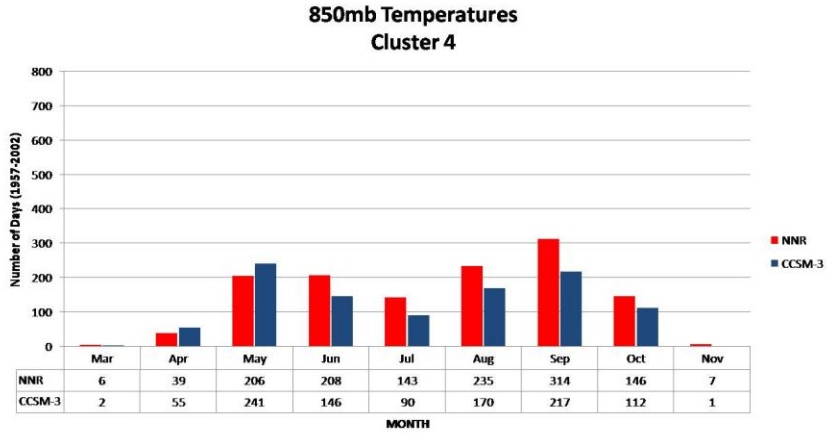

	Mar	Apr	May	Jun	Jul	Aug	Sep	Oct	Nov
NNR	6	39	206	208	143	235	314	146	7
CCSM-3	2	55	241	146	90	170	217	112	1

Figure 7 – Continued.

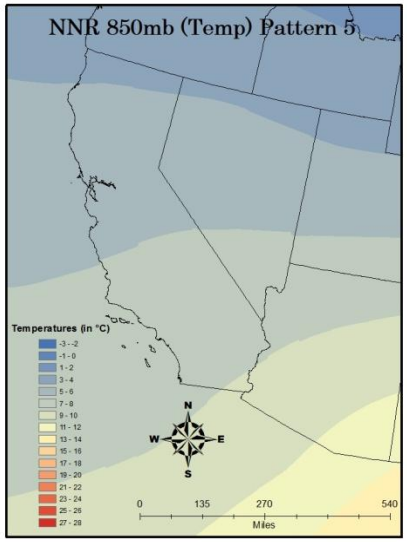

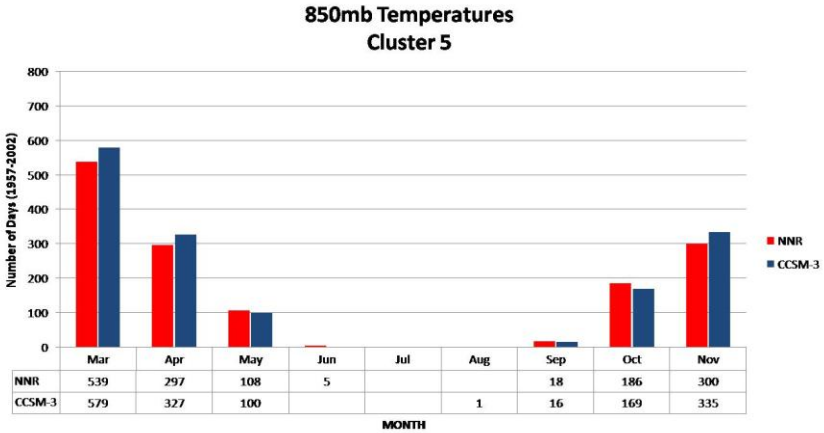

	Mar	Apr	May	Jun	Jul	Aug	Sep	Oct	Nov
NNR	539	297	108	5			18	186	300
CCSM-3	579	327	100			1	16	169	335

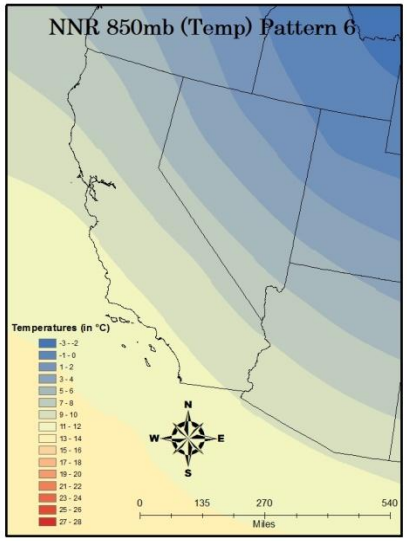

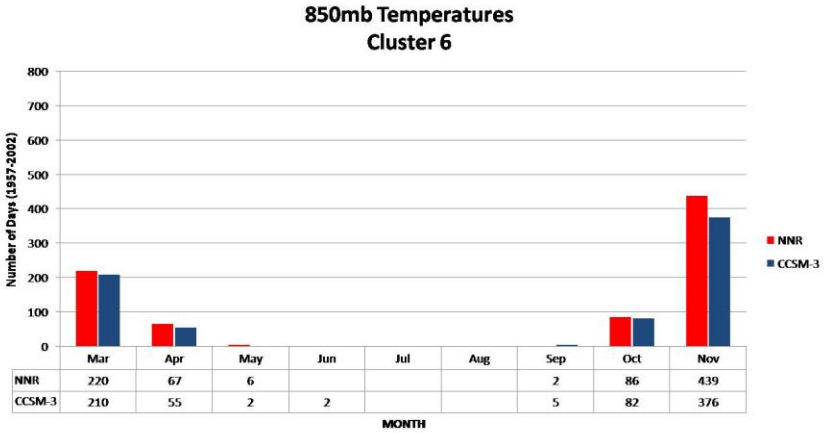

	Mar	Apr	May	Jun	Jul	Aug	Sep	Oct	Nov
NNR	220	67	6				2	86	439
CCSM-3	210	55	2	2			5	82	376

Figure 7 – Continued.

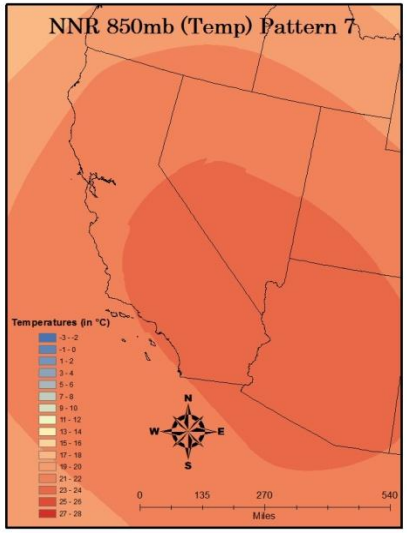

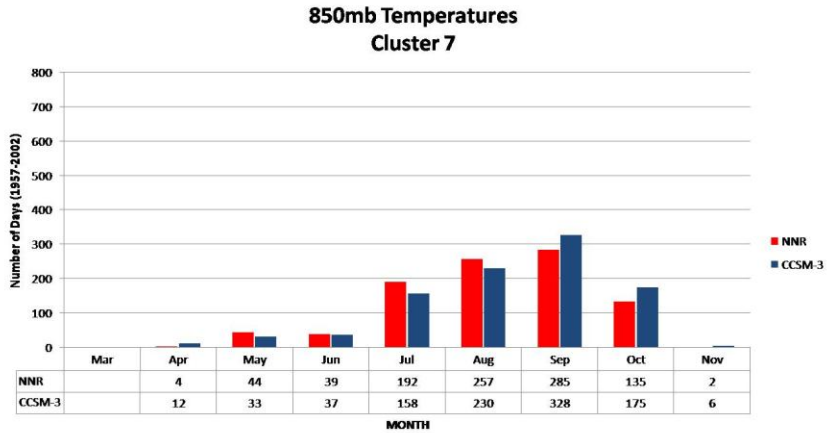

	Mar	Apr	May	Jun	Jul	Aug	Sep	Oct	Nov
NNR		4	44	39	192	257	285	135	2
CCSM-3		12	33	37	158	230	328	175	6

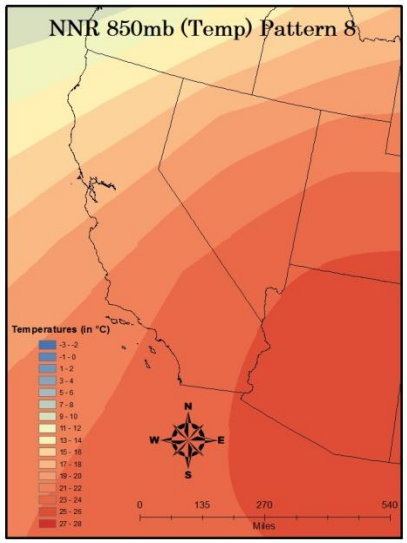

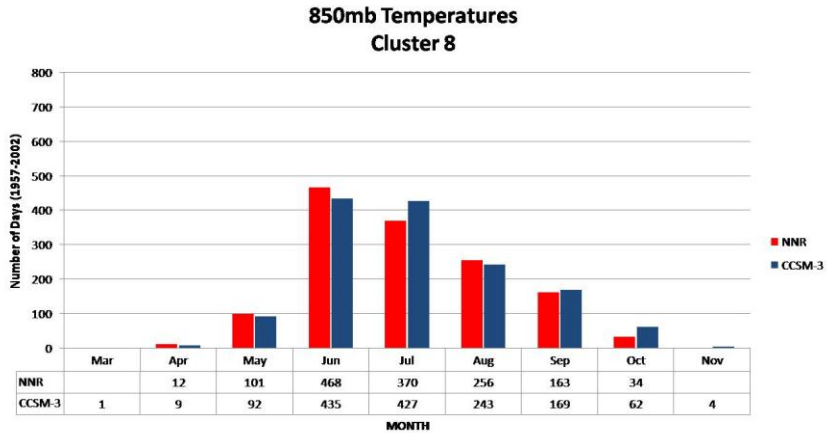

	Mar	Apr	May	Jun	Jul	Aug	Sep	Oct	Nov
NNR		12	101	468	370	256	163	34	
CCSM-3	1	9	92	435	427	243	169	62	4

Figure 7 – Continued.

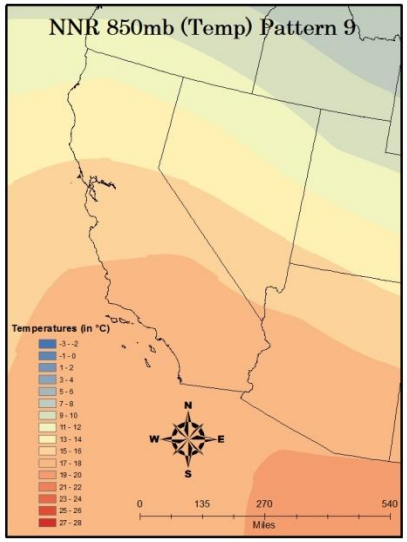

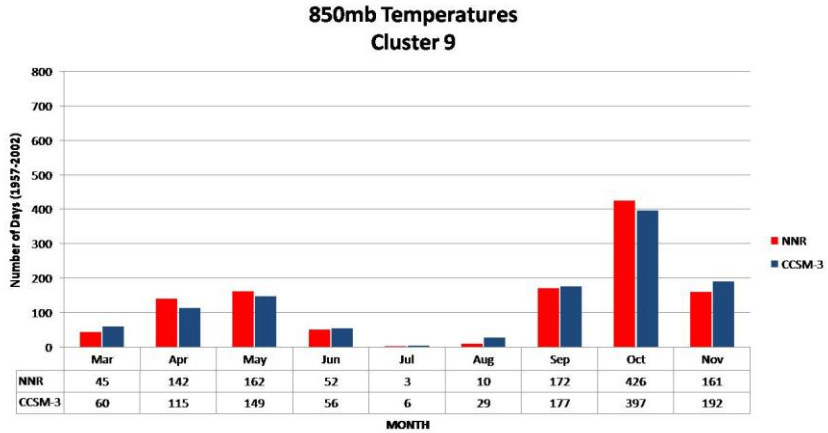

	Mar	Apr	May	Jun	Jul	Aug	Sep	Oct	Nov
NNR	45	142	162	52	3	10	172	426	161
CCSM-3	60	115	149	56	6	29	177	397	192

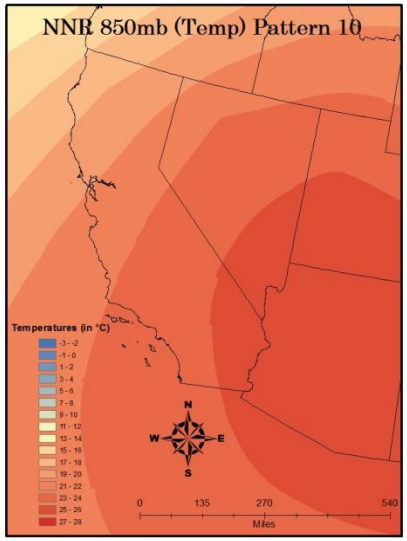

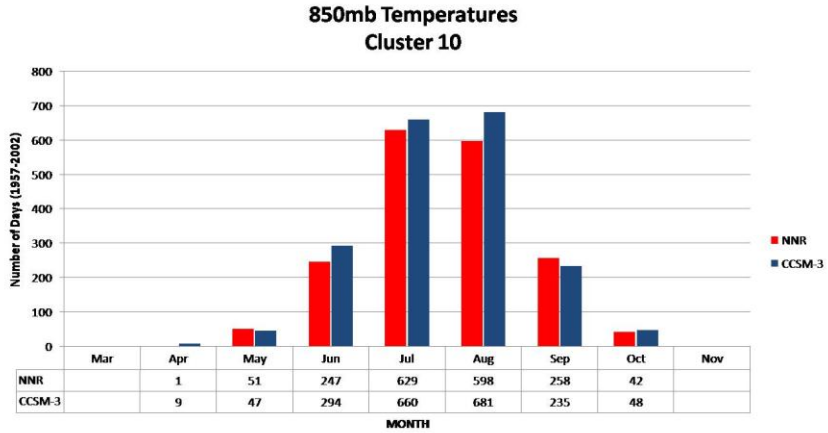

	Mar	Apr	May	Jun	Jul	Aug	Sep	Oct	Nov
NNR		1	51	247	629	598	258	42	
CCSM-3		9	47	294	660	681	235	48	

Figure 7 – Continued.

3.2 – Future Circulation Type Frequencies

There are important changes in the upper level patterns based on modeled results for the 2050s and 2090s. Some patterns that historically occurred in summer have shift seasons. Others become more dominant in summer (Figures 8 through 10).

This shift is readily apparent in the 500mb patterns (Figure 8). Pattern 5, which is predominantly summer-oriented at present, is no longer so in any of the models for the mid- or late-2000s. In both the 2050s and 2090s, pattern 5 is predominantly found in the spring, with a secondary peak in autumn. While pattern 5 presently exhibits the greatest frequency in June, the peak is shifted one month sooner and occurs between 20-40 percent of the time in May during future decades. The B1 scenario, which assumes more stringent CO_2 emissions controls, best resembles the present among all the models, but still peaks in May during future decades.

Patterns 8 and 9, which represent the two other predominant summer 500mb patterns at present, also show important changes in frequency and seasonality in the GCM data. Pattern 8 is the pre-eminent summer pattern today, but decreases in frequency during the 2050s and 2090s. Pattern 9 becomes the most common summer pattern for the future decades, particularly for the 2090s, where it occurs over 90 percent of the time during peak summer months based on the "business as usual" scenario A1FI. Again, not surprisingly, the B1 scenario shows the greatest similarity to present conditions, and under these conditions, pattern 8 predominates in late summer, while pattern 9 is most important during early summer.

There are some important shifts at 700mb as well (Figure 9). Pattern 3 is no longer a predominant summer classification during either the 2050s or 2090s, and gains influence in spring, particularly May (at present, it is most frequent in June). Under the A1FI scenario, this pattern shows a particular predominance in spring, while in the B1 scenario, the pattern exhibits a strong secondary peak in fall, almost as large as the spring mode. Nevertheless, for all future models, pattern 3 becomes almost nonexistent in July and August. There is also a shift in patterns 1 and 4, the two remaining summer patterns at 700mb. In the 20th Century, pattern 1 is clearly the most important summer category, particularly in July and August, with more than twice the frequency of pattern 4. During both the 2050s and 2090s, however, pattern 4 becomes much more important, particularly for the A1FI scenario. With more emissions controls, pattern 4 becomes less common and pattern 1 re-emerges as most important, particularly for the B1 scenario.

At the 850mb level, there are four patterns that are quite frequent in summer: 4, 7, 8, and 10 (Figure 10). Pattern 4 presently shows a slight shoulder season peak, and this is exacerbated during the decades of the 2050s and 2090s. By the latter half of the 21st Century, pattern 4 becomes quite rare in summer, and by the 2090s is most common in May and October.

At present, pattern 7 predominates in late summer and pattern 8 is most common in early summer. The A1FI run shows pattern 7 peaking in August, while the more environmentally conscious B1 model run indicates a peak in September. The summer frequency of pattern 8 decreases through the 21st century. By 2090, pattern 8 occurs about 40-50 percent of the time in June and almost disappears by August, making this pattern a late spring dominant pattern.

Pattern 10 becomes the most important 850mb pattern during the latter decades, increasing in frequency by over 30 percent for the business-as-usual (A1FI) model run. This pattern, demonstrating a strong ridge over the Desert Southwest, is undoubtedly associated with exceedingly hot conditions over Arizona and most of California. Under the A1FI scenario, it can occur on up to 80 percent of the days during a typical summer, thus suggesting a large increase in the frequency of excessive heat in this region.

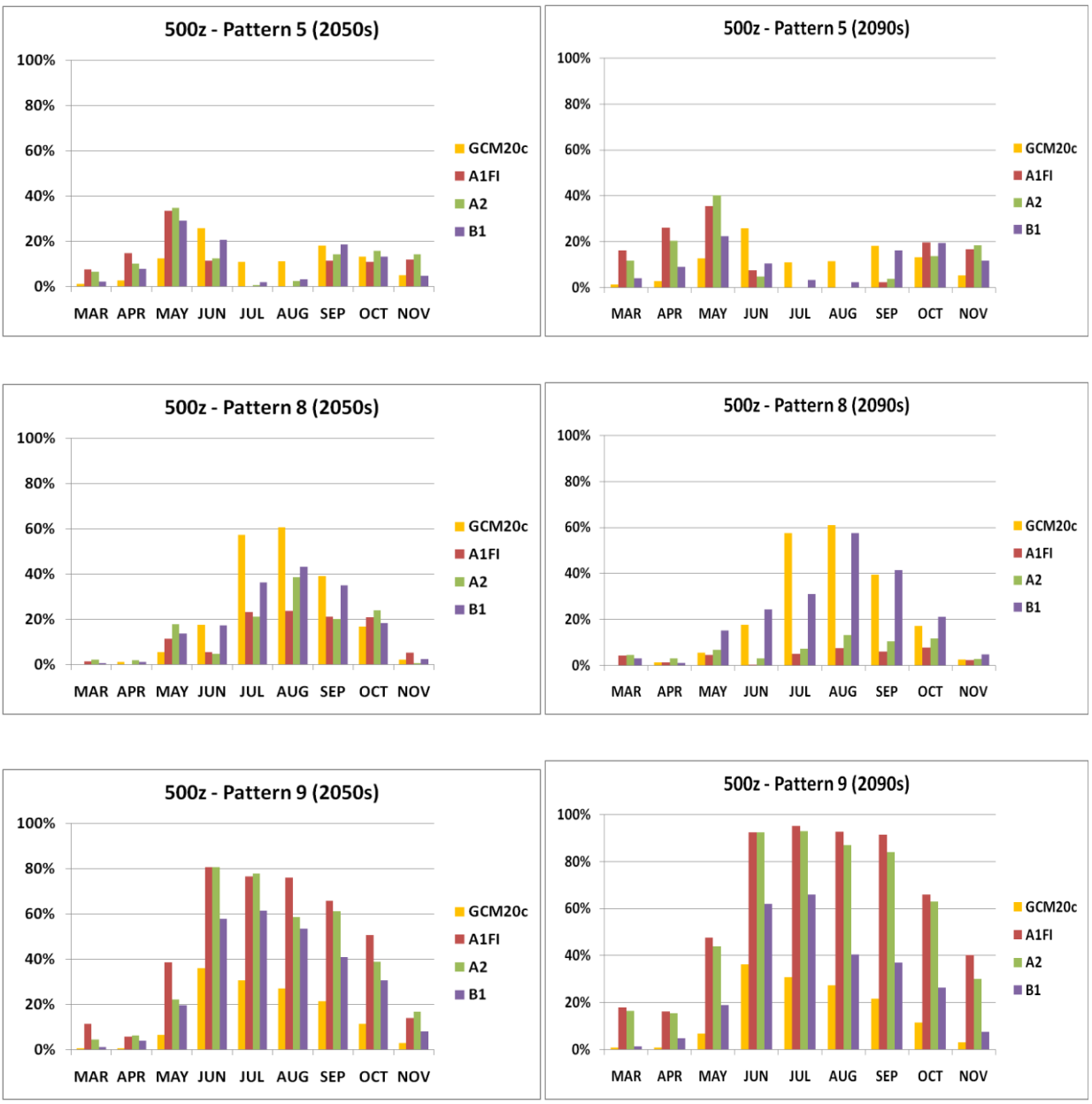

Figure 8 – Monthly frequency of selected summer 500z circulation patterns in the 2050s (left) and 2090s (right).

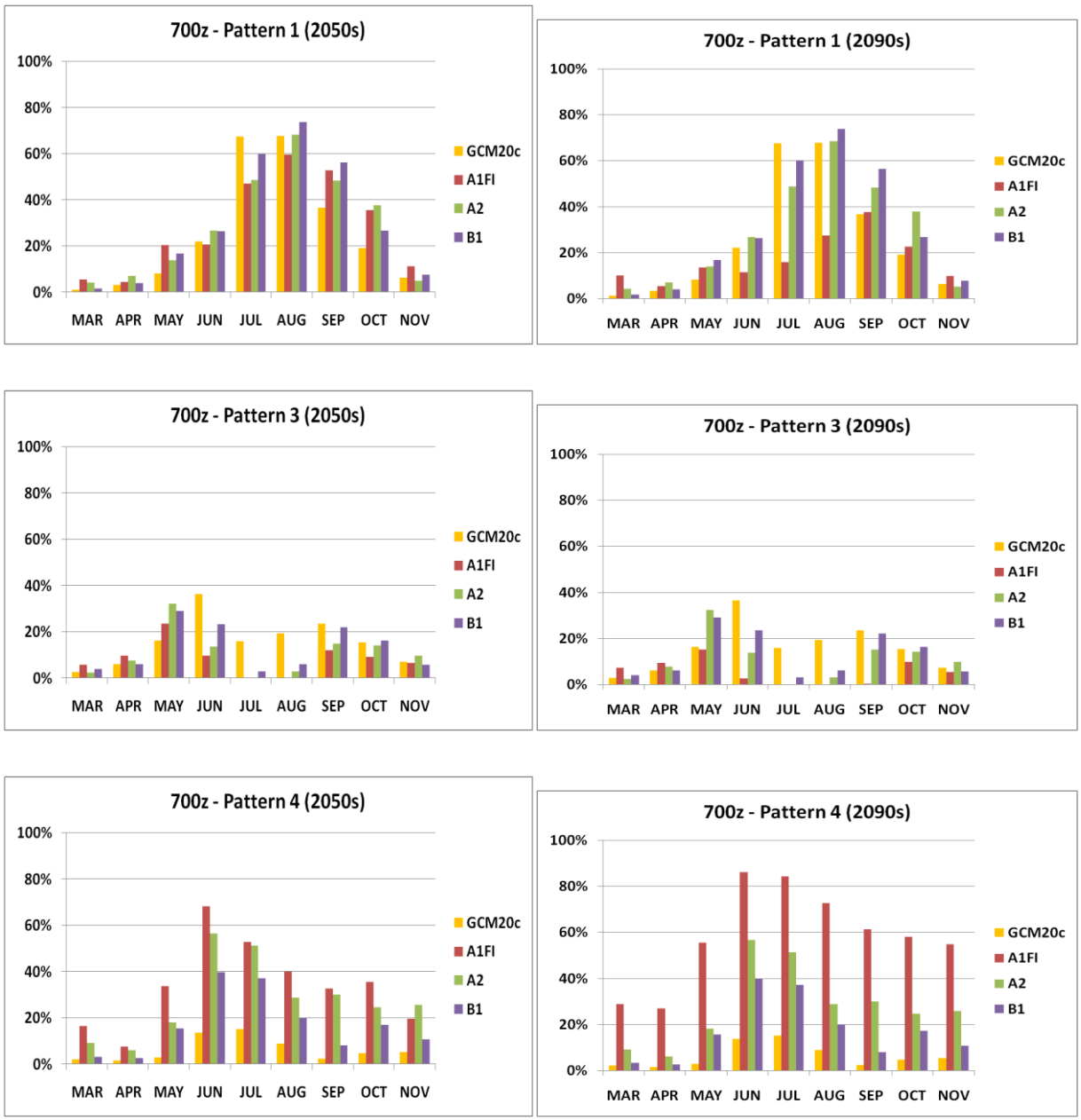

Figure 9 – Monthly frequency of selected summer 700z circulation patterns in the 2050s (left) and 2090s (right).

Figure 10 – Monthly frequency of selected summer 850t circulation patterns in the 2050s (left) and 2090s (right).

3.3 – Present and Future Weather Type Frequencies

An evaluation of seasonal frequencies and biases (for the entire March through November period) shows that both the CCSM3 and CGCM3 models duplicate reality with reasonable accuracy, which helps validate the future weather type frequency estimates (Tables 6 and 7). Comparing the actual average seasonal frequencies with the NNR and GCM20c models shows that rarely are they more than 5 percent apart. In one or two cases, there are some diverging values (e.g. El Toro DM frequencies for all models), but well over 50 percent of the values are within +/– 3 percent of the observed historical frequency. Chi-square tests on the annual mean frequency of SSC types show no statistically significant differences between the NNR and GCM20c frequencies, for either CGCM3 or CCSM3. Statistically significant differences occur between the observed SSC frequencies and both models' GCM20c output at the three coastal locations, and for Riverside for the CCSM3 only. When examining the statistical differences by SSC type (yellow boxes in Tables 6 and 7), the majority of the cases in which differences are observed are the polar weather types, especially MP. Given the interest in this research is the frequency of tropical weather types, these differences are more critical. Only several differences emerge: at Miramar, the NNR and both GCMs systematically underrepresent MT ($p=.02$ to $p=.05$); the CGCM3 overrepresents DT at Miramar ($p = .048$), and the CCSM3 underrepresents DT at both Riverside ($p = .022$) and El Toro ($p = .014$).

California covers a broad range of climates, which makes it no surprise that weather type frequencies vary considerably among the locales evaluated in this study (Figures 11 through 16). Dry tropical (DT) air dominates the summer situation in Fresno, Riverside, and Sacramento, while moist tropical (MT) air increases in frequency at Miramar (San Diego), Mountain View (Bay Area), and El Toro (Los Angeles). In northern California, MT air has a decidedly spring proclivity, especially at Mountain View. However, in southern California, which is influenced somewhat by the late-summer "Southwest Monsoon," MT frequencies are biased toward the fall, particularly at Miramar – the southernmost SSC station used in this research.

The frequencies of these two "oppressive" weather types, which are most commonly associated with heat-related deaths, will change dramatically if the models for future decades are correct. For example, in Fresno, the summer DT weather type will be almost totally predominant, reaching frequencies of over 80 percent during both the 2050s and 2090s under all three scenarios in the CCSM3 model. For the business as usual A1FI scenario, DT will approach 100 percent frequency. Although the results are less dramatic for the CGCM3 model runs, DT will make up nearly 2/3 of all summer days in Fresno in the 2050s and about 80 percent of the days in the 2090s. MT is already rare in Fresno during summer and will remain that way under all scenarios. However, there are indications that MT frequencies will increase

rather sharply during early spring, with projected frequency as high as 35 percent of March days in the 2090s in the CCSM3 A1FI scenario.

At Miramar, summer DT weather type frequency will likely remain low as indicated by all the model scenarios, although late spring frequencies will potentially more than double to nearly 30 to 40 percent of days by the 2090s. However, the Southwest Monsoon effect is estimated to greatly increase, as indicated by the large increase in frequency of MT days in both models. Under CCSM3, all scenarios show a greater-than-double present-day frequency for MT in the August through October period, approaching and exceeding 60 percent in September in the 2050s, and near or above 80 percent in September during the 2090s. These numbers in the 2090s represent a tripling or more of MT frequency, particularly for A1FI. Although less dramatic, even the CGCM3 numbers indicate a substantial increase in autumn frequency of MT days. Although the greatest occurrences of MT will still be in the fall, both future scenarios indicate a sharp increase in spring frequencies as well.

Mountain View, another locale with more MT than DT days at present, will also show increases in DT and MT frequency, particularly in early summer MT days. DT frequencies are only indicated to rise slightly, but May and June MT days are shown to rise much more dramatically. For example, in June at present, MT occurs about 10 percent of all days in an average summer. This number will rise to near 40 percent for all scenarios in the 2050s (CCSM3), and to about 50 percent under A1FI and A2. Although virtually no MT occurs in Mountain View presently in summer, it will occur with some frequency in the 2090s, particularly under CCSM3 model runs, where its springtime occurrence extends into early summer in the A1FI scenarios (55 percent in June, 21 percent in July).

El Toro conditions are projected to change dramatically under all three scenarios. DT takes on a strong double modal appearance for both CCSM3 and CGCM3, increasing dramatically in October and November (and in early spring as well in CGCM3), to frequencies as high as 25 percent. But the greatest increases will be in the MT weather type, which will also demonstrate a strong dual modal appearance. September MT frequency will skyrocket, particularly in the 2090s, to as much as 80 percent of days in the A1FI scenario, in comparison to less than 10 percent of days today. Summer MT frequencies will also increase dramatically under CGCM3, and the peak will be earlier in the summer, particularly in the 2090s.

Riverside is already dominated by the DT weather type in all seasons, particularly midsummer. This will only increase, with frequencies reaching and exceeding 80 percent of the days in June and July. The greatest percentage increases in DT frequencies will be in early summer. MT days will also show some sizable increases, particularly in late summer and fall, where in the

more extreme scenarios it exceeds 20 percent of days, but will remain a rather rare weather type as compared to DT.

Sacramento will show a similar pattern to Fresno, with sharp increases in DT presence during the late summer, to frequencies exceeding 80 percent of days for CCSM3 A1FI and A2. However, CCSM3 also indicates a very rapid upturn in MT air in spring, particularly in April, with frequencies approaching 60 percent of days by the 2090s. Sacramento demonstrates what all the cities seem to show: expected very large increases in one or both of the offensive weather types. The seasonal extent in which these weather types are common will be broadened at virtually all locales. MT will become quite predominant in coastal areas, while DT will occur more predominately in inland locations.

Table 6 – Weather type frequency (and model bias) for each SSC station. Historical weather type frequencies based off of 1960-1999 averages. Future weather type frequencies are based off of 2050-2059 (2050s) and 2090-2099 (2090s) averages in CCSM3. Boxes in yellow represent cases where the SSC type frequency is statistically significantly different from the observed weather type frequency ($p < .05$).

Station	SSC Type	ACTUAL AVG	CCSM3 20TH CENTURY AVG				CCSM3 - FUTURE					
			NNR	NNR MODEL BIAS	GCM20c	GCM20c MODEL BIAS	A1FI		A2		B1	
							2050s	2090s	2050s	2090s	2050s	2090s
Fresno	DM	50.8%	46.5%	-4.3%	46.8%	-4.0%	34.2%	27.0%	37.8%	32.2%	41.4%	43.1%
	DP	9.0%	11.3%	2.3%	11.7%	2.7%	3.0%	1.7%	5.6%	2.1%	7.0%	5.9%
	DT	30.5%	28.7%	-1.8%	27.6%	-2.8%	48.2%	54.6%	45.1%	54.5%	40.0%	39.9%
	MM	5.2%	5.1%	-0.1%	6.0%	0.8%	4.5%	3.5%	4.6%	3.2%	5.0%	4.9%
	MP	2.5%	6.0%	3.5%	4.9%	2.4%	1.8%	0.3%	2.4%	0.2%	3.5%	2.0%
	MT	2.0%	2.4%	0.4%	2.9%	0.9%	8.3%	12.9%	4.4%	7.8%	3.1%	4.2%
Miramar	DM	54.3%	53.7%	-0.5%	53.7%	-0.6%	38.2%	24.8%	44.1%	28.2%	47.8%	44.7%
	DP	2.2%	7.2%	4.9%	7.2%	4.9%	2.2%	0.5%	2.9%	0.4%	5.6%	2.7%
	DT	6.5%	9.3%	2.7%	10.0%	3.5%	15.8%	21.3%	15.7%	23.7%	12.6%	13.6%
	MM	14.5%	12.2%	-2.3%	12.8%	-1.7%	10.5%	8.7%	10.0%	7.3%	9.8%	11.1%
	MP	6.6%	7.1%	0.5%	6.6%	0.0%	1.3%	0.4%	1.9%	0.3%	3.4%	3.4%
	MT	15.9%	10.6%	-5.3%	9.7%	-6.2%	32.0%	44.3%	25.5%	40.0%	20.8%	24.5%
Mountain View	DM	55.1%	59.1%	4.0%	54.4%	-0.7%	43.9%	28.3%	49.0%	33.3%	50.8%	47.4%
	DP	1.6%	5.2%	3.6%	5.0%	3.4%	0.8%	0.2%	2.3%	0.3%	3.7%	2.2%
	DT	7.6%	10.5%	2.8%	11.1%	3.5%	13.3%	18.8%	13.2%	20.8%	12.1%	14.4%
	MM	16.8%	12.0%	-4.8%	14.2%	-2.6%	21.8%	19.2%	18.3%	18.5%	16.8%	19.5%
	MP	10.9%	4.5%	-6.4%	6.1%	-4.8%	1.6%	0.3%	1.6%	0.2%	2.9%	1.8%
	MT	8.0%	8.8%	0.8%	9.1%	1.1%	18.6%	33.3%	15.5%	27.0%	13.6%	14.6%
El Toro	DM	50.4%	67.7%	17.4%	66.1%	15.8%	57.1%	41.5%	57.0%	42.1%	63.4%	59.9%
	DP	2.4%	1.1%	-1.3%	1.3%	-1.1%	0.3%	0.2%	0.6%	0.0%	0.6%	0.4%
	DT	10.8%	7.2%	-3.6%	7.7%	-3.1%	10.3%	15.1%	12.7%	16.6%	10.5%	10.3%
	MM	15.7%	11.9%	-3.9%	13.6%	-2.1%	7.4%	5.5%	9.1%	4.6%	8.8%	9.7%
	MP	6.8%	3.1%	-3.7%	3.4%	-3.4%	0.8%	0.3%	0.8%	0.2%	2.3%	1.1%
	MT	13.9%	9.1%	-4.8%	7.8%	-6.0%	24.1%	37.4%	19.8%	36.5%	14.4%	18.5%
Riverside	DM	36.5%	34.6%	-1.9%	33.7%	-2.8%	24.0%	17.7%	24.9%	19.2%	28.2%	27.8%
	DP	10.7%	12.0%	1.3%	11.7%	1.0%	3.5%	1.6%	5.5%	1.8%	7.5%	5.6%
	DT	29.7%	33.1%	3.4%	33.0%	3.3%	55.4%	62.3%	52.9%	63.4%	45.1%	47.7%
	MM	9.9%	7.9%	-2.0%	9.8%	-0.2%	6.6%	4.7%	6.7%	4.1%	7.4%	8.8%
	MP	3.6%	6.4%	2.9%	7.0%	3.4%	1.7%	0.3%	2.1%	0.4%	4.4%	2.9%
	MT	9.5%	5.9%	-3.6%	4.8%	-4.7%	8.9%	13.4%	7.8%	10.9%	7.3%	7.1%
Sacramento	DM	58.2%	53.1%	-5.1%	54.8%	-3.4%	34.6%	21.1%	40.3%	26.8%	46.5%	45.5%
	DP	6.8%	8.7%	1.9%	8.9%	2.2%	2.3%	1.0%	4.0%	1.5%	4.2%	4.0%
	DT	20.9%	19.9%	-1.0%	18.3%	-2.6%	36.4%	42.8%	33.3%	42.7%	29.3%	30.1%
	MM	7.1%	8.0%	1.0%	9.1%	2.1%	11.0%	12.1%	9.7%	9.0%	9.5%	9.6%
	MP	5.3%	5.8%	0.5%	4.4%	-0.9%	1.7%	0.6%	2.6%	0.4%	3.2%	2.3%
	MT	1.8%	4.5%	2.8%	4.4%	2.7%	14.0%	22.4%	10.1%	19.5%	7.3%	8.5%

Table 7 – Weather type frequency (and model bias) for each SSC station. Historical weather type frequencies based off of 1970-1999 averages. Future weather type frequencies are based off of 2050-2059 (2050s) and 2090-2099 (2090s) averages in the CGCM3 global climate model. Boxes in yellow represent cases where the SSC type frequency is statistically significantly different from the observed weather type frequency ($p < .05$).

Station	SSC Type	ACTUAL AVG	CGCM3 20TH CENTURY AVG				CGCM3 - FUTURE			
			NNR	NNR MODEL BIAS	GCM20c	GCM20c MODEL BIAS	A2		B1	
							2050s	2090s	2050s	2090s
Fresno	DM	50.8%	46.3%	-4.5%	47.1%	-3.7%	42.2%	31.9%	43.0%	39.5%
	DP	9.0%	10.2%	1.2%	11.0%	2.0%	5.3%	2.2%	6.3%	4.2%
	DT	30.5%	29.1%	-1.4%	28.3%	-2.2%	41.2%	52.6%	37.7%	41.6%
	MM	5.2%	5.2%	0.0%	6.0%	0.8%	3.3%	3.3%	5.4%	6.5%
	MP	2.5%	5.8%	3.3%	4.6%	2.1%	2.3%	1.2%	2.4%	1.7%
	MT	2.0%	3.4%	1.4%	2.9%	0.9%	5.7%	8.8%	5.2%	6.5%
Miramar	DM	54.3%	55.3%	1.1%	54.9%	0.6%	45.5%	31.5%	50.8%	45.5%
	DP	2.2%	6.2%	4.0%	5.3%	3.1%	1.5%	0.5%	2.6%	2.1%
	DT	6.5%	10.1%	3.6%	10.8%	4.3%	17.9%	21.4%	16.6%	16.7%
	MM	14.5%	11.9%	-2.6%	11.5%	-3.0%	8.0%	4.9%	7.7%	8.1%
	MP	6.6%	6.7%	0.0%	7.3%	0.7%	3.1%	1.0%	3.2%	3.4%
	MT	15.9%	9.8%	-6.1%	10.2%	-5.7%	24.0%	40.6%	19.0%	24.2%
Mountain View	DM	55.1%	64.0%	8.9%	59.3%	4.2%	55.4%	51.2%	59.2%	54.6%
	DP	1.6%	3.7%	2.1%	3.3%	1.7%	1.0%	0.1%	0.7%	0.7%
	DT	7.6%	9.8%	2.2%	11.6%	4.0%	13.8%	15.6%	12.5%	13.3%
	MM	16.8%	10.6%	-6.2%	13.4%	-3.4%	14.4%	11.9%	12.6%	14.7%
	MP	10.9%	3.3%	-7.6%	4.3%	-6.6%	1.0%	0.1%	1.4%	0.5%
	MT	8.0%	8.6%	0.6%	8.1%	0.1%	14.3%	21.1%	13.6%	16.2%
El Toro	DM	50.4%	60.8%	10.4%	59.5%	9.1%	54.2%	41.5%	56.4%	54.6%
	DP	2.4%	3.8%	1.4%	3.8%	1.4%	1.2%	0.6%	1.5%	1.0%
	DT	10.8%	8.4%	-2.4%	8.8%	-2.0%	14.7%	18.7%	13.0%	14.1%
	MM	15.7%	12.3%	-3.4%	13.6%	-2.2%	8.0%	3.8%	8.0%	8.9%
	MP	6.8%	5.0%	-1.8%	4.9%	-1.9%	1.3%	0.3%	2.4%	1.8%
	MT	13.9%	9.7%	-4.2%	9.4%	-4.5%	20.6%	35.2%	18.7%	19.5%
Riverside	DM	36.5%	32.6%	-3.9%	32.3%	-4.2%	26.4%	20.3%	28.9%	25.2%
	DP	10.7%	12.2%	1.5%	11.5%	0.8%	5.4%	2.1%	6.8%	4.9%
	DT	29.7%	32.8%	3.1%	33.5%	3.8%	51.9%	63.2%	47.5%	51.6%
	MM	9.9%	9.5%	-0.5%	10.8%	0.8%	7.2%	5.1%	7.3%	9.1%
	MP	3.6%	5.9%	2.3%	6.4%	2.8%	2.2%	0.7%	3.2%	2.5%
	MT	9.5%	6.9%	-2.6%	5.5%	-4.0%	6.9%	8.7%	6.3%	6.7%
Sacramento	DM	58.2%	59.5%	1.2%	61.9%	3.6%	52.8%	41.2%	56.3%	52.1%
	DP	6.8%	7.6%	0.8%	6.9%	0.1%	2.6%	0.4%	3.7%	2.2%
	DT	20.9%	18.9%	-2.0%	18.0%	-2.9%	27.4%	37.4%	24.4%	27.8%
	MM	7.1%	7.0%	-0.1%	7.0%	0.0%	5.6%	6.6%	7.3%	8.5%
	MP	5.3%	4.2%	-1.0%	3.3%	-2.0%	2.1%	1.0%	2.2%	2.0%
	MT	1.8%	2.9%	1.1%	2.9%	1.2%	9.5%	13.4%	6.1%	7.4%

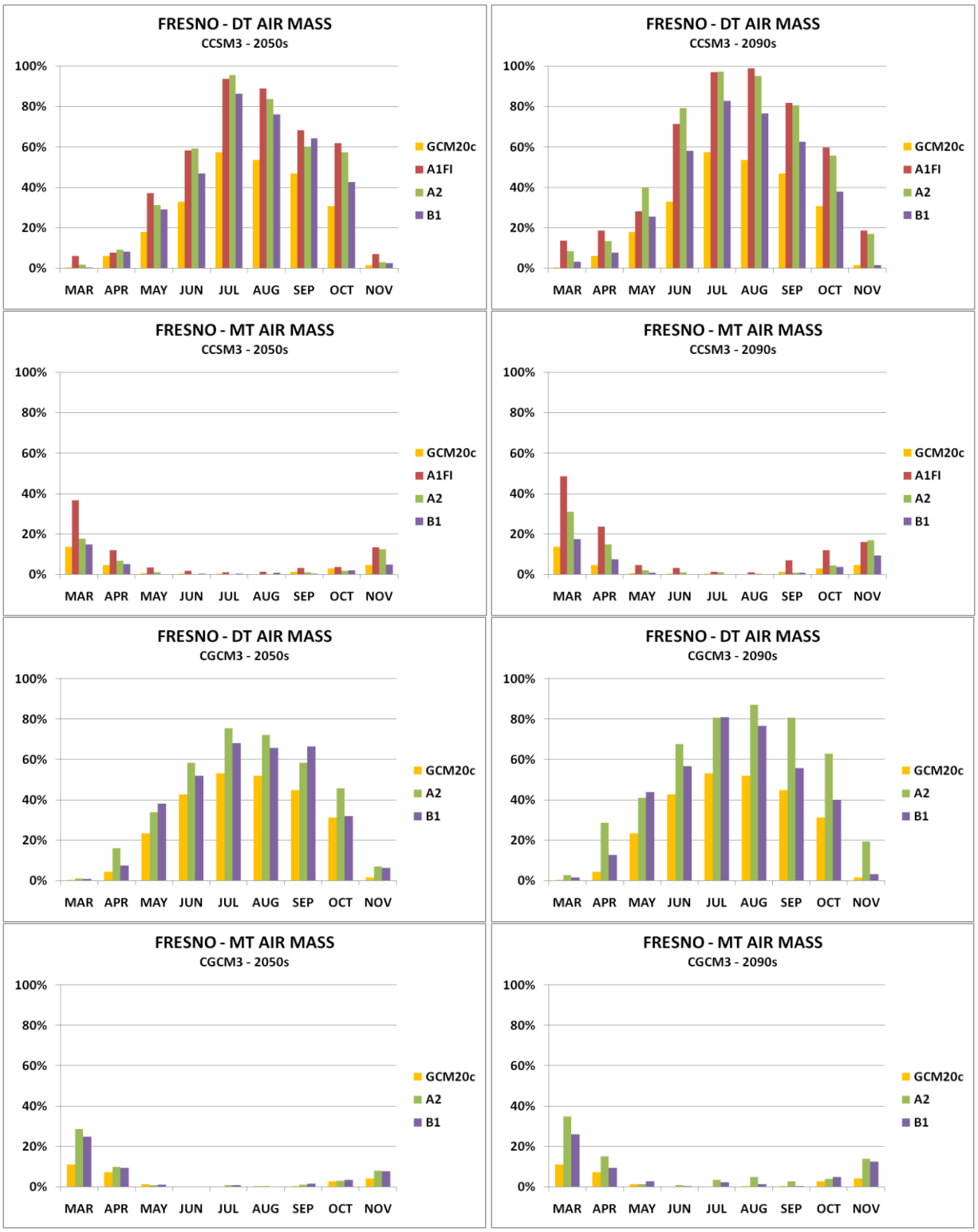

Figure 11 – Monthly frequency of the modeled DT and MT weather types at the Fresno SSC station in the 2050s (left) and the 2090s (right) in all scenarios of both the CCSM3 (top four graphs) and the CGCM3 (bottom four graphs) GCMs.

Figure 12 – Monthly frequency of the modeled DT and MT weather types at the Miramar SSC station in the 2050s (left) and the 2090s (right) in all scenarios of both the CCSM3 (top four graphs) and the CGCM3 (bottom four graphs) GCMs.

Figure 13 – Monthly frequency of the modeled DT and MT weather types at the Mountain View SSC station in the 2050s (left) and the 2090s (right) in all scenarios of both the CCSM3 (top four graphs) and the CGCM3 (bottom four graphs) GCMs.

Figure 14 – Monthly frequency of the modeled DT and MT weather types at the El Toro SSC station in the 2050s (left) and the 2090s (right) in all scenarios of both the CCSM3 (top four graphs) and the CGCM3 (bottom four graphs) GCMs.

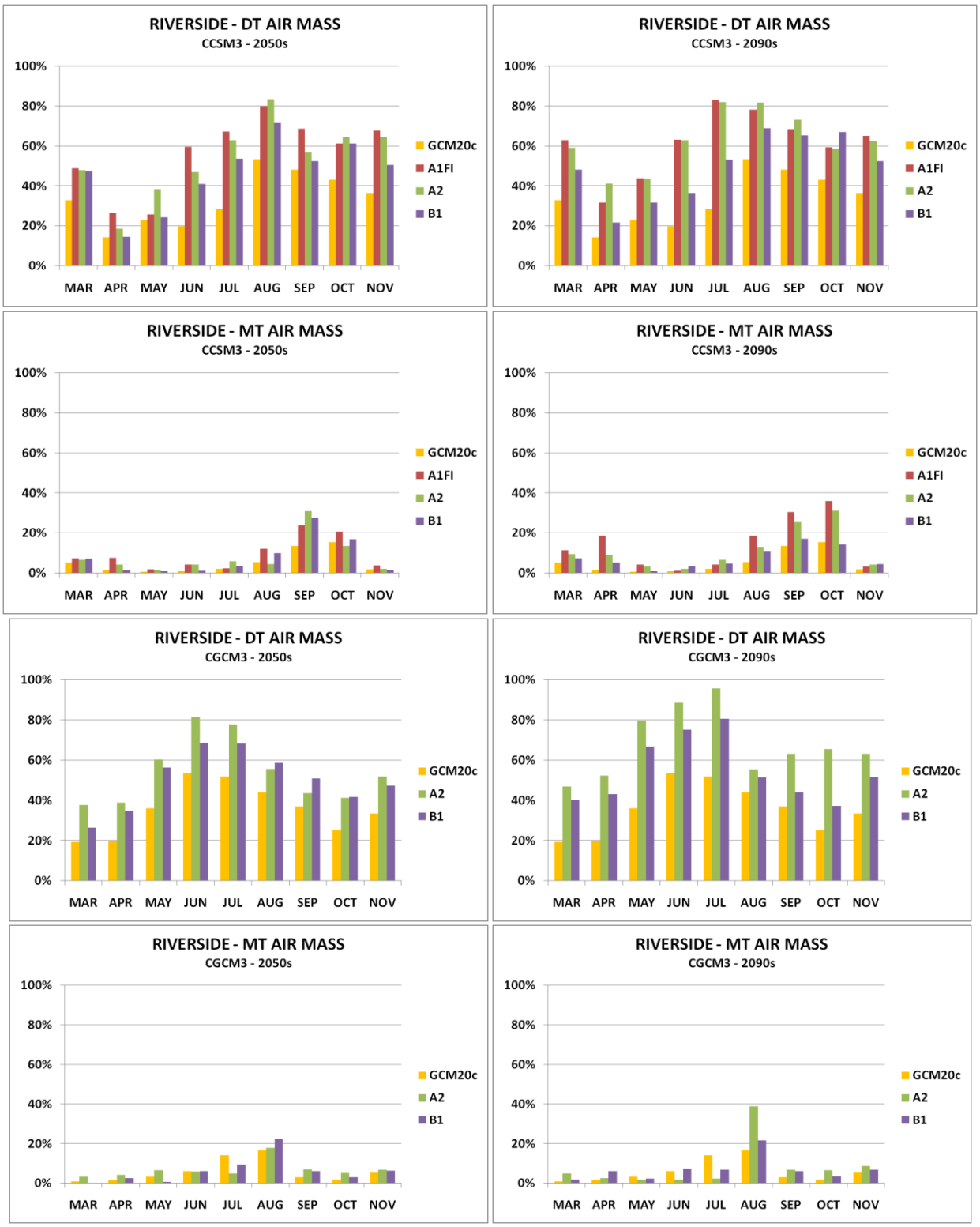

Figure 15 – Monthly frequency of the modeled DT and MT weather types at the Riverside SSC station in the 2050s (left) and the 2090s (right) in all scenarios of both the CCSM3 (top four graphs) and the CGCM3 (bottom four graphs) GCMs.

Figure 16 – Monthly frequency of the modeled DT and MT weather types at the Sacramento SSC station in the 2050s (left) and the 2090s (right) in all scenarios of both the CCSM3 (top four graphs) and the CGCM3 (bottom four graphs) GCMs.

3.4 – Historical Weather Type – Mortality Relationships

Relationships between the offensive weather types and mortality for the nine MSAs covered in this report indicate that there are clear-cut associations (Table 8). The most noticeable factor is that the relationships are most robust for the "over 74" age group based upon the number of statistically significant variables present. Variables like time of season (TOS) and day in sequence (DIS) show up more frequently in this age group; the TOS relationships are all intuitive and inverse, meaning that offensive weather type presence late in the season has a lesser impact on mortality than earlier in the season. These results are supported by considerable research that has been done in the past (Sheridan and Kalkstein 2004). Of the three times that DIS appears as statistically significant, it is directly related to mortality two times (San Diego under 65 and over 74), and inverse once (Oakland over 74). The Oakland result is counter-intuitive, which sometimes happens in pure statistical analyses like this, and is one of the only counter-intuitive relationships found in this study.

It is also clear that the DT weather type has a more detrimental impact on mortality than the other offensive weather type, MT. It occurs in the vast majority of models and is always directly related to mortality. Since these variables are applied to mortality rates (per 100,000), the results suggest that San Francisco, Oakland, and Los Angeles are most impacted by the presence of DT air, noted by the high coefficients. This is possibly due to the general rarity of this weather type at these three coastal locales. Although MT appears less frequently, Oakland and Orange County show clear sensitivities to the presence of this weather type. Many of the coefficients for MT air in the "over 74" group are rather high, showing that this weather type, in a more spatially limited sense, can have a significant direct impact on mortality.

The other variables, such as 850mb temperature at two specific model grid points, are less important in the models. With the strong presence of the weather type dummy variables, and with all these relationships being direct rather than inverse, it is not surprising that, using the climate change models and noting the greater frequency of these weather types expected in the future, mortality estimates from heat should rise dramatically as the century progresses.

Table 8 – Regression terms defining the relationship between mortality in each MSA and the SSC weather type at the corresponding SSC station.

Age Group	MSA	Constant	DT Dummy	MT Dummy	36 N 123 W	36 N 118 W	Inland Curve	Coastal Curve	DIS	TOS
UNDER 65	Fresno	0								
	Los Angeles	-0.189	0.016		0.001					
	Oakland	0.003	0.039	0.038						
	Orange County	0.002	0.015	0.041						
	Riverside	-0.768	0.012			0.003		-0.028		
	Sacramento	-0.548			0.002		-0.018			
	San Diego	0.002	0.021						0.004	
	San Francisco	0.0045								
	San Jose	0.004	0.019							
65 TO 74	Fresno	0.0383								
	Los Angeles	-1.456	0.186		0.005					
	Oakland	0.0884								
	Orange County	-0.012	0.387							
	Riverside	0.0511								
	Sacramento	0.1306								
	San Diego	0.024	0.179							
	San Francisco	0.01	0.293							
	San Jose	0.0466								
OVER 74	Fresno	-0.071	0.57							
	Los Angeles	-12.48	0.841	0.74	0.044			-0.29		
	Oakland	-12.871	1.203	1.302	0.045			-0.374	-0.148	
	Orange County	-0.065	0.583	1.114						
	Riverside	-0.186	0.556	0.927						
	Sacramento	0.299	0.74							-0.002
	San Diego	0.069		0.971					0.123	
	San Francisco	0.362	1.266							-0.002
	San Jose	-10.417	0.942		0.143	-0.103				-0.004

3.5 – Future Heat Event Estimates

Tables 9 and 10 compare the frequencies of oppressive weather type days at present (from both GCMs) with estimates of the number of such days under future model scenarios. Not surprisingly, the numbers increase significantly for both CCSM3 and CGCM3.

At present, the largest number of oppressive days occurs at the inland sites of Fresno, Riverside, and Sacramento, with Riverside clearly being the highest in all models. The lowest number is at El Toro, with Miramar and Mountain View being rather similar in number.

For consecutive day runs, there is less difference among the sites except for Riverside, which uniquely stands out. Runs of 10 days or more are presently very rare at all sites; these are the kinds of runs which will cause the greatest amount of human stress and most frequently, the largest numbers of heat-related deaths (e.g. Sheridan and Kalkstein 2004, Ostro et al. 2009, Anderson and Bell 2009).

The estimates of future offensive weather type days show increases across all cities in this analysis, but the differential between the locales diminishes, particularly for the 2090s. For example, using present-day models, the number of offensive days varies from about the lower 40s per season in El Toro to the low 100s at Riverside, well over double the El Toro number. By the 2090s, under A1FI, the difference is relatively much smaller, from the low 140s at Mountain View and El Toro to just over 200 at Riverside. Thus, all of California will experience large numbers of offensive days under the worst case A1FI scenario, and even under the more conservative scenarios.

The increase in long consecutive day strings of DT and MT days is rather substantial. Seven-day or longer events will more than double at the coastal sites for virtually all of the models for both the 2050s and 2090s. At Miramar as an example, presently such events occur about 1.5 times during a typical nine month season. This will increase to 3.7 times for the most conservative B1 scenario in the 2050s and to 4.3 times by the 2090s. Again, these increases seem steepest at the coastal locations. Possibly even more alarming are the frequencies of 14+ day events, which are exceedingly rare now, and very dangerous from a human health standpoint. Only at Riverside do such lengths of offensive days occur more than once a season at present. By the 2090s, these 14+ day runs will occur over once a year at virtually all the locales under almost all the model runs (with a few exceptions for the B1 scenarios). The increase in frequency is estimated at tenfold or greater at some of the coastal locations.

In summary, the frequencies of long consecutive day strings of offensive weather type days, which are responsible for most of the heat-related deaths in California and around the country increase dramatically in the climate change projections resulting from this research.

Table 9 – Average annual heat events and total oppressive weather type days (DT or MT) in the 20th Century (1960-1999), 2050s (2050-2059), and 2090s (2090-2099) as modeled by the CCSM3 GCM.

AVERAGE ANNUAL HEAT EVENTS		NNR 20TH CENTURY	CCSM 20TH CENTURY	CCSM3					
				A1FI		A2		B1	
				2050s	2090s	2050s	2090s	2050s	2090s
Fresno	TOTAL OPP. DAYS	84.9	83.5	154.2	184.2	135.1	170.1	117.6	120.5
	3-DAY + EVENTS	9.9	10.0	11.8	11.2	10.2	11.4	10.5	10.9
	5-DAY + EVENTS	5.8	5.7	7.5	8.3	6.9	7.0	7.2	6.5
	7-DAY + EVENTS	3.7	3.6	5.4	5.8	5.4	5.4	5.3	4.7
	10-DAY + EVENTS	2.2	1.8	3.8	4.0	3.5	3.8	3.5	3.2
	14-DAY + EVENTS	1.0	0.7	2.6	2.9	2.2	2.2	2.2	1.6
Miramar	TOTAL OPP. DAYS	54.1	53.7	130.5	179.0	112.4	174.1	91.1	103.9
	3-DAY + EVENTS	7.6	7.5	16.0	17.4	15.0	18.6	13.2	13.4
	5-DAY + EVENTS	3.1	3.3	8.1	12.9	8.2	12.1	6.5	7.5
	7-DAY + EVENTS	1.5	1.5	5.9	9.1	4.9	8.3	3.7	4.3
	10-DAY + EVENTS	0.5	0.4	3.3	5.5	2.2	5.6	1.3	1.9
	14-DAY + EVENTS	0.1	0.1	1.8	3.1	0.8	3.1	0.3	1.0
Mountain View	TOTAL OPP. DAYS	52.7	55.3	87.1	142.2	78.5	130.4	70.2	79.3
	3-DAY + EVENTS	6.6	6.8	9.9	15.1	9.2	13.6	7.6	9.6
	5-DAY + EVENTS	2.9	3.1	5.6	9.2	5.2	8.5	4.7	4.7
	7-DAY + EVENTS	1.5	1.8	3.8	5.6	3.4	5.1	2.7	3.4
	10-DAY + EVENTS	0.9	0.9	2.0	3.2	1.8	2.9	1.5	1.5
	14-DAY + EVENTS	0.4	0.4	1.0	1.9	0.4	2.0	0.6	0.7
El Toro	TOTAL OPP. DAYS	44.4	42.5	93.8	143.4	86.8	142.6	68.0	78.6
	3-DAY + EVENTS	5.6	5.5	11.0	14.7	11.8	15.6	8.9	9.1
	5-DAY + EVENTS	2.6	2.1	6.5	10.3	6.6	9.7	4.6	5.5
	7-DAY + EVENTS	1.4	1.1	4.3	7.0	3.8	7.1	2.2	3.6
	10-DAY + EVENTS	0.5	0.4	2.5	4.2	1.3	4.4	0.8	2.0
	14-DAY + EVENTS	0.2	0.2	1.0	2.2	0.5	2.0	0.2	1.0
Riverside	TOTAL OPP. DAYS	106.6	103.2	175.4	206.7	165.6	203.0	142.9	149.7
	3-DAY + EVENTS	13.8	12.7	13.4	12.7	15.7	13.2	14.0	14.0
	5-DAY + EVENTS	7.5	7.2	9.3	9.4	10.6	9.9	9.4	9.2
	7-DAY + EVENTS	4.7	4.3	6.4	6.7	7.5	7.8	6.5	6.4
	10-DAY + EVENTS	2.7	2.4	4.5	4.3	4.5	5.0	3.6	4.5
	14-DAY + EVENTS	1.2	1.1	3.3	2.8	3.1	2.9	2.5	2.3
Sacramento	TOTAL OPP. DAYS	66.7	62.0	137.6	177.9	118.5	169.8	100.0	105.5
	3-DAY + EVENTS	9.0	8.4	15.0	14.4	14.4	15.4	12.5	12.4
	5-DAY + EVENTS	3.9	3.9	9.1	10.5	8.3	10.4	7.5	7.0
	7-DAY + EVENTS	2.0	1.7	6.4	7.8	5.2	7.3	4.7	4.3
	10-DAY + EVENTS	0.9	0.6	3.9	5.0	2.8	4.7	2.2	2.3
	14-DAY + EVENTS	0.2	0.2	1.9	3.3	1.2	2.8	0.8	1.2

Table 10 – Average annual heat events and total oppressive weather type days (DT or MT) in the 20th Century (1970-1999), 2050s (2050-2059), and 2090s (2090-2099) as modeled by the CGCM3 GCM.

AVERAGE ANNUAL HEAT EVENTS		NNR 20TH CENTURY	CGCM 20TH CENTURY	CGCM3			
				A2		B1	
				2050s	2090s	2050s	2090s
Fresno	TOTAL OPP. DAYS	88.7	85.3	128.1	167.7	117.2	131.5
	3-DAY + EVENTS	10.2	10.4	13.2	15.5	12.7	15.3
	5-DAY + EVENTS	5.9	5.6	8.1	9.8	7.6	8.7
	7-DAY + EVENTS	3.9	3.4	6.0	7.3	5.0	5.2
	10-DAY + EVENTS	2.1	1.6	3.7	5.0	3.3	3.5
	14-DAY + EVENTS	1.1	0.8	1.8	3.2	1.6	1.8
Miramar	TOTAL OPP. DAYS	54.4	57.4	114.3	169.3	97.3	111.7
	3-DAY + EVENTS	8.0	8.2	16.5	18.8	13.1	14.8
	5-DAY + EVENTS	3.4	2.9	8.9	12.7	7.3	8.4
	7-DAY + EVENTS	1.2	1.3	5.2	8.3	3.5	4.6
	10-DAY + EVENTS	0.4	0.5	1.6	4.6	1.3	2.0
	14-DAY + EVENTS	0.0	0.1	0.7	2.8	0.6	0.7
Mountain View	TOTAL OPP. DAYS	50.1	53.8	76.8	100.2	71.3	80.5
	3-DAY + EVENTS	6.9	7.1	9.7	12.7	10.0	10.0
	5-DAY + EVENTS	2.4	2.9	4.4	7.3	4.3	5.0
	7-DAY + EVENTS	1.1	1.4	2.4	4.0	2.2	2.8
	10-DAY + EVENTS	0.5	0.4	1.2	2.1	0.7	1.4
	14-DAY + EVENTS	0.2	0.1	0.4	0.6	0.2	0.2
El Toro	TOTAL OPP. DAYS	49.3	49.8	96.4	147.2	86.6	91.7
	3-DAY + EVENTS	6.5	6.7	13.8	17.1	10.5	12.1
	5-DAY + EVENTS	3.1	2.9	7.3	11.3	6.7	6.1
	7-DAY + EVENTS	1.5	1.2	3.8	8.1	4.0	3.2
	10-DAY + EVENTS	0.6	0.4	1.4	4.2	1.7	1.3
	14-DAY + EVENTS	0.1	0.1	0.6	2.1	0.8	0.4
Riverside	TOTAL OPP. DAYS	108.5	106.5	160.6	196.3	146.8	159.2
	3-DAY + EVENTS	13.0	13.2	16.2	14.3	15.4	17.4
	5-DAY + EVENTS	7.8	7.2	10.4	10.6	10.5	11.5
	7-DAY + EVENTS	4.9	4.4	7.5	7.6	7.5	7.6
	10-DAY + EVENTS	2.8	2.6	4.6	5.0	4.7	4.0
	14-DAY + EVENTS	1.2	1.3	2.5	2.9	2.2	2.9
Sacramento	TOTAL OPP. DAYS	59.4	57.1	100.8	138.7	83.2	96.1
	3-DAY + EVENTS	8.0	7.9	14.0	16.0	10.9	13.6
	5-DAY + EVENTS	3.6	3.5	7.6	10.6	5.8	6.7
	7-DAY + EVENTS	2.1	1.6	3.8	7.1	3.9	3.0
	10-DAY + EVENTS	0.8	0.6	1.6	3.6	1.6	1.5
	14-DAY + EVENTS	0.1	0.2	0.5	1.8	0.3	0.5

3.6 – Future Heat-Related Mortality Estimates

Many factors must be considered when attempting to develop heat-related mortality estimates for the future, including assessment of population growth and demographic change through the 2090s, the uncertainty in the climate projections as well as the ability of GCMs in projecting the future climate, and the impact that a partial acclimatization may have upon these estimates.

Figures 17 through 25 provide a range of mortality estimates assuming no acclimatization for different model scenarios, as well as modeled estimates for present-day heat-related mortality. Although there is increasing spread in the estimates as time moves along through the century, one thing seems to be typical to all: deaths are likely to rise considerably if the climate changes as indicated by the models.

Fresno typifies what might happen to future heat-related mortality totals. During an average summer today, the number of heat-related deaths in Fresno is in the low 20s. Assuming the medium population projection, this number will increase to 132 under the "business as usual" A1FI scenario in the decade of the 2050s, and to about double that number in the 2090s. Thus, there may be approximately a tenfold increase in mortality in Fresno during the 21st century. As is typically the case, the A2 and B1 scenarios, which account for some emissions controls, suggest smaller, but still very substantial increases.

Assuming no change in the Fresno population, the results still show considerable increases, albeit much smaller. Heat-related mortality is estimated to increase by 20-30 percent by the 2050s, and slightly more than that by the 2090s for all but the B1 model.

Not surprisingly, Los Angeles will potentially have the greatest number of heat-related deaths based on model projections. Using the moderate population projection, Los Angeles's mean summer season heat-related mortality will hover around 1500 in the 2050s under the A1Fi scenario. This is approximately the average number of heat-related deaths *in the entire country* today (Kalkstein et al., 2010). Even accounting for increased emissions controls, deaths top 1000 for the B1 scenario in the 2050s, and reach 1500 by the 2090s, while A1FI totals are even higher for the 2090s. Of course, those numbers are greatly reduced if no population change is assumed, but still are over 50 percent greater than present day summer season heat-related deaths by the 2050s using the business as usual scenario. Like Fresno, there is the potential for a tenfold increase in heat-related mortality in Los Angeles by the 2090s.

For the remaining cities, proportional rises under the medium population projection are greatest through the decades for San Diego and Orange County, and least for Oakland and San Francisco. This may be attributed to a faster population growth expected through the years in the southern California locales as compared to the Bay Area. However, the increases are also greater in the south assuming no population growth (compare, for example, Oakland and Orange County, which exhibit similar heat-related mortality numbers today), suggesting that spatial variability in climate changes may be involved as well.

There are other population projections that have been used in this analysis; besides the medium level discussed above, there are low and high population growth projections (Table 11). In all cases, an unsurprising result emerges: the low population projection is higher than the "no change" scenario but lower than the medium level projection, and the high population projection is about 15 percent higher than the medium projection. While these other projections will not be discussed further here, it is clear that the population projection used has a major impact on estimated heat-related mortality, and can increase the numbers by more than fourfold in some situations (e.g. refer to the Los Angeles numbers and the differences between "none" (assuming present population) and "high").

In summary, very large increases in heat-related mortality are possible in the large California cities, particularly under the A1FI scenario. However, there are sizable increases in mortality expected even with the most conservative model runs, with the greatest proportional rises occurring in southern California.

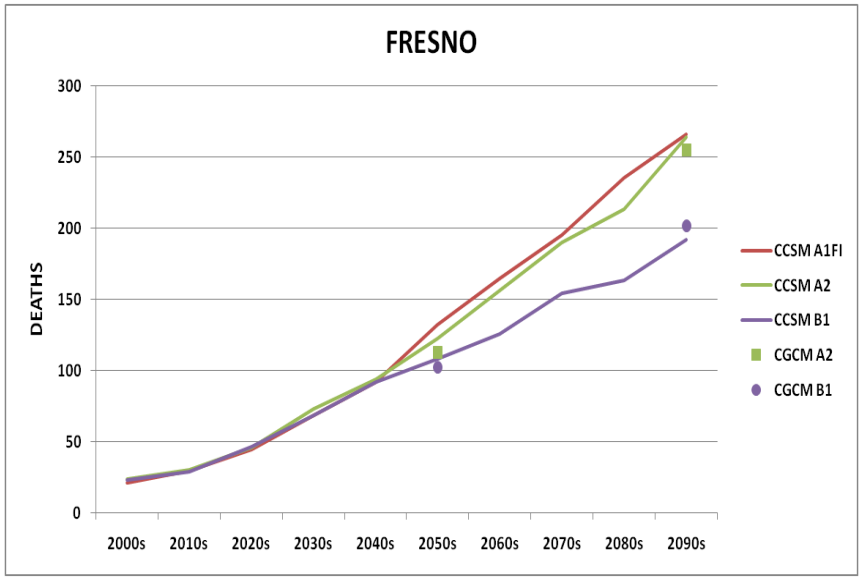

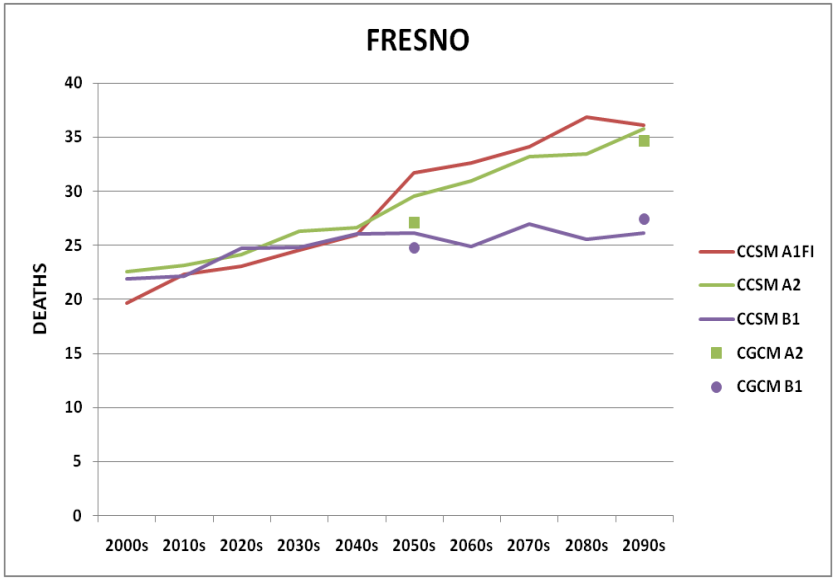

	ANNUAL AVERAGES									
	2000s	2010s	2020s	2030s	2040s	2050s	2060s	2070s	2080s	2090s
CCSM A1FI	21	29	44	69	92	132	165	195	236	266
CCSM A2	24	31	46	74	94	123	157	190	213	264
CCSM B1	23	29	47	69	92	109	126	154	164	192
CGCM A2						113				255
CGCM B1						102				202

	ANNUAL AVERAGES									
	2000s	2010s	2020s	2030s	2040s	2050s	2060s	2070s	2080s	2090s
CCSM A1FI	20	22	23	25	26	32	33	34	37	36
CCSM A2	23	23	24	26	27	30	31	33	33	36
CCSM B1	22	22	25	25	26	26	25	27	26	26
CGCM A2						27				35
CGCM B1						25				27

Figure 17 – Total projected annual future mortality under the medium population projection (left) and projected annual future mortality with steady population (right) for ages 65 and over for Fresno under all model scenarios (2000 -2099). Notice the change of scale in the vertical axis between the two graphs. Numbers represent the summed decadal totals divided by 10.

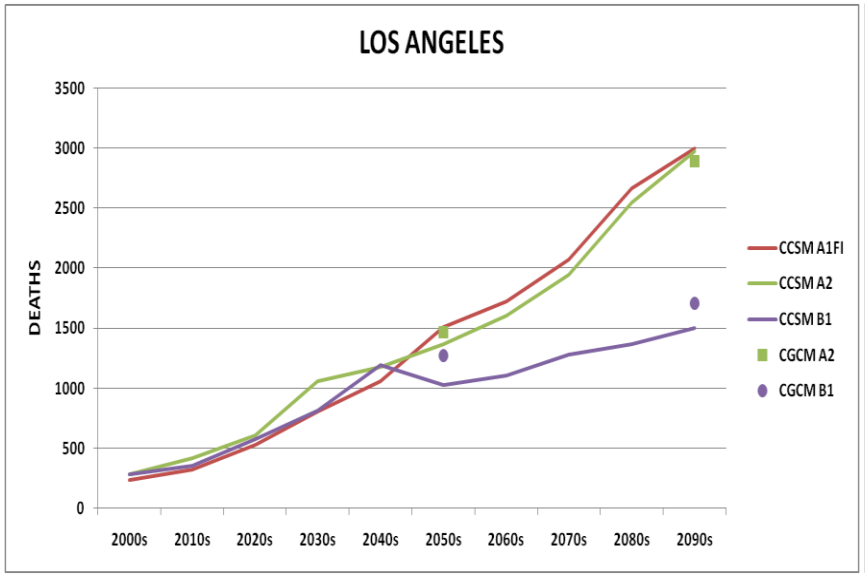

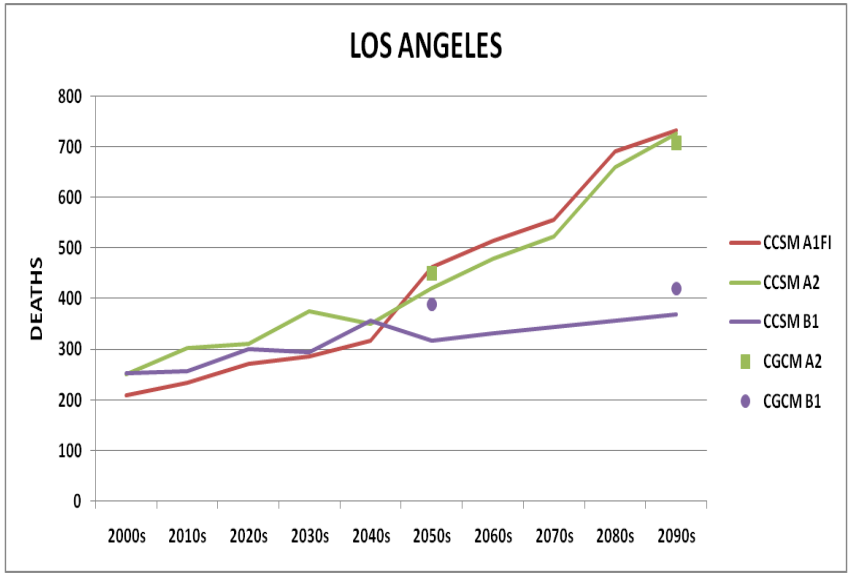

	ANNUAL AVERAGES									
	2000s	2010s	2020s	2030s	2040s	2050s	2060s	2070s	2080s	2090s
CCSM A1FI	239	325	532	812	1063	1511	1724	2073	2666	2997
CCSM A2	283	420	605	1057	1176	1369	1607	1945	2548	2973
CCSM B1	285	358	576	811	1189	1028	1103	1276	1371	1501
CGCM A2						1465				2890
CGCM B1						1273				1710

	ANNUAL AVERAGES									
	2000s	2010s	2020s	2030s	2040s	2050s	2060s	2070s	2080s	2090s
CCSM A1FI	209	234	272	285	317	462	514	556	690	732
CCSM A2	250	303	309	375	350	420	478	523	660	726
CCSM B1	252	256	299	294	355	316	330	344	356	368
CGCM A2						450				707
CGCM B1						390				420

Figure 18 – Total projected annual future mortality under the medium population projection (left) and projected annual future mortality with steady population (right) for ages 65 and over for Los Angeles under all model scenarios (2000 -2099). Notice the change of scale in the vertical axis between the two graphs. Numbers represent the summed decadal totals divided by 10.

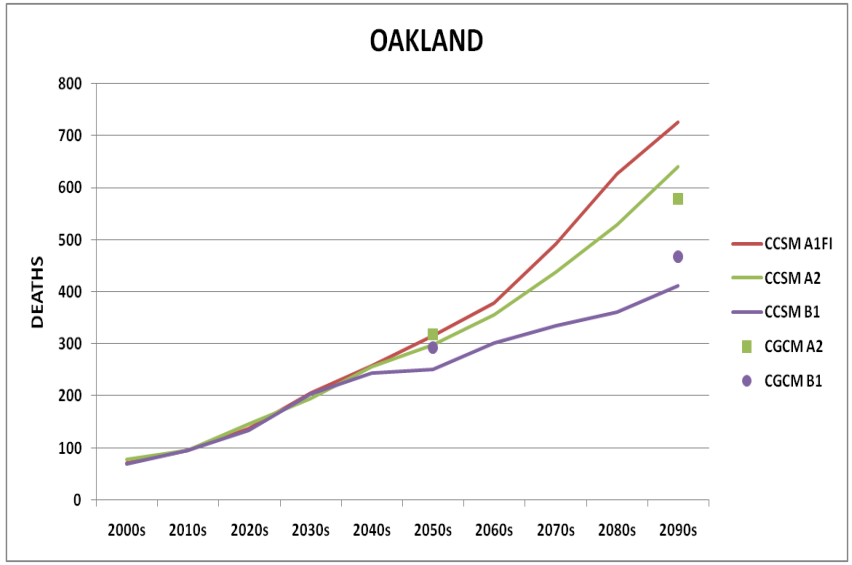

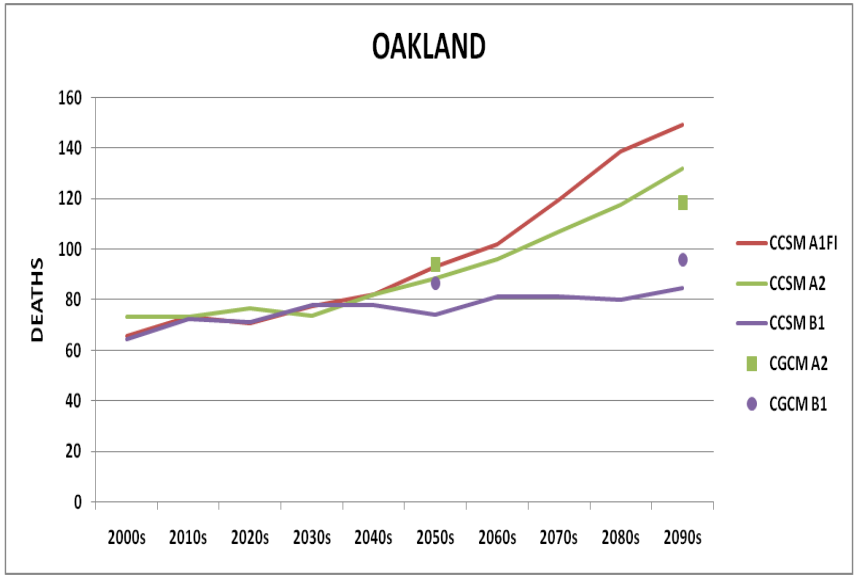

	ANNUAL AVERAGES									
	2000s	2010s	2020s	2030s	2040s	2050s	2060s	2070s	2080s	2090s
CCSM A1FI	71	96	137	205	257	315	379	492	626	726
CCSM A2	79	96	146	196	256	299	357	439	530	641
CCSM B1	69	95	135	205	244	252	303	335	361	413
CGCM A2						319				579
CGCM B1						294				468

	ANNUAL AVERAGES									
	2000s	2010s	2020s	2030s	2040s	2050s	2060s	2070s	2080s	2090s
CCSM A1FI	66	73	71	78	82	93	102	120	139	149
CCSM A2	73	73	76	74	82	88	96	107	118	132
CCSM B1	64	73	71	78	78	74	81	81	80	85
CGCM A2						94				118
CGCM B1						87				96

Figure 19 – Total projected annual future mortality under the medium population projection (left) and projected annual future mortality with steady population (right) for ages 65 and over for Oakland under all model scenarios (2000 -2099). Notice the change of scale in the vertical axis between the two graphs. Numbers represent the summed decadal totals divided by 10.

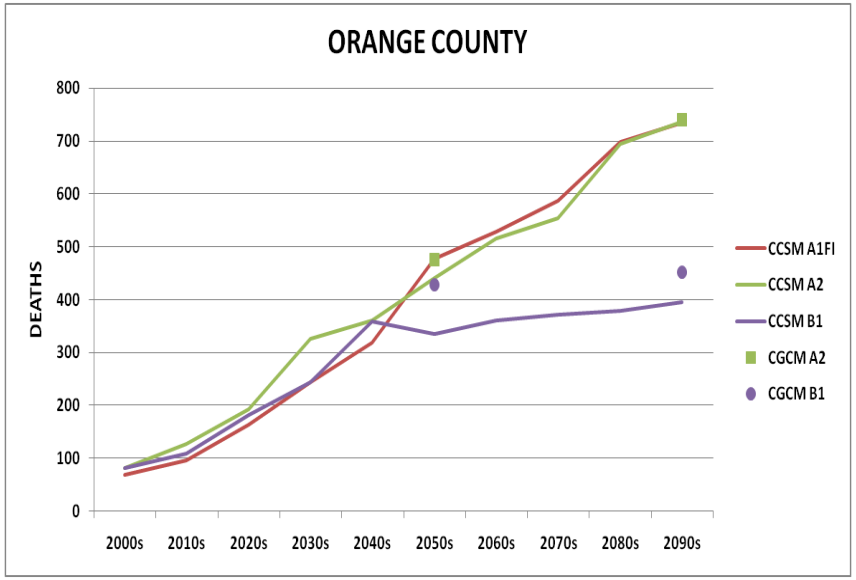

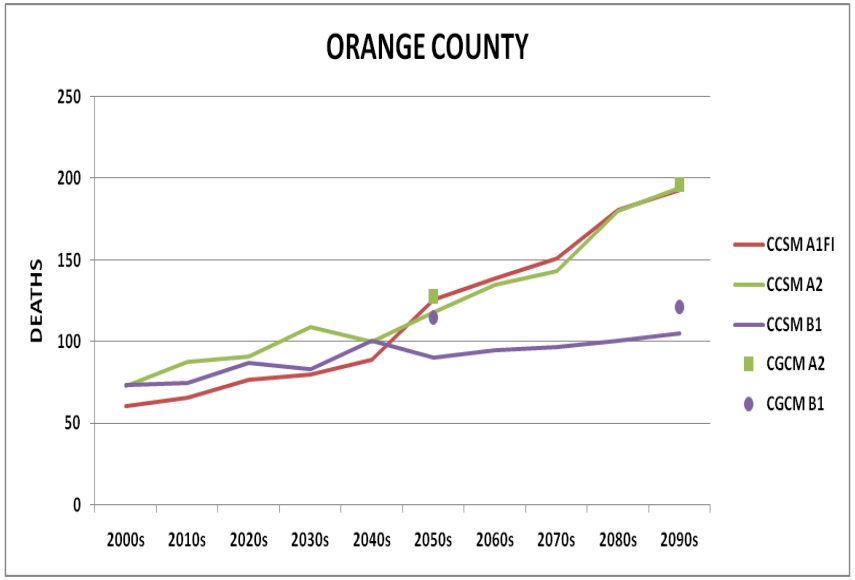

	ANNUAL AVERAGES									
	2000s	2010s	2020s	2030s	2040s	2050s	2060s	2070s	2080s	2090s
CCSM A1FI	68	96	164	243	319	477	529	586	698	735
CCSM A2	81	127	192	325	361	441	515	555	695	737
CCSM B1	82	109	182	244	359	335	361	372	379	395
CGCM A2						476				742
CGCM B1						428				452

	ANNUAL AVERAGES									
	2000s	2010s	2020s	2030s	2040s	2050s	2060s	2070s	2080s	2090s
CCSM A1FI	61	66	77	80	89	126	138	151	181	193
CCSM A2	73	88	90	109	100	118	135	143	180	194
CCSM B1	74	75	87	83	100	90	95	97	100	105
CGCM A2						128				197
CGCM B1						115				121

Figure 20 – Total projected annual future mortality under the medium population projection (left) and projected annual future mortality with steady population (right) for ages 65 and over for Orange County under all model scenarios (2000 -2099). Notice the change of scale in the vertical axis between the two graphs. Numbers represent the summed decadal totals divided by 10.

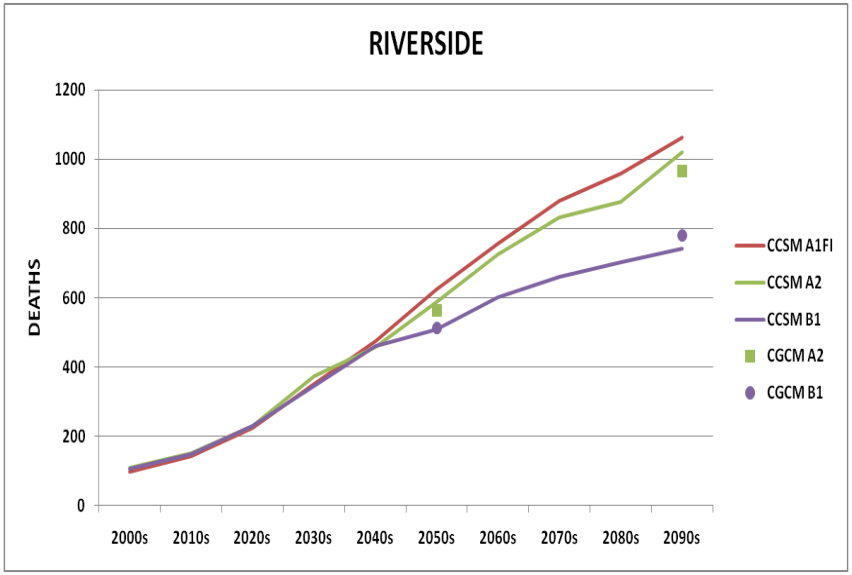

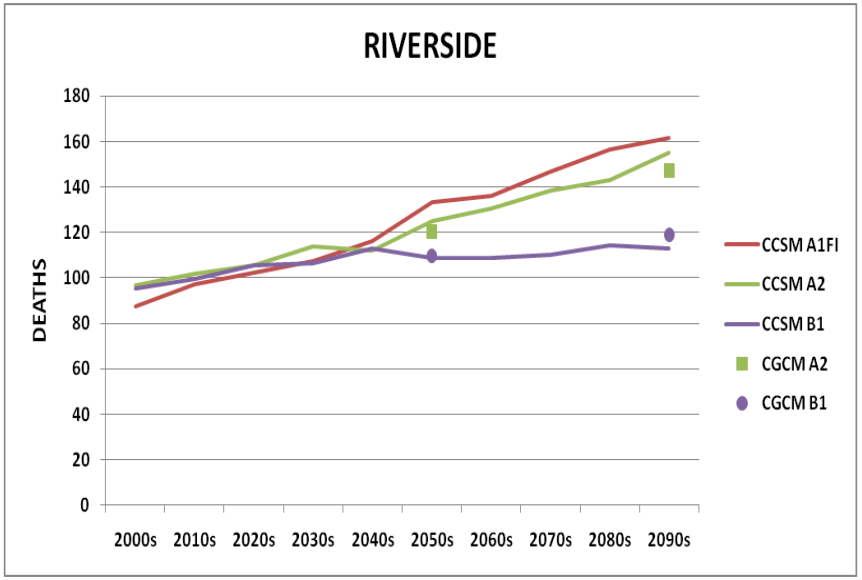

	ANNUAL AVERAGES									
	2000s	2010s	2020s	2030s	2040s	2050s	2060s	2070s	2080s	2090s
CCSM A1FI	98	143	225	352	476	625	757	881	960	1063
CCSM A2	108	151	231	372	458	586	724	831	876	1021
CCSM B1	107	148	232	345	461	509	601	659	701	741
CGCM A2						563				966
CGCM B1						513				780

	ANNUAL AVERAGES									
	2000s	2010s	2020s	2030s	2040s	2050s	2060s	2070s	2080s	2090s
CCSM A1FI	88	97	102	108	116	133	136	147	157	162
CCSM A2	97	102	105	114	112	125	131	139	143	155
CCSM B1	95	100	106	107	113	109	109	110	114	113
CGCM A2						120				147
CGCM B1						110				119

Figure 21 – Total projected annual future mortality under the medium population projection (left) and projected annual future mortality with steady population (right) for ages 65 and over for Riverside under all model scenarios (2000 -2099). Notice the change of scale in the vertical axis between the two graphs. Numbers represent the summed decadal totals divided by 10.

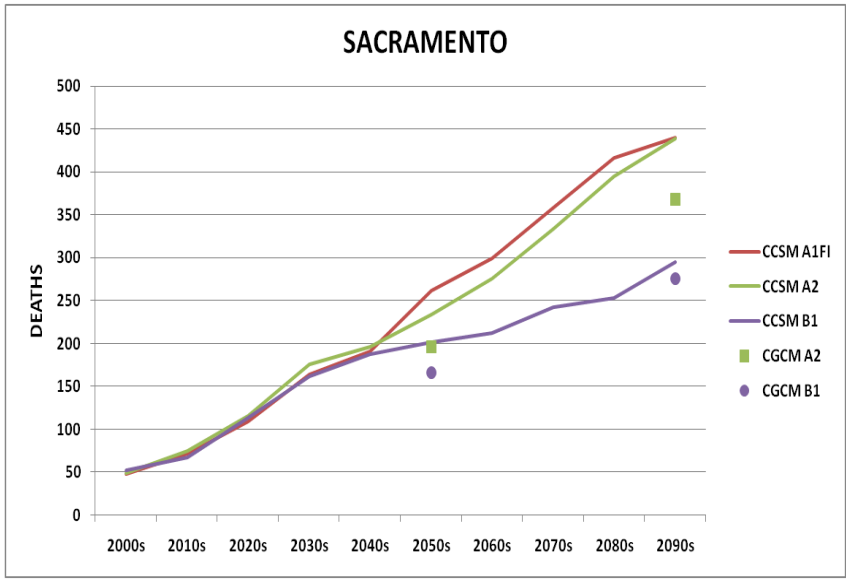

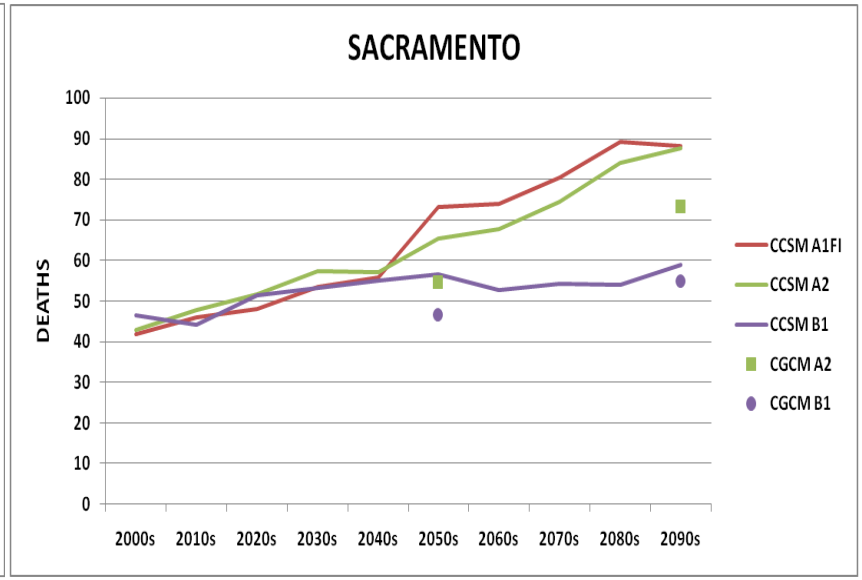

	ANNUAL AVERAGES									
	2000s	2010s	2020s	2030s	2040s	2050s	2060s	2070s	2080s	2090s
CCSM A1FI	48	71	108	164	191	262	299	358	416	440
CCSM A2	49	74	116	176	196	233	275	333	394	438
CCSM B1	53	67	114	162	188	202	213	242	253	295
CGCM A2						196				368
CGCM B1						166				275

	ANNUAL AVERAGES									
	2000s	2010s	2020s	2030s	2040s	2050s	2060s	2070s	2080s	2090s
CCSM A1FI	42	46	48	54	56	73	74	80	89	88
CCSM A2	43	48	52	57	57	65	68	75	84	88
CCSM B1	47	44	51	53	55	56	53	54	54	59
CGCM A2						55				73
CGCM B1						47				55

Figure 22 – Total projected annual future mortality under the medium population projection (left) and projected annual future mortality with steady population (right) for ages 65 and over for Sacramento under all model scenarios (2000 -2099). Notice the change of scale in the vertical axis between the two graphs. Numbers represent the summed decadal totals divided by 10.

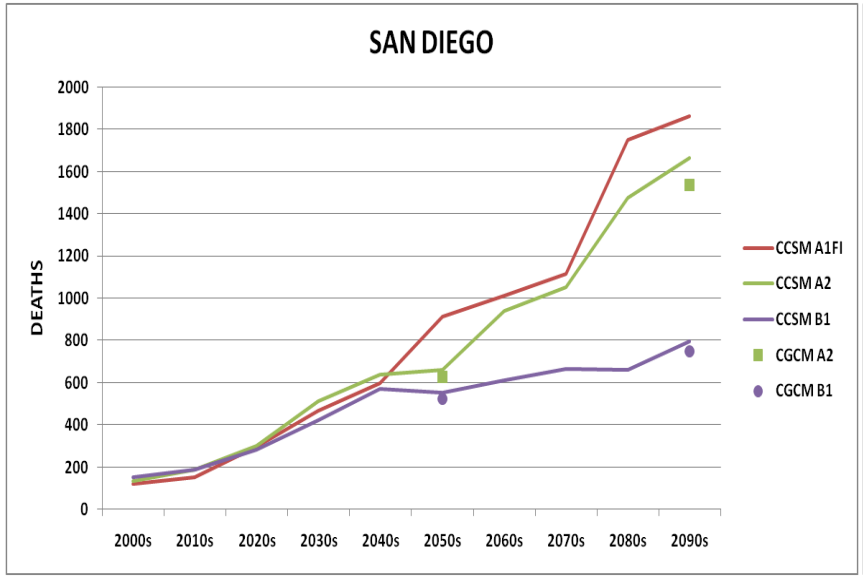

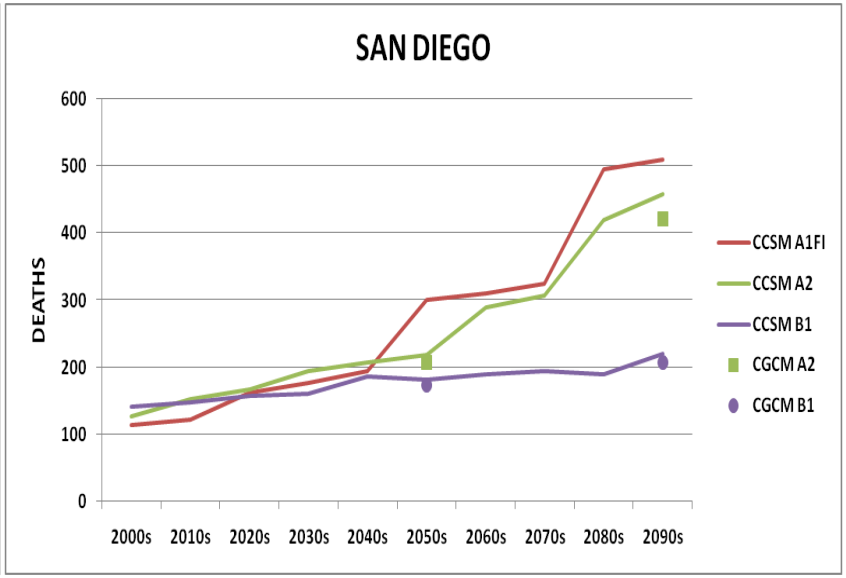

	ANNUAL AVERAGES									
	2000s	2010s	2020s	2030s	2040s	2050s	2060s	2070s	2080s	2090s
CCSM A1FI	122	153	296	466	599	916	1012	1116	1750	1865
CCSM A2	135	190	300	512	639	663	943	1056	1475	1667
CCSM B1	151	186	281	420	572	555	613	664	664	797
CGCM A2						628				1535
CGCM B1						525				750

	ANNUAL AVERAGES									
	2000s	2010s	2020s	2030s	2040s	2050s	2060s	2070s	2080s	2090s
CCSM A1FI	114	123	163	177	194	301	311	325	496	511
CCSM A2	126	152	167	194	207	219	289	307	420	458
CCSM B1	142	149	157	161	186	183	189	194	190	220
CGCM A2						208				422
CGCM B1						173				207

Figure 23 – Total projected annual future mortality under the medium population projection (left) and projected annual future mortality with steady population (right) for ages 65 and over for San Diego under all model scenarios (2000 -2099). Notice the change of scale in the vertical axis between the two graphs. Numbers represent the summed decadal totals divided by 10.

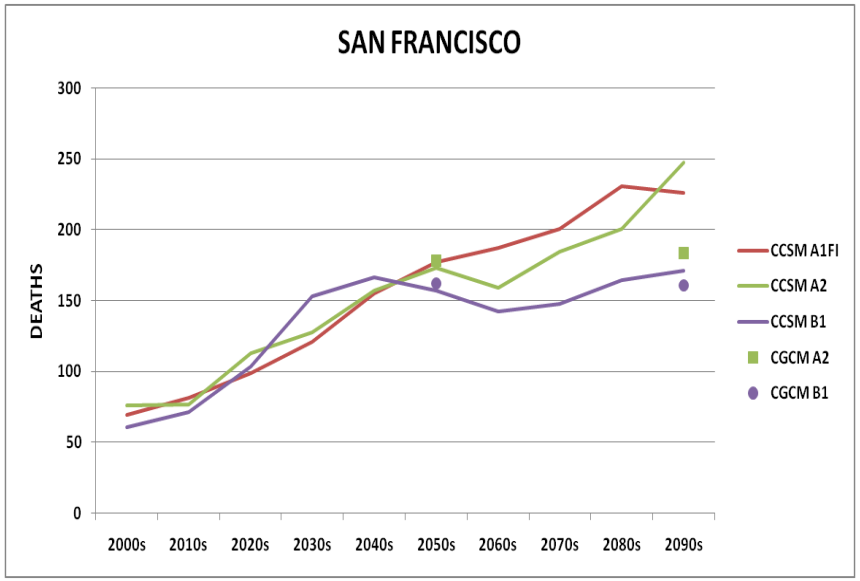

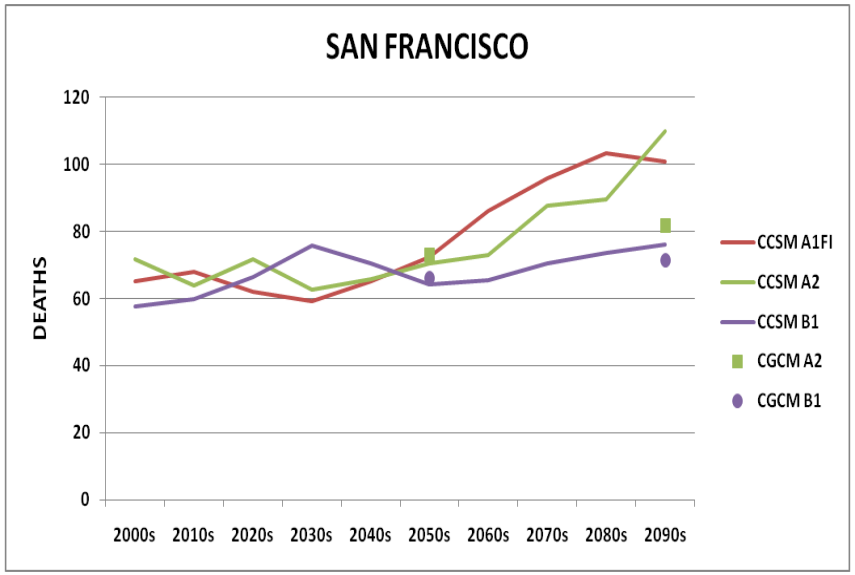

	ANNUAL AVERAGES									
	2000s	2010s	2020s	2030s	2040s	2050s	2060s	2070s	2080s	2090s
CCSM A1FI	69	82	99	121	155	178	188	200	231	226
CCSM A2	76	77	113	128	157	173	159	184	200	247
CCSM B1	61	72	104	153	167	157	143	148	165	171
CGCM A2						178				183
CGCM B1						162				161

	ANNUAL AVERAGES									
	2000s	2010s	2020s	2030s	2040s	2050s	2060s	2070s	2080s	2090s
CCSM A1FI	65	68	62	59	65	72	86	96	103	101
CCSM A2	72	64	72	63	66	71	73	88	90	110
CCSM B1	58	60	66	76	70	64	65	71	74	76
CGCM A2						73				82
CGCM B1						66				71

Figure 24 – Total projected annual future mortality under the medium population projection (left) and projected annual future mortality with steady population (right) for ages 65 and over for San Francisco under all model scenarios (2000 -2099). Notice the change of scale in the vertical axis between the two graphs. Numbers represent the summed decadal totals divided by 10.

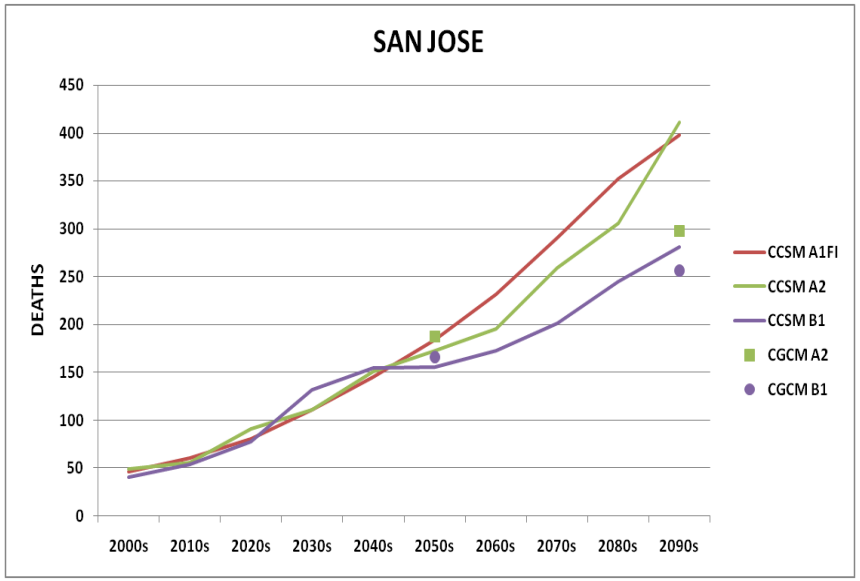

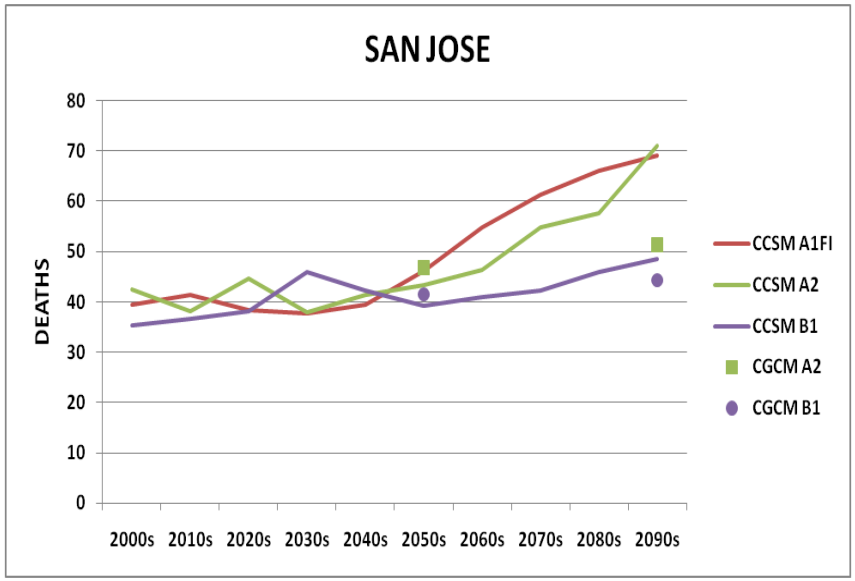

	ANNUAL AVERAGES									
	2000s	2010s	2020s	2030s	2040s	2050s	2060s	2070s	2080s	2090s
CCSM A1FI	46	60	80	110	144	184	231	291	352	398
CCSM A2	49	55	91	111	151	172	195	259	306	411
CCSM B1	41	54	78	132	155	156	173	201	246	281
CGCM A2						187				297
CGCM B1						166				256

	ANNUAL AVERAGES									
	2000s	2010s	2020s	2030s	2040s	2050s	2060s	2070s	2080s	2090s
CCSM A1FI	39	41	38	38	39	46	55	61	66	69
CCSM A2	42	38	45	38	41	43	46	55	58	71
CCSM B1	35	37	38	46	42	39	41	42	46	48
CGCM A2						47				51
CGCM B1						41				44

Figure 25 – Total projected annual future mortality under the medium population projection (left) and projected annual future mortality with steady population (right) for ages 65 and over for San Jose under all model scenarios (2000 -2099). Notice the change of scale in the vertical axis between the two graphs. Numbers represent the summed decadal totals divided by 10.

Table 11 – Mean heat-related mortality in each MSA by population projection and scenario, 2050s and 2090s. Continued on the next page.

FRESNO								
	2050s				2090s			
	LOW	MED	HIGH	NONE	LOW	MED	HIGH	NONE
CCSM A1FI	110	132	153	32	176	266	385	36
CCSM A2	102	123	143	30	174	264	383	36
CCSM B1	90	109	126	26	127	192	278	26
CGCM A2	94	113	131	27	169	255	370	35
CGCM B1	85	102	119	25	133	202	293	27
HIST. AVG	15							

LOS ANGELES								
	2050s				2090s			
	LOW	MED	HIGH	NONE	LOW	MED	HIGH	NONE
CCSM A1FI	1360	1511	2014	462	1778	2997	4499	732
CCSM A2	1229	1369	1826	420	1761	2973	4460	726
CCSM B1	924	1028	1369	316	893	1501	2250	368
CGCM A2	1314	1465	1955	450	1713	2890	4334	707
CGCM B1	1149	1273	1688	390	1014	1710	2560	420
HIST. AVG	165							

OAKLAND								
	2050s				2090s			
	LOW	MED	HIGH	NONE	LOW	MED	HIGH	NONE
CCSM A1FI	263	315	411	93	375	726	1089	149
CCSM A2	249	299	390	88	331	641	961	132
CCSM B1	209	252	329	74	213	413	619	85
CGCM A2	266	319	416	94	299	579	870	118
CGCM B1	245	294	383	87	242	468	703	96
HIST. AVG	49							

Table 11 – Continued.

ORANGE COUNTY								
	2050s				2090s			
	LOW	MED	HIGH	NONE	LOW	MED	HIGH	NONE
CCSM A1FI	414	477	625	126	508	735	1353	193
CCSM A2	382	441	577	118	509	737	1357	194
CCSM B1	290	335	438	90	273	395	724	105
CGCM A2	412	476	622	128	512	742	1362	197
CGCM B1	372	428	557	115	312	452	828	121
HIST. AVG	44							

RIVERSIDE								
	2050s				2090s			
	LOW	MED	HIGH	NONE	LOW	MED	HIGH	NONE
CCSM A1FI	518	625	747	133	862	1063	1914	162
CCSM A2	486	586	702	125	828	1021	1838	155
CCSM B1	422	509	608	109	602	741	1331	113
CGCM A2	467	563	674	120	784	966	1736	147
CGCM B1	425	513	611	110	633	780	1403	119
HIST. AVG	60							

SACRAMENTO								
	2050s				2090s			
	LOW	MED	HIGH	NONE	LOW	MED	HIGH	NONE
CCSM A1FI	213	262	318	73	317	440	727	88
CCSM A2	190	233	284	65	316	438	725	88
CCSM B1	165	202	246	56	213	295	488	59
CGCM A2	160	196	238	55	264	368	610	73
CGCM B1	136	166	201	47	198	275	457	55
HIST. AVG	27							

Table 11 – Continued.

SAN DIEGO								
	2050s				2090s			
	LOW	MED	HIGH	NONE	LOW	MED	HIGH	NONE
CCSM A1FI	810	916	1187	301	1247	1865	3163	511
CCSM A2	585	663	860	219	1116	1667	2819	458
CCSM B1	490	555	719	183	535	797	1342	220
CGCM A2	555	628	813	208	1029	1535	2592	422
CGCM B1	464	525	673	173	502	750	1266	207
HIST. AVG	68							

SAN FRANCISCO								
	2050s				2090s			
	LOW	MED	HIGH	NONE	LOW	MED	HIGH	NONE
CCSM A1FI	149	178	248	72	124	226	387	101
CCSM A2	145	173	242	71	136	247	424	110
CCSM B1	132	157	220	64	94	171	293	76
CGCM A2	149	178	249	73	101	183	314	82
CGCM B1	136	162	226	66	89	161	275	71
HIST. AVG	53							

SAN JOSE								
	2050s				2090s			
	LOW	MED	HIGH	NONE	LOW	MED	HIGH	NONE
CCSM A1FI	145	184	241	46	169	398	594	69
CCSM A2	136	172	227	43	175	411	615	71
CCSM B1	123	156	205	39	120	281	421	48
CGCM A2	147	187	246	47	127	297	444	51
CGCM B1	131	166	218	41	109	256	383	44
HIST. AVG	27							

3.7 – Future Heat-Related Mortality Estimates with Acclimatization

If the earth warms as the models forecast, there is the possibility that humans will partially adapt to this situation, rendering the unacclimatized estimates above as the upper limit in terms of heat-related mortality estimates. We have devised two techniques to determine what the impacts of acclimatization might be: DIS-2 and DIS-4; both of these procedures are described in the Methods chapter. Values presented in Tables 12 and 13 estimate the reduction in heat-related mortality utilizing these two acclimatization levels.

For Fresno, using the DIS-2 acclimatization procedure, in which the heat-related mortality on the first day of a heat event is assumed to be offset, reductions in heat-related mortality will vary between 12-20 percent in the 2050s and 8-19 percent in the 2090s. In general, the "business as usual" model run (A1FI) demonstrates the lowest decrease in acclimatized heat-related mortality, while the most demanding emissions control scenarios (B1) show the largest. This is possibly because there are many more offensive weather type days in the business as usual scenario, and the number of consecutive day runs of these days will remain relatively high. Los Angeles exhibits a higher decrease in mortality than Fresno under the DIS-2 acclimatization methodology. Reductions range from 24-34 percent in the 2050s and 17 to 31 percent in the 2090s. Like Fresno, the A1FI scenario shows the smallest decrease, and B1 the largest. The percentage decreases under acclimatization are greater in the 2050s estimates than in the 2090s, because of the inherently longer duration of heat events in the 2090s.

While all the cities studied show the same general characteristics, some regional differentiation is apparent. The three Bay Area regions of Oakland, San Francisco, and San Jose demonstrate the greatest decrease in mortality attributed to acclimatization, averaging in the 30-40 percent range for the DIS-2 procedure. The inland cities of Riverside, Sacramento, and Fresno show the smallest decreases in mortality, generally between 15 and 20 percent. Los Angeles and Orange County are somewhere intermediate, and only San Diego seems to be an outlier, with similar smaller decreases as the inland cities.

Not surprisingly, in all cities, the DIS-4 assumption, that all heat-related mortality in the first three days of a heat event is negated, leads to greater decreases in acclimatized mortality. A regionality similar to the DIS-2 procedure exists, but in some cases (e.g. Oakland) the decreases approach 80 percent or slightly above for the B1 scenario. That would render Oakland's acclimatized mortality similar to today's unacclimatized heat-related mortality in that region. Many of the DIS-4 decreases are beyond 50 percent of the unacclimatized numbers, but slightly less at the inland locales.

Thus, we can consider the unacclimatized numbers presented in Section 3.6 as the high end estimates for heat-related mortality, and the DIS-4 numbers as lower end. With few exceptions, even the acclimatized estimates are considerably higher than the present day levels of heat-related mortality in the California cities.

Table 12 – Comparison of each MSA's non-acclimatized mortality versus the acclimatized mortality using the DIS-2 method. Values represent total annual mortality by MSA for the 2050s and 2090s under each model scenario for the medium population projection (for age 65+). GCM20c values are historical annual means from 1980-1999. Continued on the next page.

FRESNO								
	2050s				2090s			
	NOT ACC.	ACC.	DIFF	% DIFF	NOT ACC.	ACC.	DIFF	% DIFF
CCSM3 A1FI	132	117	-15	-12%	266	244	-22	-8%
CCSM3 A2	123	106	-17	-14%	264	237	-27	-10%
CCSM3 B1	109	92	-16	-15%	192	162	-30	-16%
CGCM3 A2	113	93	-20	-18%	255	220	-36	-14%
CGCM3 B1	102	82	-20	-20%	202	163	-39	-19%
20c AVG.	15	11	-3	-23%				

LOS ANGELES								
	2050s				2090s			
	NOT ACC.	ACC.	DIFF	% DIFF	NOT ACC.	ACC.	DIFF	% DIFF
CCSM3 A1FI	1511	1155	-356	-24%	2997	2474	-524	-17%
CCSM3 A2	1369	970	-399	-29%	2973	2386	-586	-20%
CCSM3 B1	1028	682	-346	-34%	1501	1112	-389	-26%
CGCM3 A2	1465	1082	-383	-26%	2890	2327	-563	-19%
CGCM3 B1	1273	933	-340	-27%	1710	1177	-533	-31%
20c AVG.	165	102	-63	-38%				

OAKLAND								
	2050s				2090s			
	NOT ACC.	ACC.	DIFF	% DIFF	NOT ACC.	ACC.	DIFF	% DIFF
CCSM3 A1FI	315	190	-125	-40%	726	472	-254	-35%
CCSM3 A2	299	172	-127	-42%	641	419	-223	-35%
CCSM3 B1	252	144	-108	-43%	413	248	-165	-40%
CGCM3 A2	319	183	-136	-43%	579	351	-228	-39%
CGCM3 B1	294	161	-133	-45%	468	271	-196	-42%
20c AVG.	49	28	-21	-43%				

ORANGE COUNTY								
	2050s				2090s			
	NOT ACC.	ACC.	DIFF	% DIFF	NOT ACC.	ACC.	DIFF	% DIFF
CCSM3 A1FI	477	360	-117	-25%	735	602	-132	-18%
CCSM3 A2	441	313	-128	-29%	737	587	-150	-20%
CCSM3 B1	335	219	-116	-35%	395	294	-102	-26%
CGCM3 A2	476	348	-128	-27%	742	594	-148	-20%
CGCM3 B1	428	312	-116	-27%	452	304	-148	-33%
20c AVG.	44	27	-17	-39%				

Table 12 – Continued.

RIVERSIDE								
	2050s				2090s			
	NOT ACC.	ACC.	DIFF	% DIFF	NOT ACC.	ACC.	DIFF	% DIFF
CCSM3 A1FI	625	548	-76	-12%	1063	967	-96	-9%
CCSM3 A2	586	499	-88	-15%	1021	919	-102	-10%
CCSM3 B1	509	431	-77	-15%	741	619	-122	-16%
CGCM3 A2	563	459	-104	-18%	966	851	-114	-12%
CGCM3 B1	513	421	-91	-18%	780	642	-138	-18%
20c AVG.	60	45	-14	-24%				

SACRAMENTO								
	2050s				2090s			
	NOT ACC.	ACC.	DIFF	% DIFF	NOT ACC.	ACC.	DIFF	% DIFF
CCSM3 A1FI	262	213	-49	-19%	440	384	-56	-13%
CCSM3 A2	233	179	-54	-23%	438	381	-57	-13%
CCSM3 B1	202	154	-48	-24%	295	225	-70	-24%
CGCM3 A2	196	143	-53	-27%	368	294	-73	-20%
CGCM3 B1	166	119	-47	-28%	275	198	-77	-28%
20c AVG.	27	18	-9	-34%				

SAN DIEGO								
	2050s				2090s			
	NOT ACC.	ACC.	DIFF	% DIFF	NOT ACC.	ACC.	DIFF	% DIFF
CCSM3 A1FI	916	785	-131	-14%	1865	1725	-140	-7%
CCSM3 A2	663	542	-121	-18%	1667	1526	-141	-8%
CCSM3 B1	555	451	-104	-19%	797	667	-131	-16%
CGCM3 A2	628	515	-113	-18%	1535	1387	-149	-10%
CGCM3 B1	525	421	-104	-20%	750	610	-140	-19%
20c AVG.	68	47	-20	-30%				

SAN FRANCISCO								
	2050s				2090s			
	NOT ACC.	ACC.	DIFF	% DIFF	NOT ACC.	ACC.	DIFF	% DIFF
CCSM3 A1FI	178	116	-62	-35%	226	162	-64	-28%
CCSM3 A2	173	106	-67	-39%	247	183	-64	-26%
CCSM3 B1	157	101	-56	-36%	171	113	-58	-34%
CGCM3 A2	178	116	-62	-35%	183	123	-60	-33%
CGCM3 B1	162	96	-66	-41%	161	107	-54	-33%
20c AVG.	53	33	-20	-37%				

Table 12 – Continued.

SAN JOSE								
	2050s				2090s			
	NOT ACC.	ACC.	DIFF	% DIFF	NOT ACC.	ACC.	DIFF	% DIFF
CCSM3 A1FI	184	129	-55	-30%	398	302	-96	-24%
CCSM3 A2	172	116	-57	-33%	411	320	-92	-22%
CCSM3 B1	156	106	-51	-32%	281	201	-80	-29%
CGCM3 A2	187	127	-60	-32%	297	205	-92	-31%
CGCM3 B1	166	103	-62	-38%	256	176	-80	-31%
20c AVG.	27	18	-9	-33%				

Table 13 – Comparison of each MSA's non-acclimatized mortality versus the acclimatized mortality using the DIS-4 method. Values represent total annual mortality by MSA for the 2050s and 2090s under each model scenario for the medium population projection (for age 65+).. GCM20c values are historical annual means from 1980-1999. Continued on the next page.

FRESNO								
	2050s				2090s			
	NOT ACC.	ACC.	DIFF	% DIFF	NOT ACC.	ACC.	DIFF	% DIFF
CCSM3 A1FI	132	96	-36	-27%	266	212	-54	-20%
CCSM3 A2	123	85	-38	-31%	264	201	-63	-24%
CCSM3 B1	109	70	-39	-36%	192	123	-69	-36%
CGCM3 A2	113	65	-48	-43%	255	167	-88	-35%
CGCM3 B1	102	55	-47	-46%	202	108	-94	-46%
20c AVG.	15	7	-8	-52%				

LOS ANGELES								
	2050s				2090s			
	NOT ACC.	ACC.	DIFF	% DIFF	NOT ACC.	ACC.	DIFF	% DIFF
CCSM3 A1FI	1511	725	-786	-52%	2997	1763	-1235	-41%
CCSM3 A2	1369	539	-830	-61%	2973	1650	-1323	-45%
CCSM3 B1	1028	338	-690	-67%	1501	680	-821	-55%
CGCM3 A2	1465	598	-867	-59%	2890	1576	-1315	-45%
CGCM3 B1	1273	536	-737	-58%	1710	605	-1105	-65%
20c AVG.	165	45	-120	-73%				

OAKLAND								
	2050s				2090s			
	NOT ACC.	ACC.	DIFF	% DIFF	NOT ACC.	ACC.	DIFF	% DIFF
CCSM3 A1FI	315	77	-238	-75%	726	202	-524	-72%
CCSM3 A2	299	63	-236	-79%	641	178	-463	-72%
CCSM3 B1	252	56	-196	-78%	413	90	-322	-78%
CGCM3 A2	319	59	-260	-81%	579	134	-444	-77%
CGCM3 B1	294	54	-240	-82%	468	89	-379	-81%
20c AVG.	49	9	-39	-81%				

ORANGE COUNTY								
	2050s				2090s			
	NOT ACC.	ACC.	DIFF	% DIFF	NOT ACC.	ACC.	DIFF	% DIFF
CCSM3 A1FI	477	227	-249	-52%	735	437	-298	-41%
CCSM3 A2	441	178	-263	-60%	737	405	-332	-45%
CCSM3 B1	335	109	-226	-68%	395	179	-216	-55%
CGCM3 A2	476	189	-287	-60%	742	406	-335	-45%
CGCM3 B1	428	184	-245	-57%	452	154	-298	-66%
20c AVG.	44	12	-32	-74%				

Table 13 – Continued.

RIVERSIDE								
	2050s				2090s			
	NOT ACC.	ACC.	DIFF	% DIFF	NOT ACC.	ACC.	DIFF	% DIFF
CCSM3 A1FI	625	449	-175	-28%	1063	838	-225	-21%
CCSM3 A2	586	382	-205	-35%	1021	782	-239	-23%
CCSM3 B1	509	324	-184	-36%	741	466	-275	-37%
CGCM3 A2	563	329	-234	-42%	966	702	-264	-27%
CGCM3 B1	513	302	-211	-41%	780	458	-322	-41%
20c AVG.	60	29	-31	-52%				

SACRAMENTO								
	2050s				2090s			
	NOT ACC.	ACC.	DIFF	% DIFF	NOT ACC.	ACC.	DIFF	% DIFF
CCSM3 A1FI	262	147	-114	-44%	440	309	-131	-30%
CCSM3 A2	233	111	-122	-52%	438	294	-145	-33%
CCSM3 B1	202	94	-108	-54%	295	139	-157	-53%
CGCM3 A2	196	79	-117	-60%	368	195	-173	-47%
CGCM3 B1	166	65	-101	-61%	275	102	-173	-63%
20c AVG.	27	8	-19	-71%				

SAN DIEGO								
	2050s				2090s			
	NOT ACC.	ACC.	DIFF	% DIFF	NOT ACC.	ACC.	DIFF	% DIFF
CCSM3 A1FI	916	600	-316	-34%	1865	1500	-365	-20%
CCSM3 A2	663	369	-294	-44%	1667	1287	-380	-23%
CCSM3 B1	555	303	-252	-45%	797	480	-318	-40%
CGCM3 A2	628	331	-298	-47%	1535	1135	-400	-26%
CGCM3 B1	525	274	-251	-48%	750	401	-348	-46%
20c AVG.	68	24	-44	-65%				

SAN FRANCISCO								
	2050s				2090s			
	NOT ACC.	ACC.	DIFF	% DIFF	NOT ACC.	ACC.	DIFF	% DIFF
CCSM3 A1FI	178	59	-119	-67%	226	98	-128	-56%
CCSM3 A2	173	46	-127	-74%	247	109	-138	-56%
CCSM3 B1	157	55	-103	-65%	171	53	-118	-69%
CGCM3 A2	178	54	-125	-70%	183	67	-116	-63%
CGCM3 B1	162	35	-127	-78%	161	49	-112	-70%
20c AVG.	53	14	-38	-73%				

Table 13 – Continued.

SAN JOSE								
	2050s				2090s			
	NOT ACC.	ACC.	DIFF	% DIFF	NOT ACC.	ACC.	DIFF	% DIFF
CCSM3 A1FI	184	68	-115	-63%	398	190	-208	-52%
CCSM3 A2	172	54	-119	-69%	411	199	-213	-52%
CCSM3 B1	156	57	-99	-64%	281	101	-180	-64%
CGCM3 A2	187	58	-129	-69%	297	111	-186	-63%
CGCM3 B1	166	39	-126	-76%	256	79	-177	-69%
20c AVG.	27	8	-19	-69%				

4. DISCUSSION

The goal of this project has been to develop the most robust estimates of projected changes in heat-related mortality over the next century for nine major urban areas in California. Those estimates are found in Chapter 3, along with estimates on frequencies of synoptic patterns, excessive heat event days (numbers of offensive weather type days), and unacclimatized and acclimatized estimates of mortality. Of course, there are a number of uncertainties surrounding the mortality estimates, and they have been discussed as well. In this chapter, we will try to evaluate all of the data in Chapter 3 and discuss the significance of the findings.

We determined a number of synoptic patterns at the 500, 700, and 850mb levels that contribute to heat during the summer. Most all of these patterns are identified as exhibiting a strong ridge over the western United States, which is frequently associated with descending air aloft and at the surface. The ramifications of this flow are twofold: descending air inhibits cloud and precipitation development, and these dry conditions and increased solar radiation income contribute to hotter temperatures at the surface.

Using the various GCM models and emissions scenarios for the 2050s and 2090s, is the results strongly suggest that the most extreme of these synoptic patterns, with the strongest ridge development, will become more predominant during these future decades. This contributes to a much greater number of "offensive weather type" days, where DT and MT situations will predominate even more than they do today. Not surprisingly, the dry, generally clear, and very hot DT weather type will become much more frequent in Fresno, Riverside, and Sacramento, inland locales where atmospheric moisture is relatively low. The very warm and much more humid MT weather type will be more frequent in Miramar, Mountain View, and Los Angeles, where relative humidities are naturally higher than the more inland locales. Of course, the increases in the projected frequency of these synoptic patterns vary by model and scenario, with the "business as usual" scenario showing the largest increases. The range in weather type frequency that occurs between GCMs is significant. For example, in Miramar, the offensive MT weather type can vary over 30 percent between models in the very warm month of September. Similar variations are found at some of the other locations. Even if we consider this large range to be part of a "sensitivity analysis", it is difficult for a decision-maker come to grips with these large variations among models.

The regression terms regarding the relationship between mortality at each locale and SSC weather type show some intuitive trends but also some unexplainable ones. For example, the importance of the DT weather type is very apparent, and the DT dummy variable is statistically

significant in 18 of the 27 regressions. The MT variable is only important in the "over 74" regressions, which intuitively are the strongest models among the different age groups. Particularly within the "over 74" models, it seems clear that regression coefficients are highest among the older, more established California cities, such as Oakland, Los Angeles, and San Francisco. These cities undoubtedly support a larger population of individuals who would be most susceptible to heat-related issues.

One surprise is the comparative lack of importance of the "day in sequence" (DIS) and "time of season" (TOS) variables. Each appears only three times in the 27 regression models, and most of these appearances are in the oldest age group models. All the TOS variables, when statistically significant, are properly inversely related, indicating that heat late in the summer season has less of an impact on mortality than early season heat. However, only 2 of the 3 DIS variables are intuitive and directly related to mortality. This is a lower representation of these variables than occurs in the US cities that have synoptic heat watch-warning systems (HWWS), particularly those in the eastern and Midwestern United States (Sheridan and Kalkstein 2004).

One important indicator of how important climate change might be on human health is the evaluation of consecutive day offensive events shown in Figures 9 and 10. In some of the inland locations, there is already a sizable number of long consecutive day offensive weather type events; for example, about 2 events of 10 or more days duration occur at present in a typical summer in Fresno, and over 4 of these long events occurs seasonally on average at Riverside. These numbers increase predictably in the 2050s and 2090s, using all model scenarios. But maybe even more problematic are the increases in frequency of these events at the cooler, coastal locations. At all three coastal stations, an event of 7 days or more occurs slightly over 1 time per summer on average. These numbers generally double for the 2050s and triple for the 2090s (even higher for A1FI) for most of the stations.

We suggest that these rises in the frequency of long-duration heat events at coastal locations are more significant than those in the inland stations, even though there will still remain slightly more long events inland under the various models. Since long consecutive day offensive events are so rare in Los Angeles, San Diego, and in the Bay Area, a sharp rise will most likely contribute to very large increases in heat-related mortality. Intuitively, these increases should be larger than those found in Riverside, Fresno, and Sacramento. It is a well-known bioclimatological principle that extreme meteorological events have a greater negative impact on humans and animals than the more frequent ones. Thus, the inland locales are already exposed to a few episodes per year of at least week-long heat events; the coastal locales are exposed to many less today. A tripling of such events within the coastal population centers can thus be expected to have an inordinate impact on heat-related mortality in those cities.

There are a number of uncertainties when developing the future heat-related mortality estimates. Among them are:

- The assumptions inherent in utilizing the output of GCMs, which vary considerably from one to another in their ability to reproduce certain features of the climate; this is also true about the emissions scenarios;
- The uncertainty of how the population totals and demographics may change during the upcoming 50-90 years;
- The impact of acclimatization upon the mortality estimates.

All of these may have a significant impact on mortality estimates. Nevertheless, there is certainly some value in developing these estimates, which can be used as high-, low- and mid-bounds and can provide some range of how heat-related mortality may change in future decades. A range of policy issues can then be considered, and they can be altered as the future situation becomes more precisely known. However, it is important to view these numbers as rough projections, and they should be quoted with care to express the lack of certainty therein.

Figures 17-25 demonstrate the range of estimates for the different model possibilities and emissions scenarios. The range in estimates between the A1FI and B1 scenarios is highly variable from region to region. For Fresno as an example, the range is relatively small, even for the 2090s estimates. The B1 mortality estimate for an average summer is in the 190s, much higher than today's seasonal heat-related mortality, but only within 70 deaths of the highest (A1FI) estimate. The difference between the lowest and highest estimate is only 26 percent. Conversely, for San Diego, the range between B1 and A1FI is much larger. In the 2090s, the B1 scenario estimates almost 800 heat-related deaths in an average summer in San Diego, while the A1FI estimate is well over double, at 1865 deaths. Interestingly, the largest ranges between the model estimates are found in the Southern California regions of Los Angeles, San Diego, and Orange County. These all show spreads in the 2090 of double the number of estimated heat-related deaths between the B1 and A1FI scenarios. Conversely, the smallest variations between scenarios are found in the hot, dry inland cities of Fresno and Riverside.

The mortality increases for the various emissions scenarios are regionally coherent as well. For example, for the A1FI scenario, the greatest increases in heat-related mortality between the 2000s and 2050s are also in the Southern California cities. San Diego leads the group, with a 650% rise in average summer season heat-related mortality between the present and the 2050s. This is followed by Orange County (601% increase) and Los Angeles (532% increase). The smallest increases are in Oakland (343%), San Jose (300%), and San Francisco (157%). Of course, ALL the California cities exhibit a rapid rise in mortality for the A1FI scenario, but clearly the most dramatic of these increases are in the southern portion of the state.

For the B1 scenario mortality differences between the 2000s and 2050s, there is still good regional coherence, but the largest increases are in the hot, dry cities of Fresno (379%) and Riverside (375%). The Southern California and Bay Area cities show lower increases and are quite similar in response (e.g. San Diego, 267%; Oakland, 265%; Los Angeles, 260%). Again, while there are regional similarities, the reasons why the hot, dry cities would have the largest increases for the B1 scenario are not known. Of course, the B1 mortality estimates are considerably lower than the A1FI.

When evaluating the projected mortality increases from the 2050s to 2090s, across the board the percentage increases are lower than the period from the 2000s to 2050s. There is also much less spatial coherence among the California cities. For example, for the A1FI scenario, the city with the greatest percentage increase in heat-related mortality from the 2050s to 2090s is Oakland, with a 130% increase between those decades, followed by San Jose (116%). The lowest percentage increase areas, Orange County (54%) and San Francisco (26%) clearly have little in common in terms of climate and urban structure . For the B1 scenario, not surprisingly the 2050s to 2090s percentage mortality increases are considerably lower, with San Jose and Fresno showing the steepest increases (around 80%) and San Francisco illustrating the smallest (9%). Obviously, for virtually all the cities, we can expect significant rises in heat-related mortality, but policy-makers will have to contend with the spread of estimates between the different emissions scenarios and climate models.

Of course, another source of variation is the implementation of a population growth scenario. The figures cited above assume a medium population growth, but the numbers may vary greatly if the population grows faster or slower than expected (Table 11). For the 2050s for Fresno, for example, assuming no population growth at all (probably an unrealistic assumption), only 32 people are estimated to die of heat during an average summer. Using a high population growth model, this number balloons to 153 deaths. Similar ranges are found for the other cities as well. Thus, for the purposes here, and to reduce another layer of uncertainty, we have chosen to concentrate on the medium population projection.

The final source of variation is the role of acclimatization on heat-related mortality. Our procedure, which assumes that in an acclimatized world, we will react with less sensitivity during consecutive day runs of offensive weather type days, shows significant reductions when compared to the unacclimatized results. The decreases of around 20-40 percent, as we found, are similar to acclimatized mortality decreases reported in other literature (Gosling et al. 2009, Knowlton et al. 2007). The greatest mortality reductions will occur in the Bay Area locales, and the smallest will occur within the hot inland cities. This seems intuitive, since even using our

DIS-2 and DIS-4 procedure, there will be a greater number of offensive days in the hottest cities. This noted, there is a large level of uncertainty with the acclimatized results, as we have chosen a new acclimatization procedure to utilize for this research. Not least, there is considerable uncertainty with regard to adaptive capacity. Given California's unique climate, an increase in heat events over coastal California within its relatively mild climate may mean that physiological adaptation in coastal areas will be less efficient than inland where hotter conditions will become more constant. However, these same coastal locations are ones for which it is likely that significant increases in behavioral mechanisms (e.g., air conditioning prevalence) will take place, in comparison to inland locations where such mechanisms are already near saturation.,.

The results from this analysis are generally intuitive, and cities in a similar climate environment generally respond similarly in terms of heat-mortality response. However, as advised previously, these results should always be reviewed with caution because of the number of uncertainties involved, including those related to the variations among the climate models and various emissions scenarios. However, even with these caveats, the numbers provide useful guidance in trying to determine how a changing climate will alter the number of heat-related deaths in major California cities.

5. SUMMARY AND CONCLUSIONS

To help assess the impacts of climate change on human health, the goal of this project was to provide a range of 21st century heat-related mortality projections for nine major urban centers in the state of California (Table 14). Previous research has shown that increased heat-related mortality in each urban area can be related to the incidence of oppressive weather types – most notably, Dry Tropical (DT) and Moist Tropical (MT) weather types (Sheridan and Kalkstein 2004, Sheridan et al. 2009). Based upon similar studies and the expertise of the researchers involved, synoptic climatological methods were utilized to incorporate the variables that general circulation models (GCMs) project best in order to make these estimations.

Using 45 years of warm-season (March-November) climate data, a novel six-step method was utilized to develop historical mid-tropospheric circulation patterns at three levels of the atmosphere, which could then be related to the oppressive weather types (DT or MT). Once an historical relationship between patterns and types was established, future projections of the frequency and seasonality of these patterns were used to determine the future occurrence of oppressive weather types.

Historical relationships between weather and mortality were derived to assess potential impacts of heat on human mortality using data from 1975-2004 for the nine regions. Mortality rates accounted for weather type, weather type persistence, and seasonality, and were developed separately for three separate age groups. These relationships were then utilized along with the future weather type projections to estimate the changes in heat-related mortality for each urban area.

At both the 500 mb and 700 mb level, three warm patterns are prevalent in summer, while at the 850 mb level, four patterns exhibit summer seasonality. At both 500 mb and 700 mb, the frequency of the more zonal early-summer pattern is projected to increase in the 2050s and 2090s, while the seasonality of these patterns broadens deeper into both the spring and autumn. At the 850 mb level, the disparity between the future frequency and seasonality of the summer patterns is not as evident, although the most frequent historical pattern does show the greatest increase in occurrence in future summers. At all levels, the A1FI and A2 scenarios show the greatest increases of the three scenarios used herein.

The circulation pattern results carry over into the weather type results as well. The more inland stations (Fresno, Riverside and Sacramento) show a dramatic increase in the frequency of DT weather types in every month, exacerbated in the higher emissions scenarios and deeper into the century (Table 15). These stations also show an increase in MT frequencies in the spring and autumn. The stations located closer to the coast (El Toro, Miramar and Mountain View) show a

marked increase in MT days, while DT days are also projected to increase in most months, but to a lesser extent.

These results translate into a substantial rise in prolonged heat events (Table 14). By the 2090s, 14+ consecutive day runs of oppressive weather types are projected to occur about once a year at each station, while the occurrence of 10+ day heat events is projected to increase nearly tenfold in some locations under the higher emissions scenarios.

Supporting previous research, the results here indicate that DT and/or MT weather types play a statistically significant role in increasing heat-related mortality in nearly every major urban center – especially for those over the age of 74. Thus, the broadened future seasonality and the increase in the frequency of these weather types along with the increased frequency of consecutive day heat events, is likely to have a substantial effect on mortality. Using the medium population projection, with the exception of San Francisco, all major urban centers could have a greater than tenfold increase in heat-related mortality in those over the age of 65 by the 2090s (Table 5.1). Collectively, heat related mortality in the medium population projection would rise by more than a factor of 9, to an annual total of 4684 to 8757 deaths per year depending upon GCM scenario. However, much of this increase is due in large part to a rising and aging population. In keeping a steady (age 65+) population from 2000 through 2099, the increase in mortality due specifically to a warming climate is projected to be 1.9 times (San Francisco) to 7.5 times (San Diego) greater than current levels by the 2090s under the A1FI scenario.

Two methods were developed to account for the well-documented effect of acclimatization on heat-related mortality – DIS-2 and DIS-4 – which eliminates the increased mortality before the 2nd or 4th (respectively) day in a heat event. Using the DIS-2 method with the medium population scenario for those aged 65 and over, statewide mortality increases to between 3626 to 7371 deaths per year, lessened by anywhere from 7% (San Diego) to 35% (Oakland) in the 2090s with A1FI (Table 15). With the DIS-4 method, these mortality increases were lessened by 20% (San Diego and Fresno) to 72% (Oakland), with a statewide range of 2334 to 5919. Though acclimatization is projected to help mitigate some heat-related mortality, it is important to note that despite the lessened impact, these numbers still represent overall increases in deaths due to a warming climate.

Table 14 – Summary of Heat-Related Mortality Estimates by MSA.

Urban Area	Mean Annual Heat Related Mortality (Age 65+)				
	20th century		2090s - Medium Growth		2090s - No Growth
	Unacclimatized	Acclimatized	Unacclimatized	Acclimatized	Unacclimatized
Fresno	15	11	192 - 266	162 - 244	26 - 36
Los Angeles	165	102	1501 - 2997	1112 - 2474	368 - 732
Oakland	49	28	413 - 726	248 - 472	85 - 149
Orange County	44	27	395 - 742	294 - 602	105 - 194
Riverside	60	45	741 - 1063	619 - 967	113 - 162
Sacramento	27	18	275 - 440	198 - 384	55 - 88
San Diego	68	47	750 - 1865	610 - 1725	207 - 511
San Francisco	53	33	161 - 247	107 - 183	71 - 110
San Jose	27	18	256 - 411	176 - 320	44 - 69
TOTAL	508	329	4684 - 8757	3526 - 7371	1074 - 2051

Table 15 – Summary of Oppressive Weather Type Days and 10+ Day Heat Events by MSA.

SSC Station	Mean Annual			
	Oppressive days		Heat events >10 days	
	20th Cent.	2090s	20th Cent.	2090s
El Toro	43	79 - 147	0.4	1.3 - 4.4
Fresno	84	120 - 184	1.8	3.2 - 5.0
Miramar	54	104 - 179	0.4	1.9 - 5.6
Mountain View	55	79 - 142	0.9	1.4 - 3.2
Riverside	103	150 - 207	2.4	4.0 - 5.0
Sacramento	62	106 - 178	0.6	1.5 - 5.0

6. RECOMMENDATIONS

Results from this study indicate that heat-related mortality in the nine major urban centers of California is projected to increase substantially throughout the 21st Century. The public is generally under-educated about the dangers of extreme heat and heat waves (Sheridan 2007, Kalkstein and Sheridan 2007). Because of this, many of the most vulnerable people are unaware of the risks associated with excessive heat events or of the proper steps to take to reduce their risk to heat exposure, and are uninformed about the locally funded assistance that is available to them, such as cooling shelters or water trucks.

The impacts of heat on human health actually transcend the climate change issue, as heat is already the major weather-related killer in the United States. Thus, many communities around the country already have sophisticated heat mitigation plans in place. These not only include public education, as described above, but also increased interaction between stakeholders, politicians, and the local National Weather Service office. Some of these plans are found online; for example, look at Philadelphia's online heat resources:

http://www.phila.gov/Health/keepingCool.html (main website)
http://www.phila.gov/Health/pdfs/heat_flyer.pdf (distributed to residents of Philadelphia so they know what to do during a heat wave)
http://www.phila.gov/Health/pdfs/StayCool.pdf (more detailed advice)

The National Weather Service has partnered with local health departments, utility companies, and the U.S. EPA to develop a system of heat watch/warning systems (HWWS) at various Weather Forecast Offices in the country. These systems provide guidance to forecasters, based upon the same types of synoptic models used in this research, to inform them which days are most dangerous to human health, and to suggest when to call excessive heat warnings and advisories. **We strongly recommend that systems like these are developed for every weather forecast office in California, irrespective of the impacts of climate change.**

Many communities have a heat-health task force presently in existence. These might also exist in a number of California cities, but it is probable that most cities do not have the stakeholder collaboration to develop such a task force. **We recommend that every major California city have a heat-health task force.** In most cities, these meet several times a year, especially before the heat season, to coordinate activities and to update the efficiency of mitigation plans. We would be glad to provide assistance, if asked, to develop such urban task forces, since we've had great experience doing this in the past.

Awareness, education, and intervention are the keywords to lessen heat-related mortality now and in a potentially warmer world. In the state of California, much can be done to improve all three of these items, and hopefully this analysis has pointed to the significance of the heat/health issue in the state, both presently and in the future.

REFERENCES

Anderson B.G. and Bell M.L. (2009): Weather-Related Mortality, How Heat, Cold, and Heat Waves Affect Mortality in the United States. *Epidemiology* **20(2)**: 205-213.

Ballester J., Rodo X., Giorgi F. (2010): Future changes in Central Europe heat waves expected to mostly follow summer mean warming. *Climate Dynamics* **98:** 277-284.

Basu R., Feng W.Y., Ostro B.D. (2008): Characterizing Temperature and Mortality in Nine California Counties. *Epidemiology*, **19:** 138-145.

Basu R. (2009): High ambient temperature and mortality: a review of epidemiologic studies from 2001 to 2008. *Environmental Health* **8(40)**: 1-13.

Beniston M. (2004): The 2003 heat wave in Europe: a shape of things to come? An analysis based on Swiss climatological data and model simulations. *Geophysical Research Letters* **31**. doi:10.1029/2003GL018857.

Beniston, M. (2007): Entering into the "greenhouse century": Recent record temperatures in Switzerland are comparable to the upper temperature quantiles in a greenhouse climate. *Geophysical Research Letters* **34:** L16710, 1-5.

Boer, G.J., B. Yu, S.J. Kim, and G.M. Flato. (2004): Is there observational support for an El Nino-like pattern of future global warming? *Geophysical Research Letters* 31: art. no. L06201.

Bouchama A., Dehbi M., Mohamed G., Matthies F., Shoukri M., Menne B. (2007): Prognostic Factors in Heat Wave-Related Deaths, A Meta-analysis. *Archives of Internal Medicine* **167(20):** E1-E7.

Brazel A., Gober P., Lee S.J., Grossman-Clarke S., Zehnder J., Hedquist B., Comparri B. (2007): Determinants of changes in the regional urban heat island (1990-2004) within Metropolitan Phoenix. *Climate Research* **33**: 171-182.

California Department of Finance (2007): Demographic Reports and Research Papers. Website: http://www.dof.ca.gov/research/demographic/reports/view.php Accessed July 2007

Caruba, A. (2008): Brownouts and blackouts: Power crisis in California. American Policy Center. http://americanpolicy.com/more/brownouts.htm

Centers for Disease Control (CDC) (2004): Extreme heat: a prevention guide to promote your personal health and safety. www.bt.cdc.gov/disasters/extremeheat/heat_guide.asp.

Census (2010): Census Bureau Homepage. Website: http://www.census.gov/ Accessed July 2007.

Clark R., Brown S., Murphy J. (2006): Modeling northern hemisphere summer heat extreme changes and their uncertainties using a physics ensemble of climate sensitivity experiments. *Journal of Climate* **19**: 4418–4435.

Collins W.D., Bitz C.M., Blackmon M.L., Bonan G.B., Bretherton C.S., Carton J.A., Chang P., Doney S.C., Hack J.A., Henderson T.B., Kiehl J.T., Large W.G., McKenna D.S., Santer B.D., Smith R.D. (2006): The Community Climate System Model: CCSM3. White paper, NCAR, Boulder, Colorado, USA.

Cuell C., Bonsall B. (2009): An assessment of climatological synoptic typing by principal component analysis and k-means clustering. *Theoretical and Applied Climatology* **98**: 361-373.

Curriero F.C., Heiner K.S., Samet J.M., Zeger S.L., Strug L., Patz J.A. (2002): Temperature and mortality in 11 cities of the eastern United States. *American Journal of Epidemiology*, **155:** 80-87.

Davis R.E., Knappenberger P.C., Novicoff W.M., Michaels P.J. (2002): Decadal changes in heat-related human mortality in the Eastern US. *Climate Research* **22**: 175–184

Demuzere M., Werner M., van Lipzig N.P.M., Roeckner E. (2009): An analysis of present and future ECHAM5 pressure fields using a classification of circulation patterns. *International Journal of Climatology,* **29**, 1796-1810.

Dessai S. (2003): Heat stress and mortality in Lisbon part II. An assessment of the potential impacts of climate change. *International Journal of Biometeorology* **48**: 37–44

Donaldson G.C., Kovats R.S., Keatinge W.R., McMicheal A.J. (2001): Heat- and cold related mortality and morbidity and climate change. In: Maynard RL (ed) Health effects of climate change in the UK. Department of Health, London, pp. 70–80

Doyon B., Belanger D., Gosselin P. (2008): The potential impact of climate change on annual and seasonal mortality for three cities in Quebec, Canada. *International Journal of Health Geographics* **7:23:** 1-12.

Ebi K.L., Teisberg T.J., Kalkstein L.S., Robinson L., Weiher R.F. (2004): Heat Watch/Warning Systems Save Lives: Estimated Costs and Benefits for Philadelphia 1995-1998. *Bulletin of the American Meteorological Society*, **85**: 1067-74.

Ellis F.P. and F. Nelson F. (1978): Mortality in the elderly in a heat wave in New York City, August, 1975. *Environmental Research* **15**: 504-512.

Environment Canada (2009a): The Third Generation Coupled Global Climate Model (CGCM3), http://www.cccma.bc.ec.gc.ca/models/cgcm3.shtml, Accessed in January 2010.

Environment Canada (2009b): The Third Generation Atmospheric General Circulation Model (AGCM3), http://www.cccma.bc.ec.gc.ca/models/gcm3.shtml, as accessed in January 2010.

Gershunov A., Cayan D.R., Iacobellis S.F. (2009): The Great 2006 heat wave over California and Nevada: Signal of an Increasing Trend. *Journal of Climate*, **22(23):** 6181-6203.

Gillett N.P., Allen M.R., Williams K.D. (2003): Modeling the atmospheric response to doubled CO2 and depleted stratospheric ozone using a stratosphere-resolving coupled GCM. *Quarterly Journal of the Royal Meteorological Society*, **129**: 947-966.

Gosling S.N., Lowe, J.A., McGregor G.R, Pelling M., Malamud B.D. (2009): Associations between elevated atmospheric temperature and human mortality: a critical review of the literature. *Climatic Change* **92**: 299-341.

Greene, J.S., L.S. Kalkstein, D. Mills, and J. Samenow, under review. An examination of climate change on extreme heat events and climate/mortality relationships in large US cities. *Weather, Climate, and Society.*

Hajat S.A., Ben G., Gouveia, N., Wilkinson, P. (2005): Mortality Displacement of Heat-Related Deaths: A Comparison of Delhi, Sao Paulo, and London. *Epidemiology* **16:** 613-620.

Hajat S., Armstrong B., Baccini M., Biggeri A., Bisanti L., Russo A., Paldy A., Menne B., Kosatsky T. (2006): Impact of High Temperatures on Mortality: Is There an Added Heat Wave Effect? *Epidemiology*, **17:** 632-638.

Harlan S.L., Brazel A.J., Prashad L., Stefanov W.L., Larsen L. (2006): Neighborhood microclimates and vulnerability to heat stress. *Social Science & Medicine* **63**: 2847-2863.

Hayhoe K., Cayan D., Field C.B., Frumhoff P.C., Maurer E.P., Miller N.L., Moser S.C., Schneider S.H., Cahill K.N., Cleland E.E., Dale L., Drapek R., Hanemann R.M., Kalkstein L.S., Lenihan J., Lunch C.K., Neilson R.P., Sheridan S.C., Verville J.H. (2004): Emissions

pathways, climate change, and impacts on California. *Proceedings of the National Academy of Sciences U S A* **101**: 12422–12427.

Hayhoe, K., Sheridan S.C., Kalkstein L.S., Greene J.S. (2010): Climate change, heat waves, and mortality projections for Chicago. *Journal of Great Lakes Research*, in press.

Hope, P.K. (2006): Projected future changes in synoptic systems influencing southwest Western Australia. *Climate Dynamics* **26:** 765-780.

Intergovernmental Panel on Climate Change (IPCC) (2001): Climate change 2001: impacts adaptation and vulnerability. In: McCarthy J.J., Canziani O.F., Leary N.A., Dokken D.J., White K.S. (eds) Cambridge University Press, Cambridge, 1032 pp.

Johnson D.P., Wilson J.S., Luber G.C. (2009): Socioeconomic indicators of heat-related health risk supplemented with remotely sensed data. *International Journal of Health Geographics* **8(57).**

Kalkstein, A.J., and S.C. Sheridan (2007): The social impacts of the heat-health watch/warning system in Phoenix, Arizona: Assessing the perceived risk and response of the public. *International Journal of Biometeorology* **52**: 43-55.

Kalkstein L.S. and K.M. Valimont K.M. (1987): Climate effects on human health. In: Potential Effects of Future Climate Changes on Forests and Vegetation, Agriculture, Water Resources, and Human Health. *EPA Science and Advisory Committee Monograph* **25389**: 122-152.

Kalkstein, L.S., Greene, J.S., Mills, D.,Perrin, A., Samenow, J., and Cohen, J-C. (2008): Analog European Heat Waves for U.S. Cities to Analyze Impacts on Heat-Related Mortality. *Bulletin of the American Meteorological Society* **89**: 75-86.

Kalkstein, L.S, Greene, J.S., Mills D., and Samenow, J. (2010): An Evaluation of the Progress in Reducing Heat-Related Human Mortality in Major U.S. cities. *Natural Hazards,* DOI 10.1007/s11069-010-9552-3.

Kalnay, E., Kanamitsu, M., Kistler, R., Collins, W, Deaven, D., Gandin, L., Iredell, M., Saha, S., White, G., Woollen, J., Zhu, Y., Chelliah, M., Ebisuzaki, W., Higgins, W., Janowiak, J., Mo, K.C., Ropelewski, C., Wang, J., Leetmaa, A., Reynolds, R., Jenne, R., Joseph, D. (1996): The NCEP/NCAR 40-Year Reanalysis Project. *Bulletin of the American Meteorological Society* **77**: 437-471.

Keatinge W.R., Donaldson G.C., Cordioloi E., Martinelli M., Kunst A.E., Mackenbach J.P., Nayha S. (2000): Heat related mortality in warm and cold regions of Europe: observational study. *British Medical Journal* **321**: 670–673.

Kinney P., O'Neill M.S., Bell M.L., Schwartz J. (2008): Approaches for estimating effects of climate change on heat-related deaths: challenges and opportunities. *Environmental Science & Policy*, **11:** 87-96.

Klinenberg E. (2002): Heat wave: a social autopsy of disaster in Chicago. University of Chicago Press, Chicago.

Knapp P.A. (1992): Correlation of 700mb height data with seasonal temperature trends in the Great Basin (western USA): 1947-1987. *Climate Research* **2**, 65-71.

Knowlton K., Lynn B., Goldberg R.A., Rosenzweig C., Hogrefe C., Rosenthal J.K., Kinney P.L. (2007): Projecting heat-related mortality impacts under a changing climate in the New York City region. *American Journal of Public Health* **97**: 2028–2034.

Knowlton K., Rotkin-Ellman M., King G., Margolis H.G., Smith D., Solomon G., Trent R., English P. (2009): The 2006 California Heat Wave: Impacts on Hospitalizations and Emergency Department Visits. *Environmental Health Perspectives* **117(1):** 61-67.

Kovats R.S. and Hajat S. (2008): Heat Stress and Public Health: A Critical Review. *Annual Review of Public Health* **29**: 41-55.

Kysely J. (2009): Recent severe heat waves in central Europe: how to view them in a long-term prospect? *International Journal of Climatology* **30(1):** 89-109.

Kysely J., Huth R., Kim J. (2009): Evaluating heat-related mortality in Korea by objective classifications of 'air masses.' *International Journal of Climatology* **30(10):** 1484-1501.

Lee, C.C. (2010): The Relationship of Large-Scale Atmospheric Circulation Patterns to Tornadoes and the Impacts of Climate Change. Masters Thesis, Kent State University, Kent, Ohio, USA. 263 pp.

Luber, G. and McGeehin M. (2008): Climate Change and Extreme Heat Waves. *American Journal of Preventative Medicine* **35(1)**: 429-435.

Meehl G.A., and Tebaldi C. (2004): More intense, more frequent, and longer lasting heatwaves in the 21st century. *Science* **305**: 994–997.

Meehl G.A., Stocker T.F., Collins W.D., Friedlingstein P., Gaye A.T., Gregory J.M., Kitoh A., Knutti R., Murphy J.M., Noda A., Raper S.C.B., Watterson I.G., Weaver A.J., Zhao Z-C. (2007): Global climate projections. In: Solomon S., Qin D., Manning M., Chen Z., Marquis M., Averyt K.B., Tignor M., Miller H.L. (eds) Climate change 2007: the physical science basis. Contribution of working group I to the fourth assessment

report of the Intergovernmental Panel on Climate Change. Cambridge University Press, Cambridge, UK

National Climate Data Center (NCDC) (2007): Billion-dollar weather disasters, 1980-2006. Website: http://www.ncdc.noaa.gov/ol/reports/billionz.html. Accessed 13 March 2007

Nicholls N. (2009): Estimating changes in mortality due to climate change. *Climactic Change* **97:** 313-320.

O'Neill M.S. (2003): Air conditioning and heat-related health effects. *Applied Environmental Science and Public Health* **1**: 9-12.

O'Neill M.S., Carter R., Kish J.K., Gronlund C.J., White-Newsome J.L., Manarolla X., Zanobetti A., Schwartz J.D. (2009): Preventing heat-related morbidity and mortality: New approaches in changing climate. *Maturitas* **64:** 98-103.

Ostro B.D., Roth L.A., Green R.S., Basu R. (2009): Estimating the mortality effect of the July 2006 California heat wave. *Environmental Research* **109:** 614-619.

Schär C., Vidale P.L., Lüthi D., Frei C., Häberli C., Liniger M.A., Appenzeller C. (2004): The role of increasing temperature variability in European summer heatwaves. *Nature* **427**: 332–336.

Saunders I.R., Byrne J.M. (1999) Using surface and geopotential height fields for generating grid-scale precipitation. *International Journal of Climatology,* **19**, 1165-1176.Sheridan, S.C. (2007): A survey of public perception and response to heat warnings across four North American cities: an evaluation of municipal effectiveness. *International Journal of Biometeorology*, **52**: 3-15.

Sheridan S.C. (2002): The redevelopment of a weather type classification scheme for North America. *International Journal of Climatology* **22:** 51-68.

Sheridan S.C., Kalkstein L.S. (2004): Progress in heat watch-warning system technology. *Bulletin of the American Meteorological Society* **85**: 1931–1941

Sheridan, S.C., Kalkstein A.J., and Kalkstein L.S. (2009): Trends in heat-related mortality in the United States, 1975-2004. *Natural Hazards* **50**: 145-160. DOI:10.1007/s11069-008-9327-2

Sheridan, S.C. and Kalkstein A.J. (2010): Seasonal variability in heat-related mortality across the United States. *Natural Hazards*, in press.

Sheridan, S.C. and C.C. Lee (2010): Synoptic Climatology and the General Circulation Model. *Progress in Physical Geography* **34(1)**: 101-109.

Smoyer K.E. (1998): Putting risk in its place: methodological considerations for investigating extreme event health risk. *Social Science & Medicine* **47**: 1809–1824

Stone D.A., Weaver A.J., and Stouffer R.J. (2001): Projection of climate change onto modes of atmospheric variability. *Journal of Climate* **14**: 3551-3565.

Stott P.A., Stone D.A., Allen M.R. (2004): Human contribution to the European heatwave of 2003. *Nature* **432**: 610–613

Tebaldi C., Hayhoe K., Arblaster J.M., Meehl G.A. (2006): Going to Extremes, An Intercomparison of Model-Simulated Historical and Future Changes in Extreme Events. *Climactic Change,* **79**: 185-211.

Valleron, A.J. and Boumendil, A. (2004): Epidemiology and heat waves: analysis of the 2003 episode in France. *Comptes Rendus Biologies* **327**: 1125-1141.

Vrac, M., Hayhoe, K. and Stein, M. (2007): Identification and intermodal comparison of seasonal circulation patterns over North America. *International Journal of Climatology* **27:** 603-620.

Wilks, D.S. (2006): Statistical Methods in the Atmospheric Sciences, Second Edition. Academic Press, Elsevier, Burlington, Massachusetts, USA; San Diego, California, USA; London, UK. 627 pp.

Yarnal, B. (1993): Synoptic Climatology in Environmental Analysis: A primer. Belhaven Press, London and CRC Press, Inc., Boca Raton, Florida, USA. 192 pp.

GLOSSARY

500z – Geopotential height values (in meters) at which the atmospheric pressure is estimated to be 500 millibars.

700z – Geopotential height values (in meters) at which the atmospheric pressure is estimated to be 700 millibars.

850t – Air temperature values (in °C) at the 850 millibar pressure surface

A1FI – An extreme, non environmentally-friendly, emissions scenario for GCM model runs (sometimes referred to as the 'business as usual' scenario).

A2 – An intermediate emissions scenario for GCM model runs

AO – Arctic Oscillation

AOGCM – Atmospheric and Oceanic General Circulation Model – referred to normally as a GCM

B1 – A conservative, environmentally-friendly, emissions scenario for GCM model runs

CCSM3 – The Community Climate System Model 3, a coupled atmospheric and oceanic GCM from the

CDC – Centers for Disease Control and Prevention

CGCM3 – The Coupled Global Climate Model – version 3

CSA – Combined Statistical Area

Debias – The process of removing the mean monthly model bias at each grid point from a GCM's 20th Century data set and applying it to all of the same GCM's future data sets.

DFA – Discriminant Function Analysis

DIS – Day in Sequence. The number of consecutive days on which an oppressive (DT or MT) weather type occurred

DIS-2 – A method of accounting for acclimatization, where mortality from the first day of a heat event is ignored and only the increased mortality from the second day forward is included

DIS-4 – A method of accounting for acclimatization, where mortality from the first three days of a heat event is ignored, and only the increased mortality from the fourth day forward is included

DM – Dry Moderate weather type

DP – Dry Polar weather type

DT – Dry Tropical weather type

ENSO – El Nino / Southern Oscillation

FAT – The Fresno SSC station code

GCM – Global Climate Model or General Circulation Model

GCM20c – The 20th Century data from a GCM

HWWS – Heat Watch Warning System

IPCC – Intergovernmental Panel on Climate Change

MLR – Multinomial Logistic Regression

MM – Moist Moderate weather type

MP – Moist Polar weather type

MSA – Metropolitan Statistical Area

MT – Moist Tropical weather type

NAO – North Atlantic Oscillation

NKX – The Miramar SSC station code

NCAR – National Center for Atmospheric Research

NCEP – National Centers for Environmental Prediction

NNR – The NCEP/NCAR Reanalysis data set

NUQ – The Mountain View SSC station code

Oppressive Weather type – Any tropical SSC weather type – either Dry Tropical (DT) or Moist Tropical (MT)

NZJ – The El Toro SSC station code

PC – A principal component score created from a PCA

PCA – Principal Component Analysis

RIV – The Riverside SSC station code

SAC – The Sacramento SSC station code

SPSS – The Statistical software package used for analysis in this report

SRES – Special Reports on Emissions Scenarios

SSC – The Spatial Synoptic Classification

TOS – Time of Season. The day of the year.

TSC – The Two-Step Cluster analysis

APPENDIX A

The maps and graphs in Appendix A represent the synoptic circulation patterns and the monthly frequency of the CGCM3 global climate model. The 500z and 700z patterns are in meters, while the 850t patterns are in terms of °C. Contours for the 500z patterns are in 60m intervals, for 700z at 30m intervals, and for 850t at 2°C intervals. The bar graphs show the monthly frequency of each pattern in the GCM20c portion of the results (as averaged over the years 1970-1999) and the 2090s in the A2 and B1 scenarios.

CGCM3 500z Patterns and Seasonality

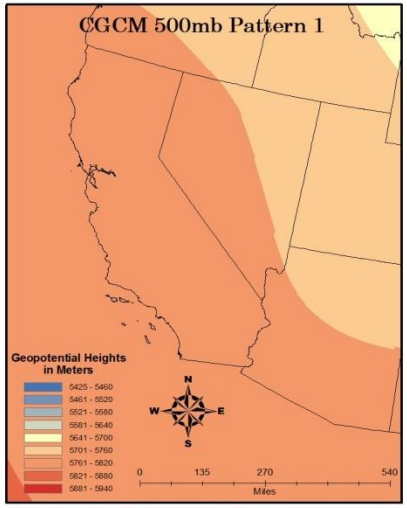

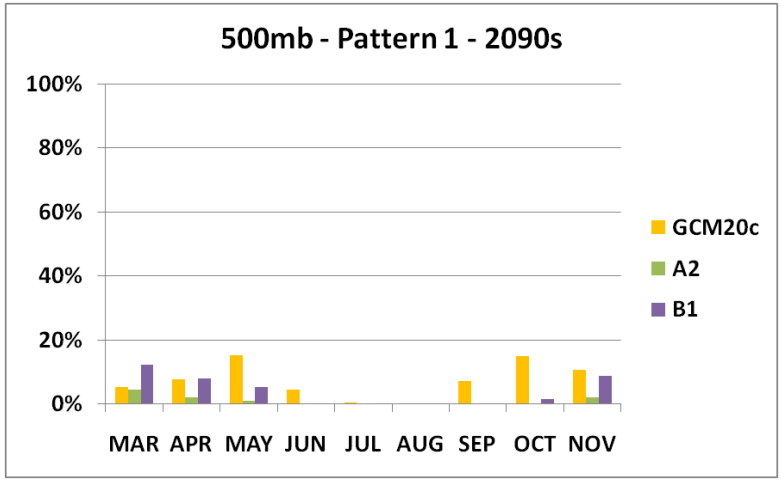

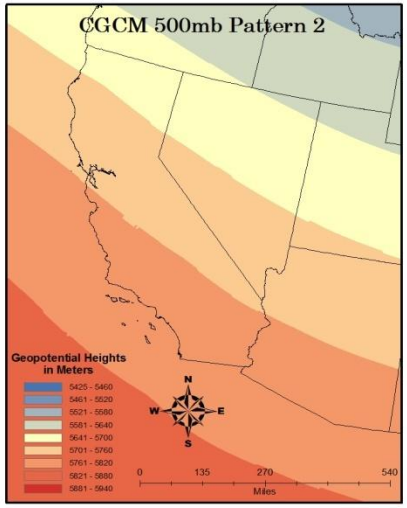

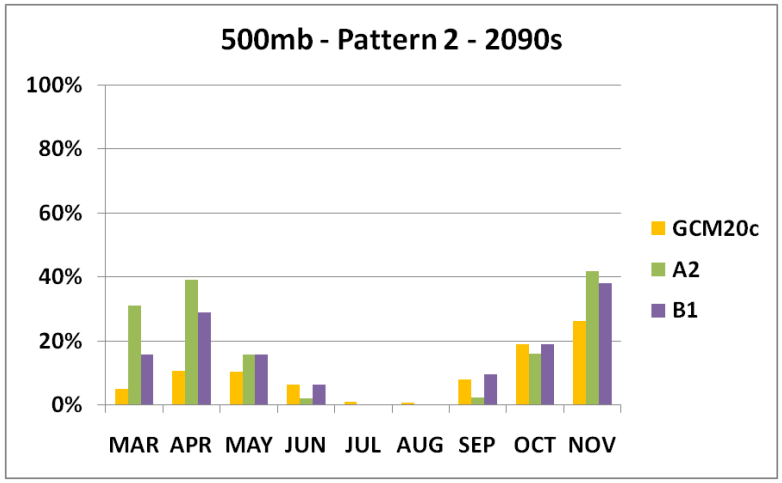

Figure A.1 – CGCM3 500z patterns and monthly frequency. Continued on the next page.

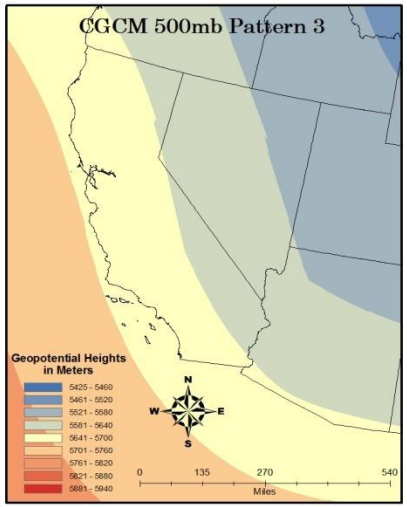

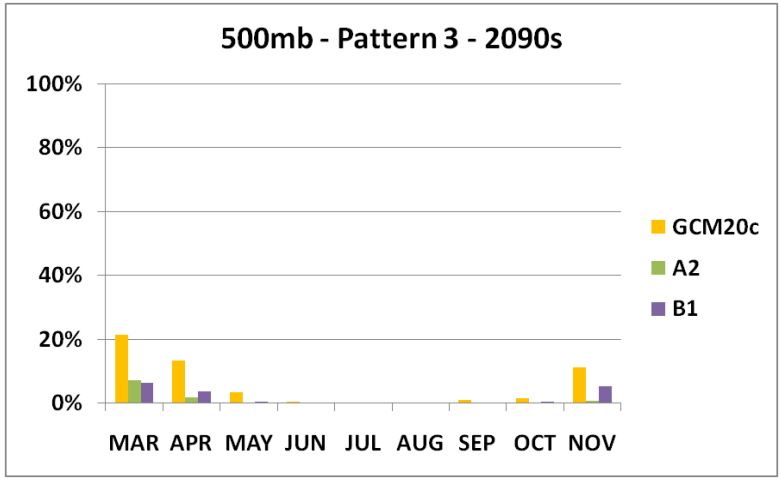

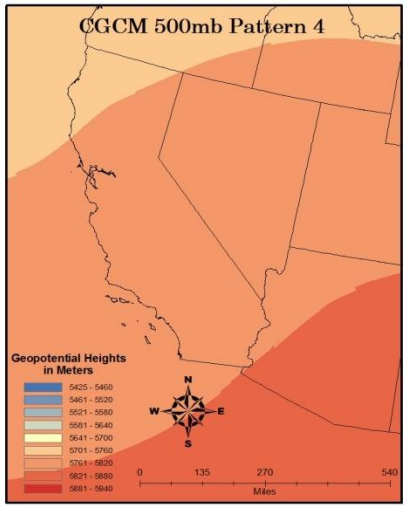

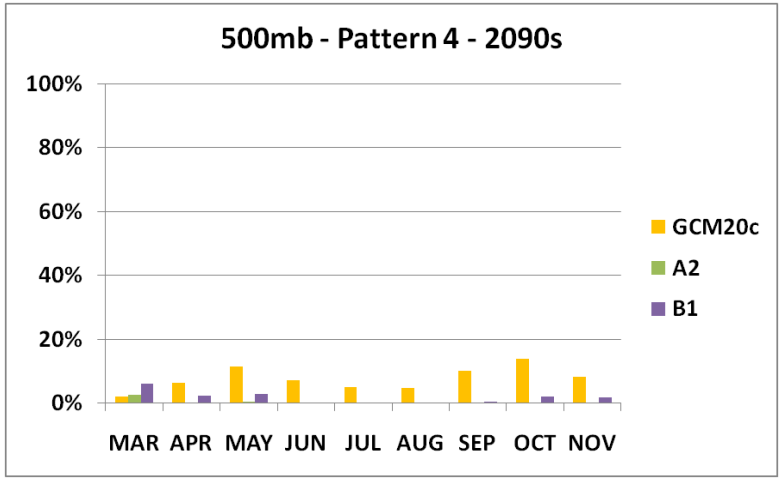

Figure A.1 – continued

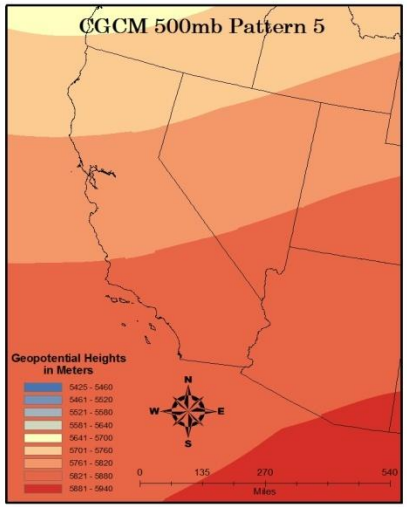

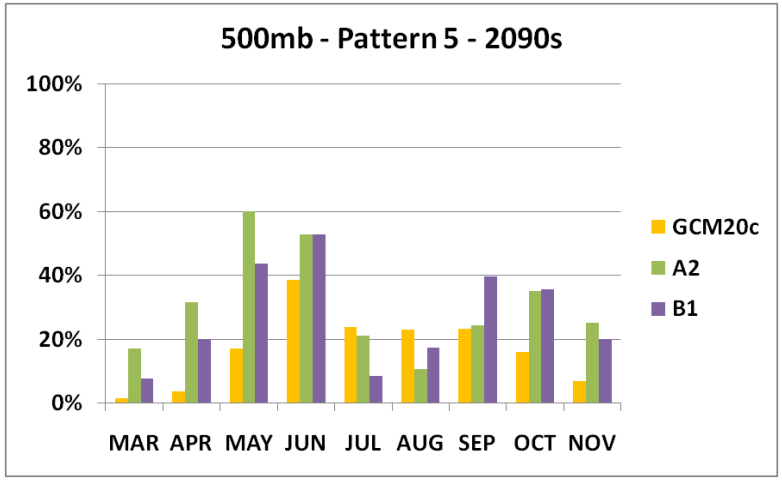

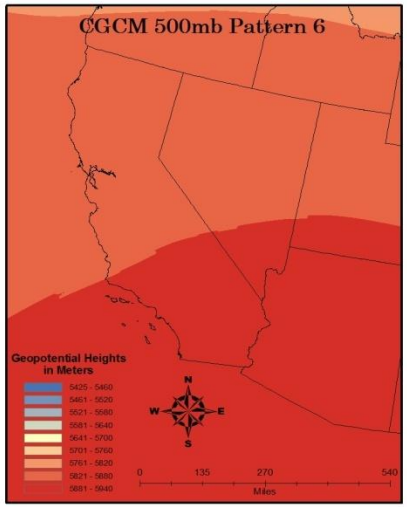

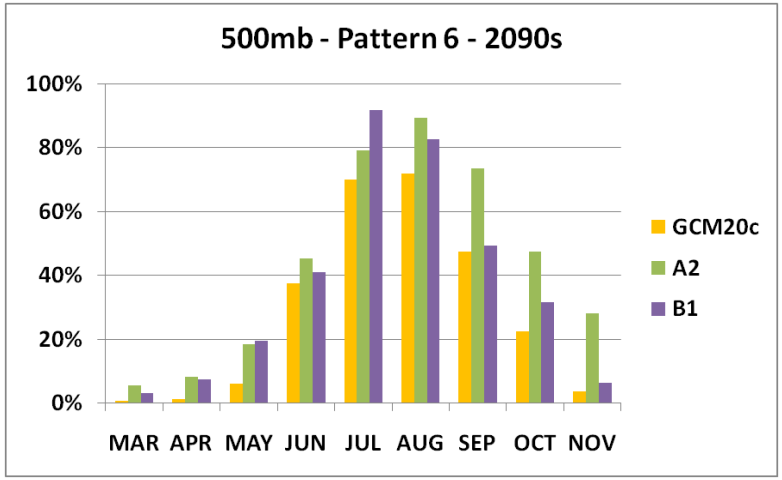

Figure A.1 – continued

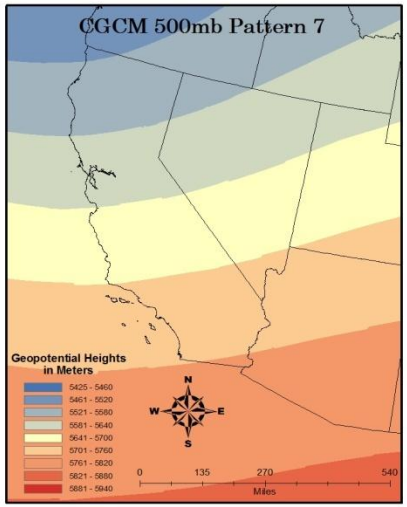

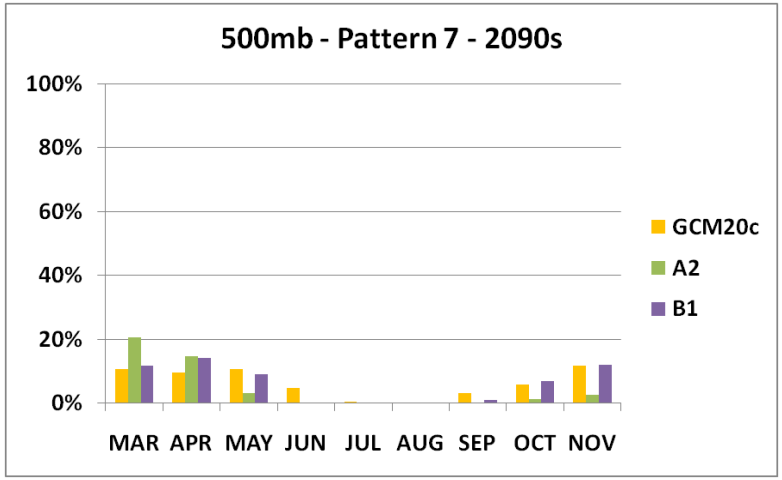

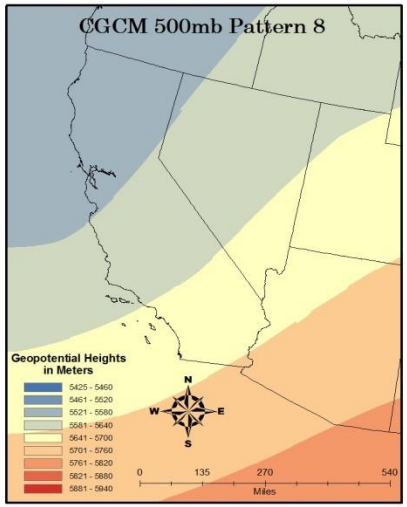

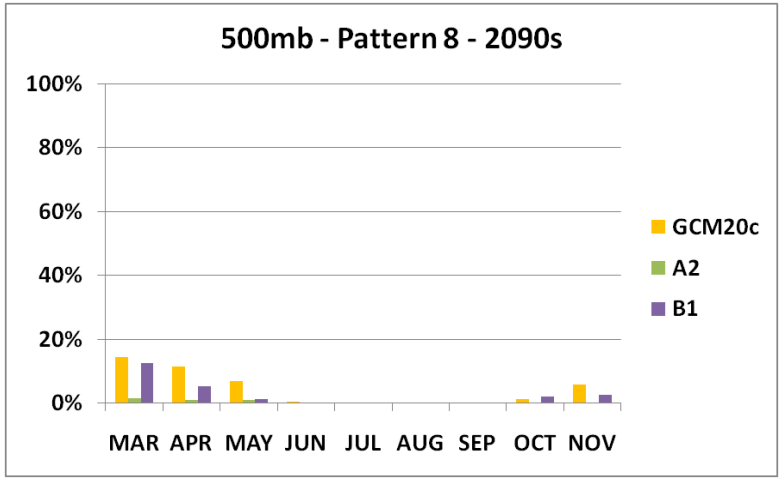

Figure A.1 – continued

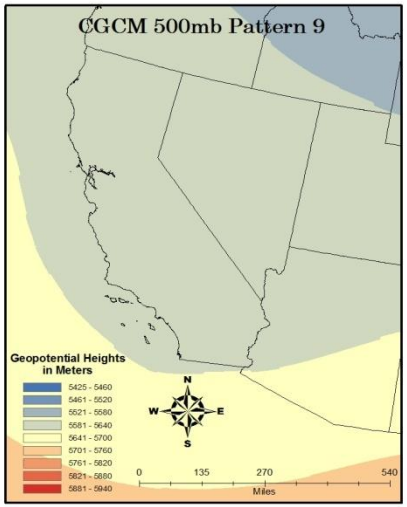

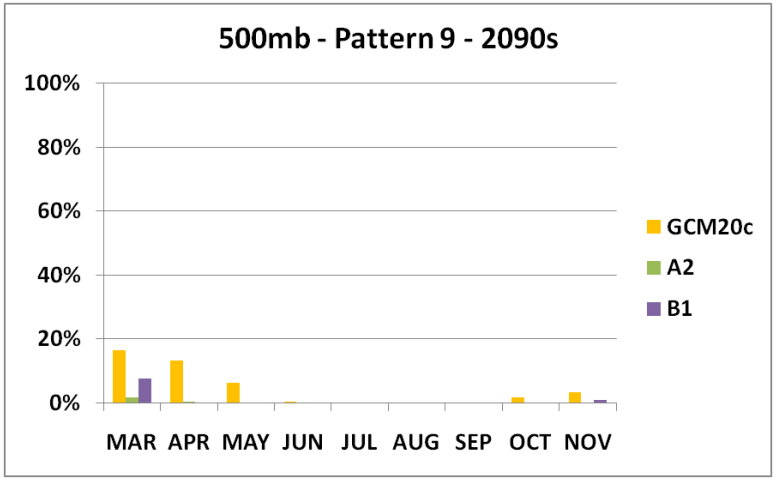

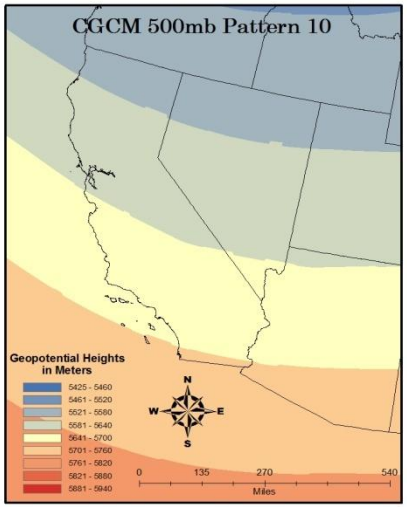

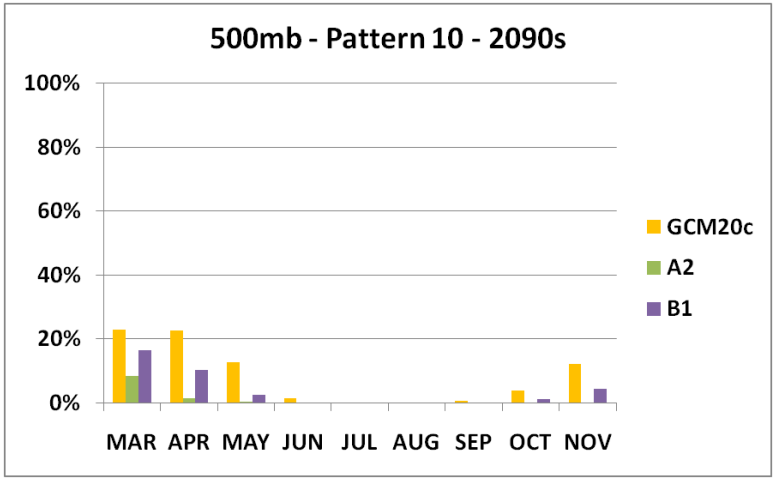

Figure A.1 – continued

CGCM3 700z Patterns and Seasonality

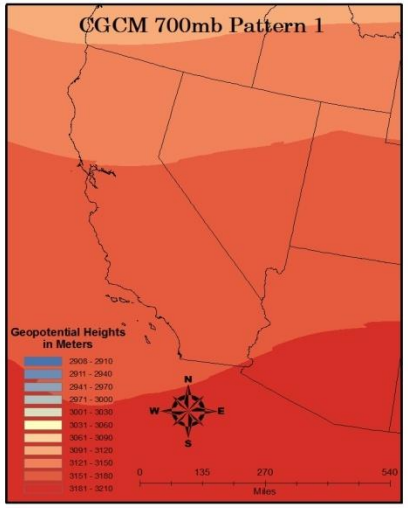

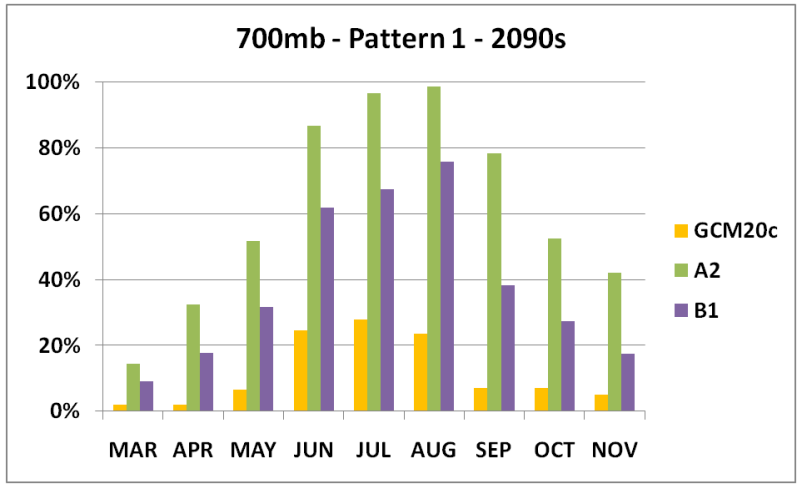

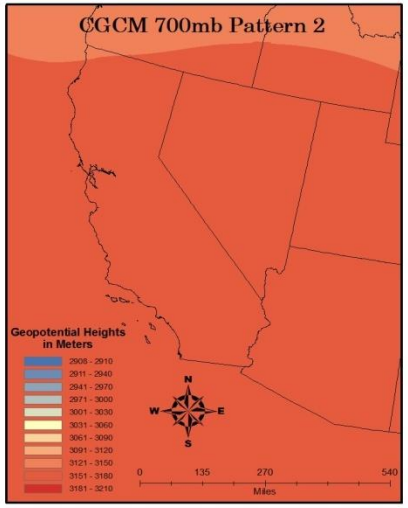

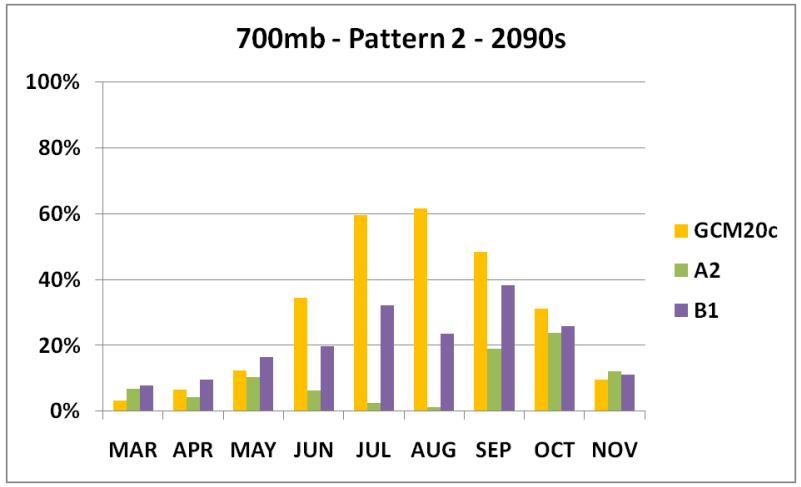

Figure A.2 – CGCM3 700z patterns and monthly frequency. Continued on the next page.

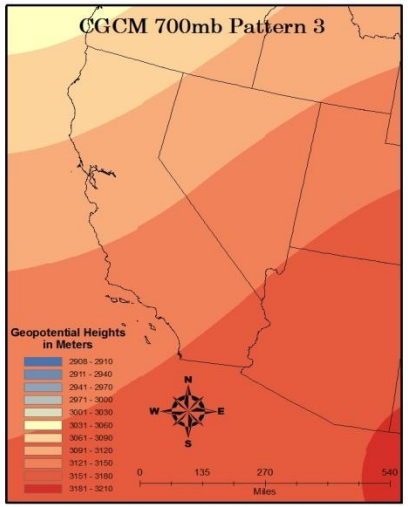

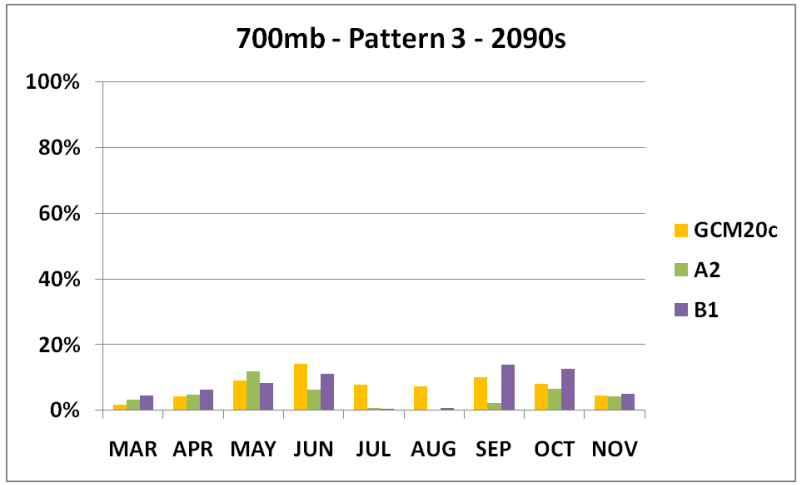

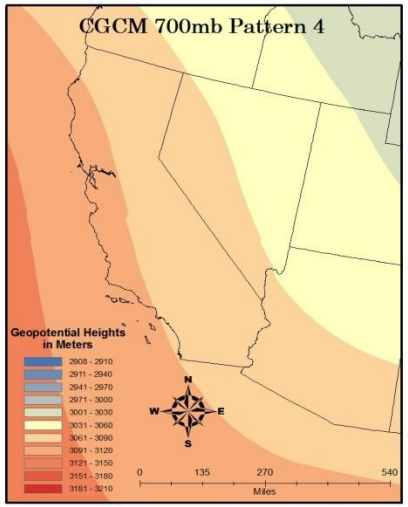

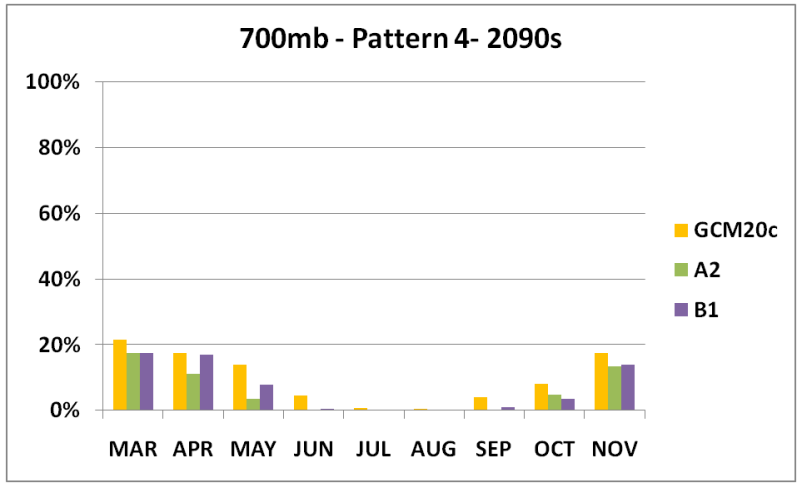

Figure A.2 – continued

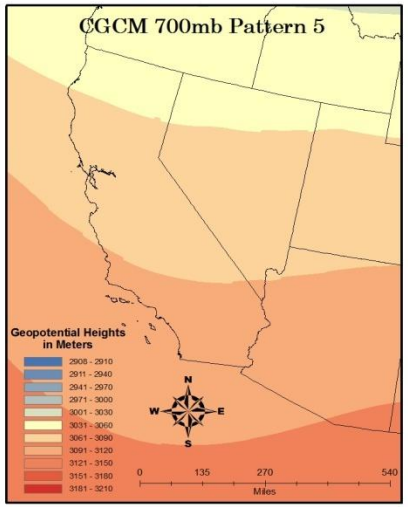

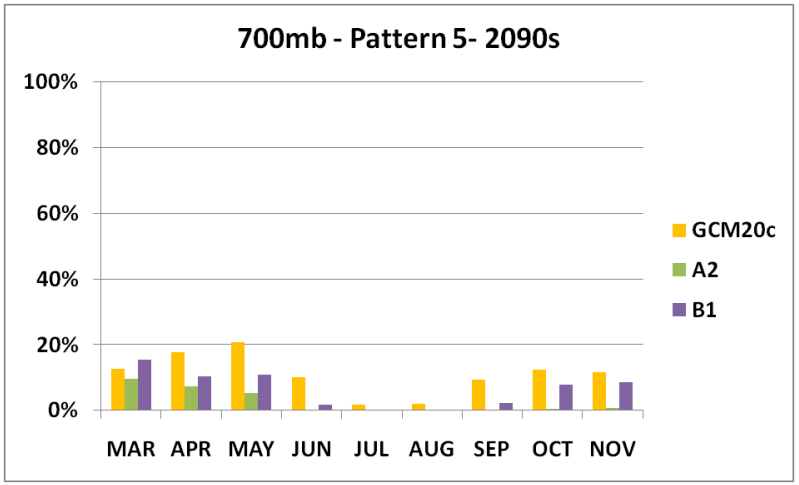

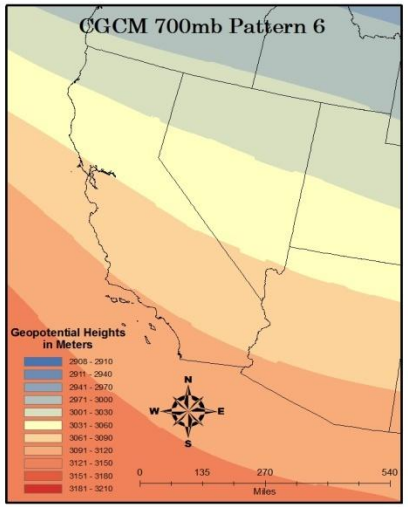

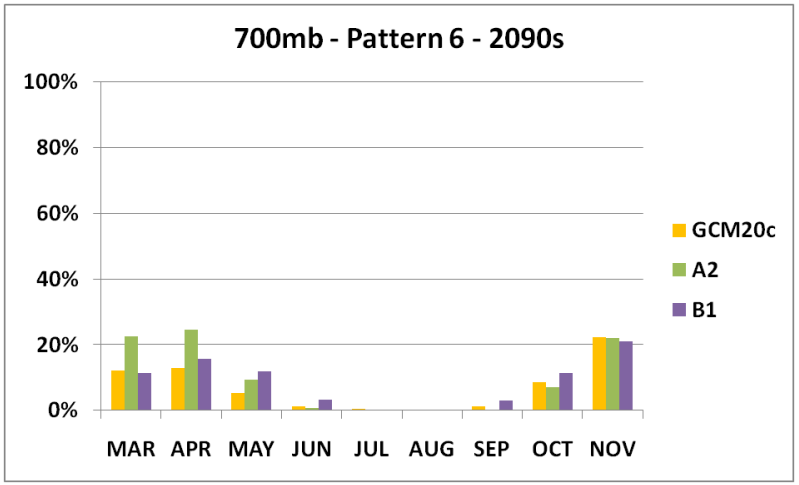

Figure A.2 – continued

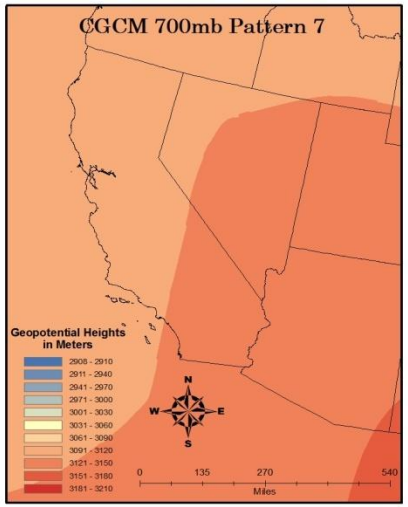

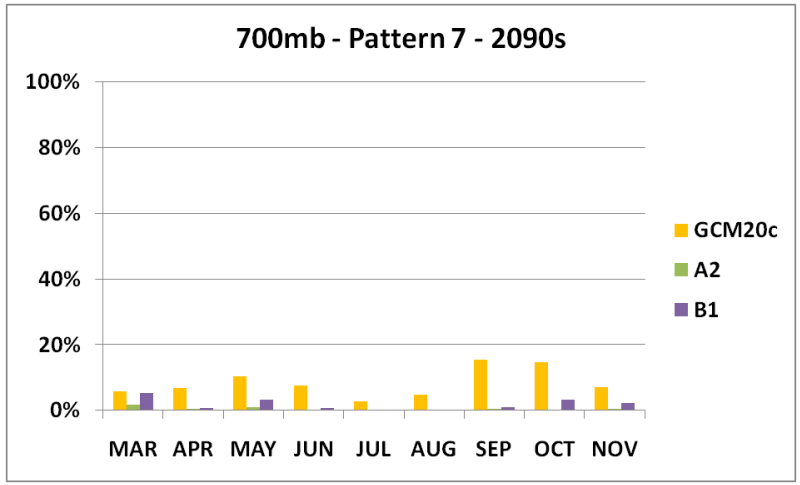

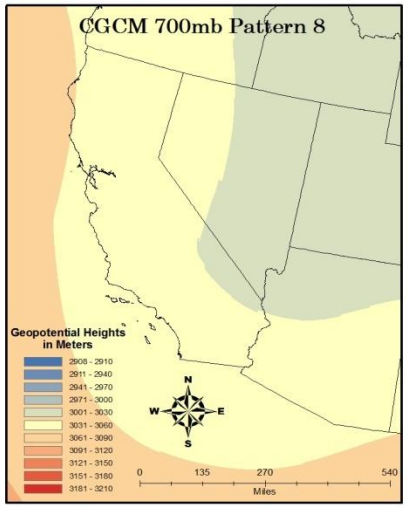

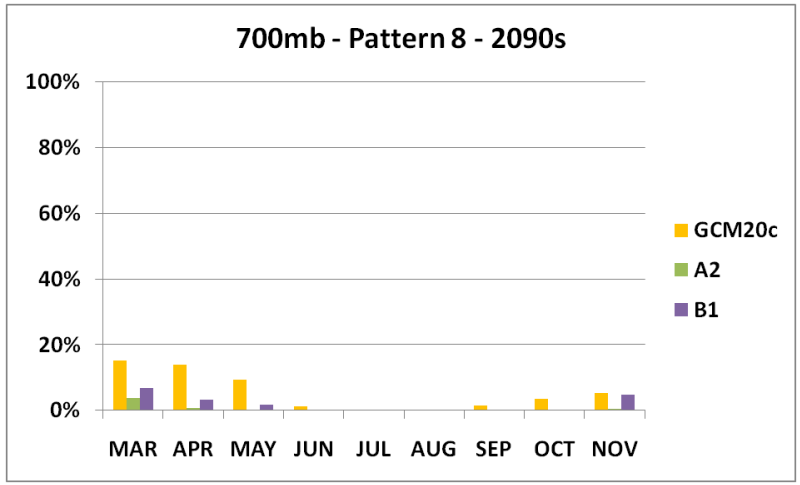

Figure A.2 – continued

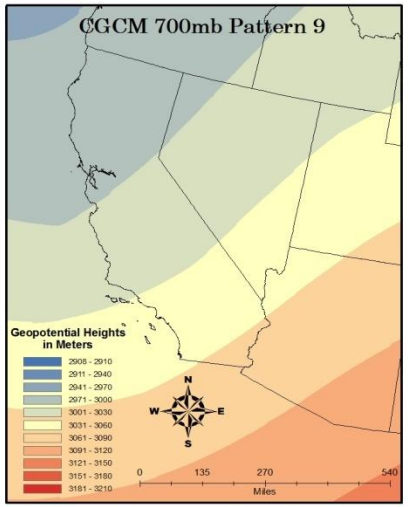

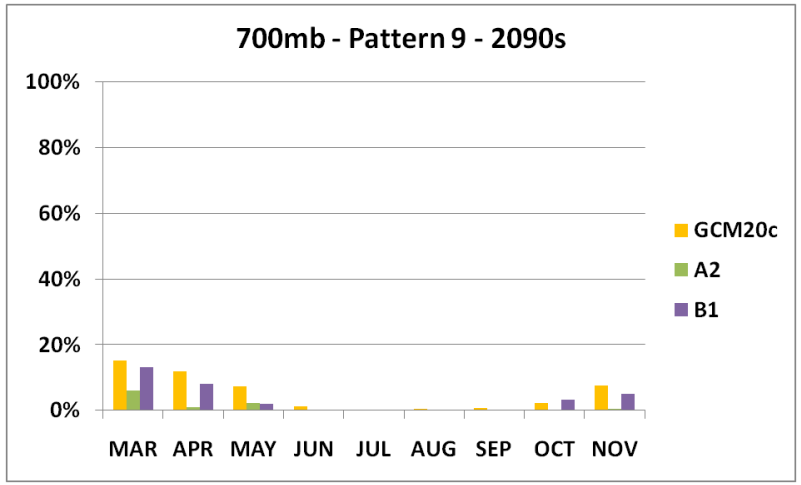

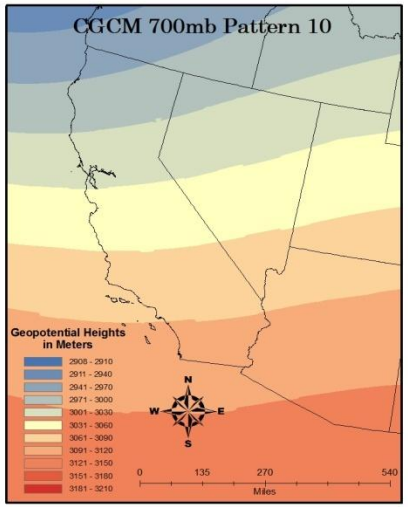

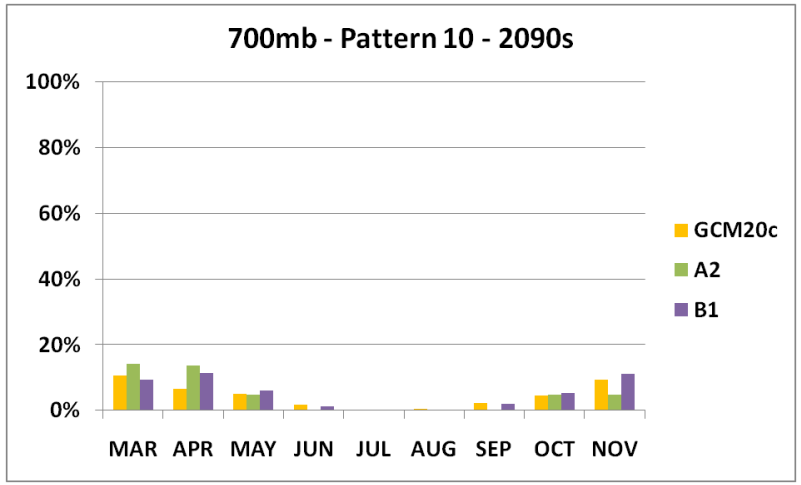

Figure A.2 – continued

CGCM3 850t Patterns and Seasonality

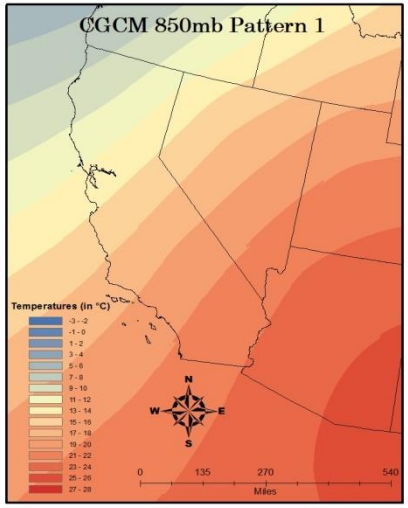

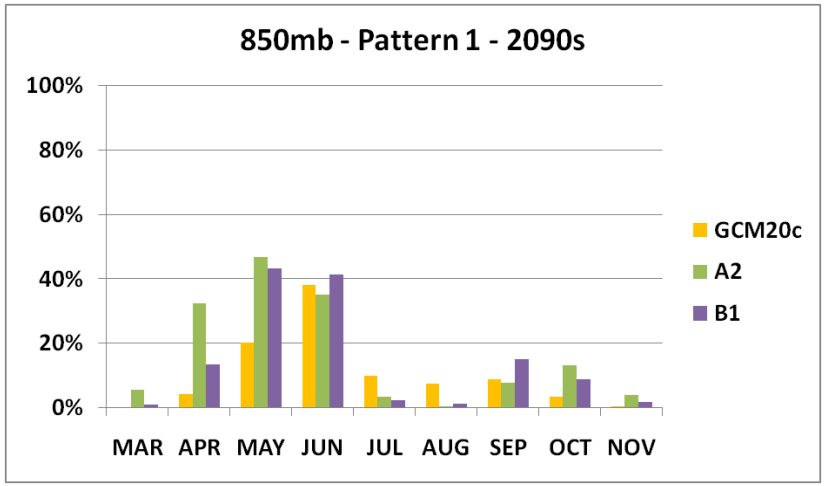

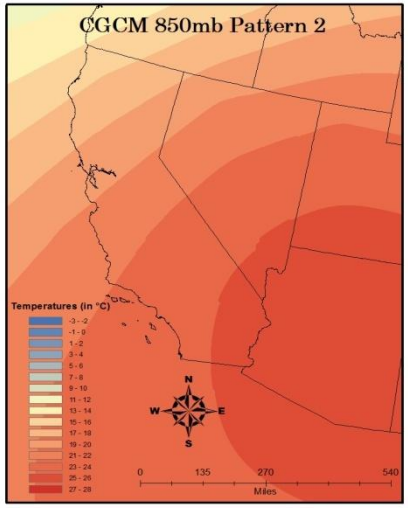

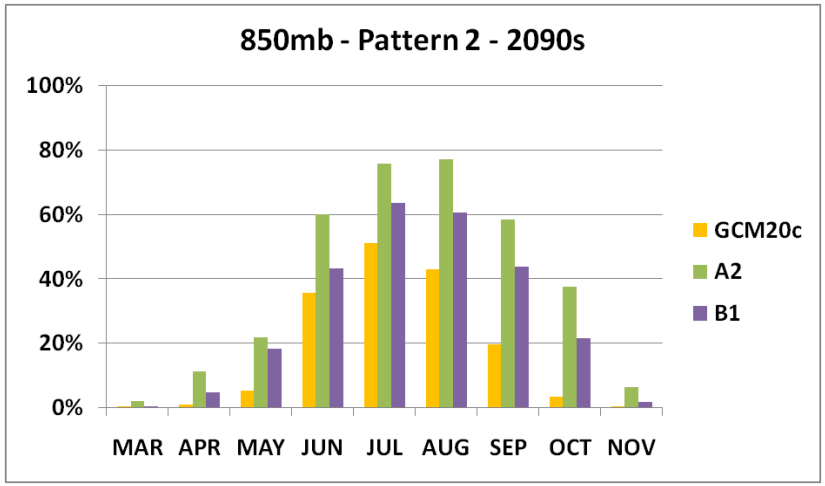

Figure A.3 – CGCM3 850t patterns and monthly frequency. Continued on the next page.

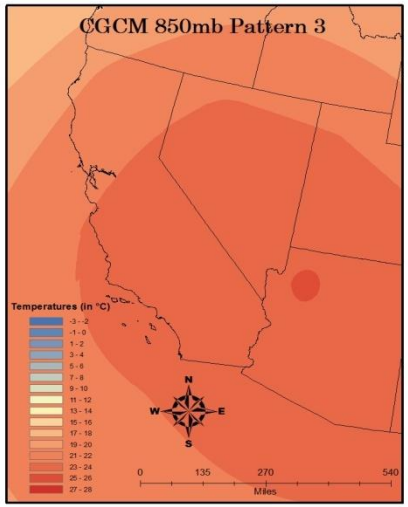

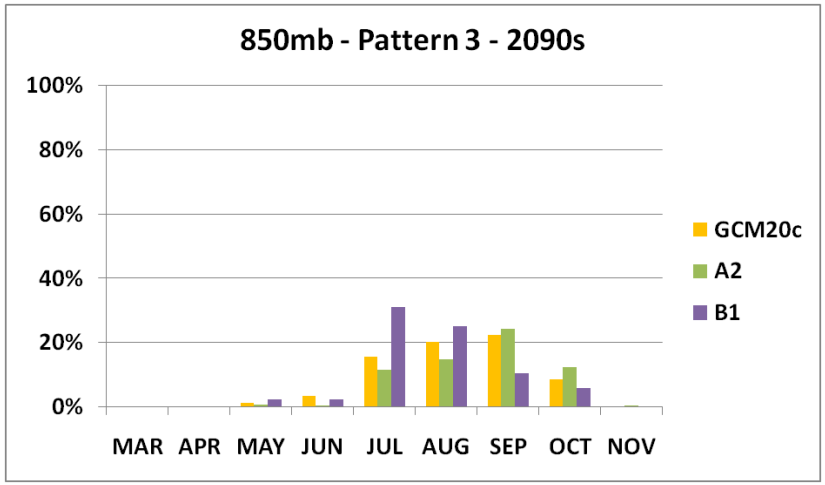

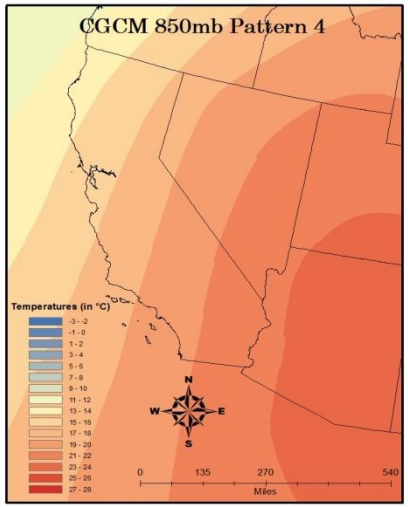

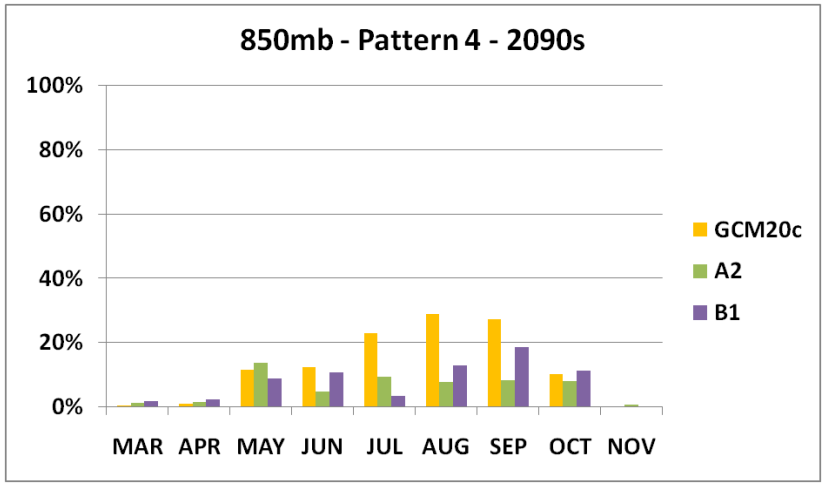

Figure A.3 – continued

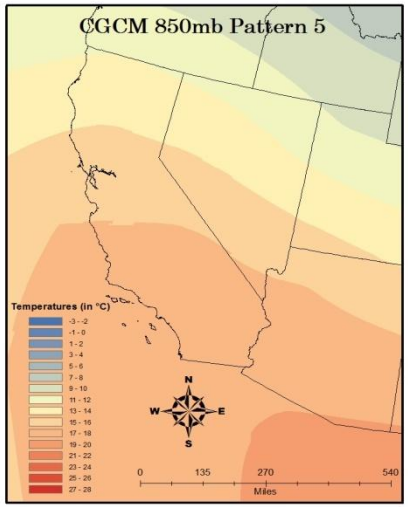

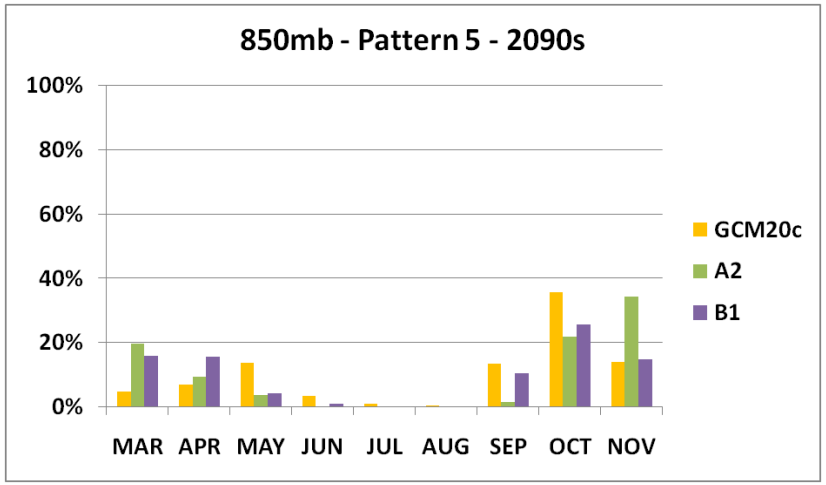

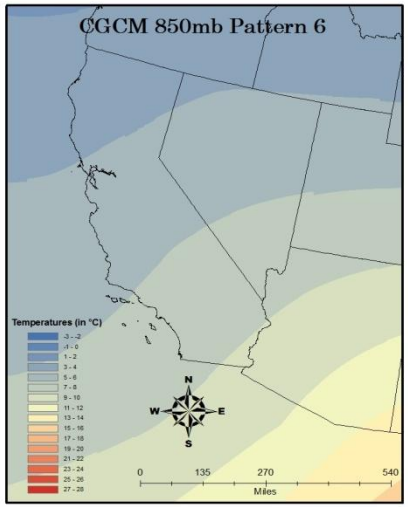

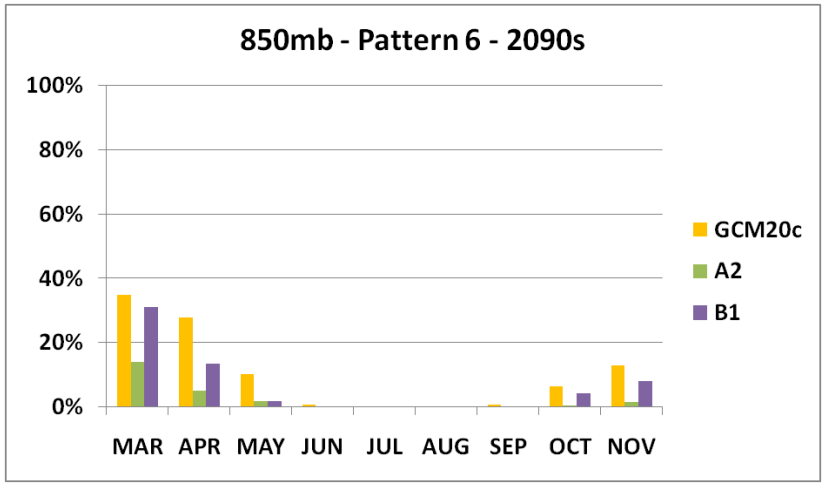

Figure A.3 – continued

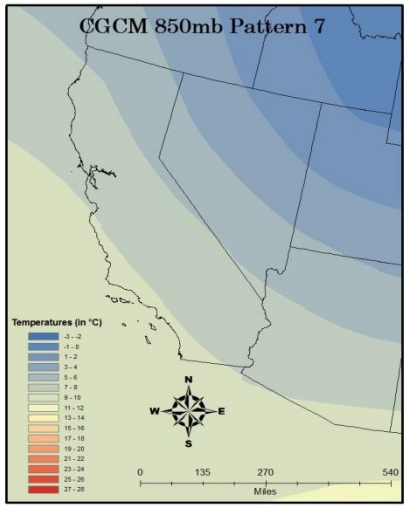

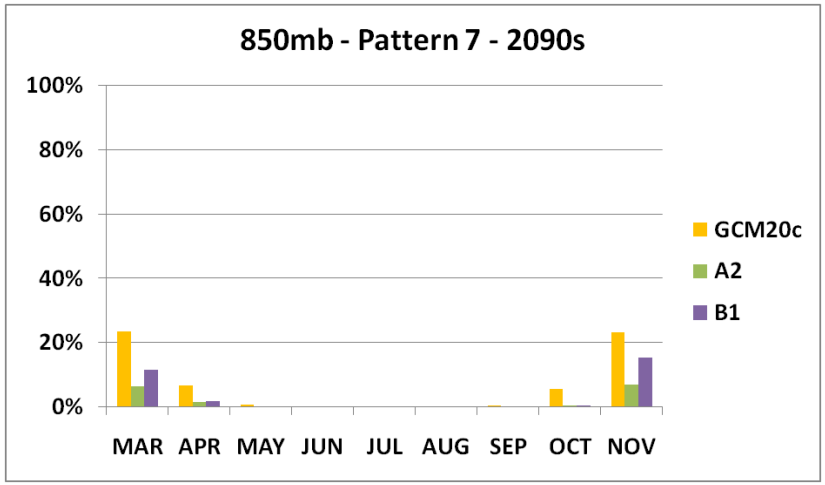

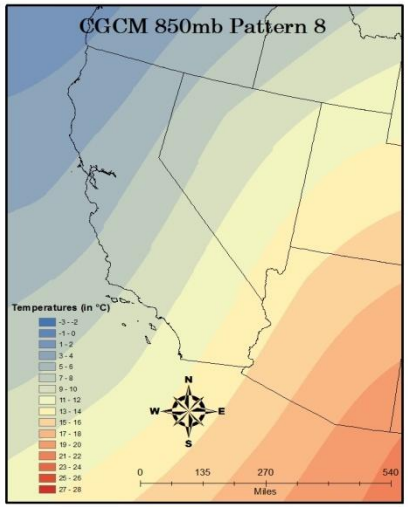

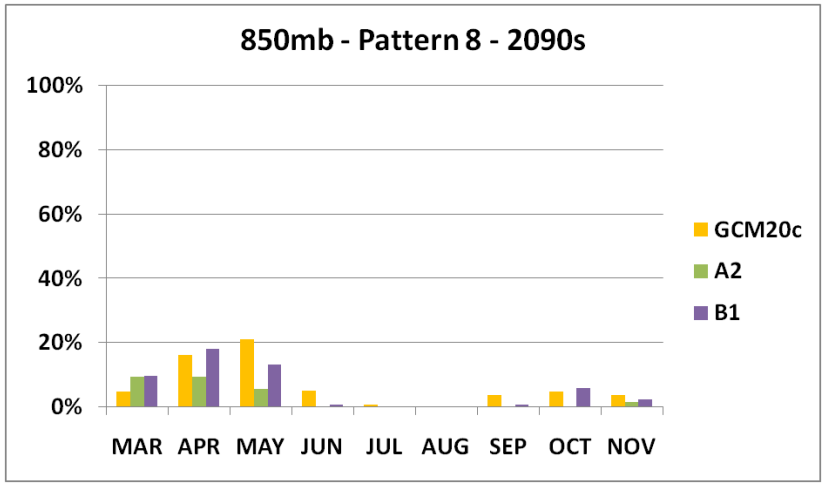

Figure A.3 – continued

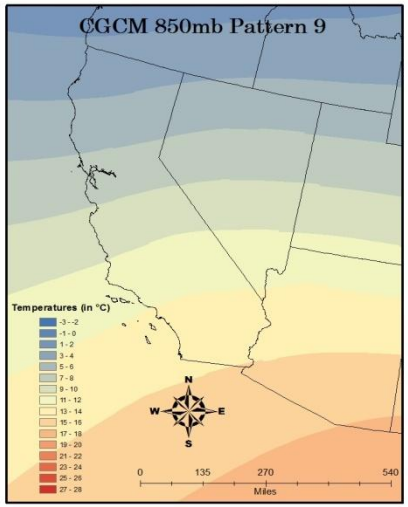

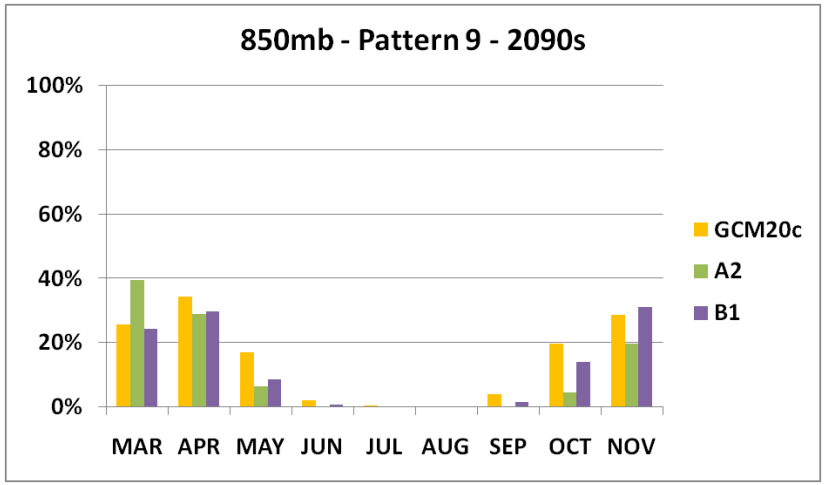

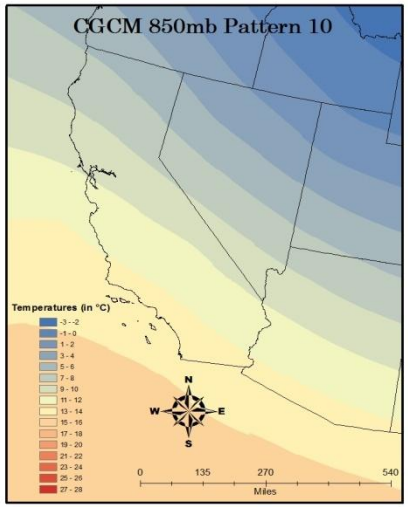

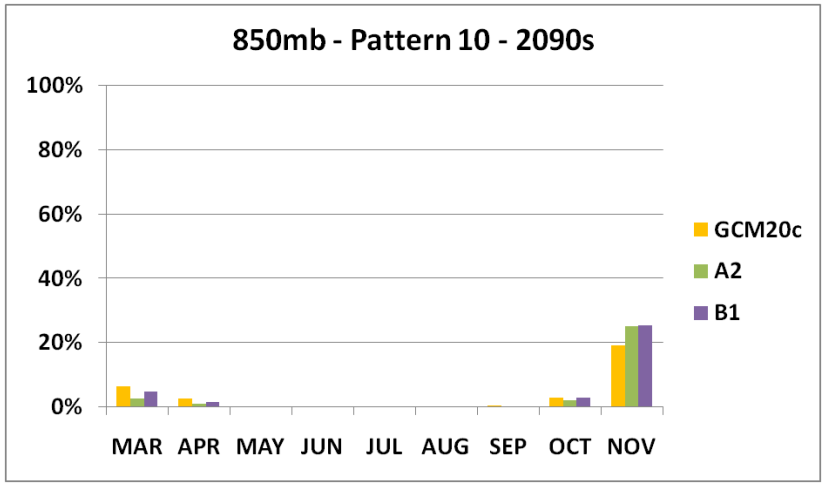

Figure A.3 – continued

APPENDIX B

The tables in Appendix B represent the mean monthly frequency of the CCSM3 and CGCM3 patterns created at each level – both in the GCM20c portion of the results, and in the 2050s or 2090s. The first three tables are of the 500z, 700z and 850t patterns (respectively) in the CCSM3 for the 2050s. The next three are for CCSM3 in the 2090s. Those six tables are then repeated in the same order for the CGCM3 global climate model.

Table B.1 – The mean monthly frequency of the 10 CCSM3 synoptic patterns created at the 500z level. GCM20c percentages are based off of 1960-1999 averages. Future model scenarios are based off of 2050-2059 averages.

CCSM3 - 500mb - 2050s																				
	1				2				3				4				5			
	GCM20c	A1FI	A2	B1	GCM20c	A1FI	A2	B1	GCM20c	A1FI	A2	B1	GCM20c	A1FI	A2	B1	GCM20c	A1FI	A2	B1
MAR	19.5%	10.6%	12.6%	15.8%	20.3%	9.0%	3.9%	13.2%	20.2%	13.5%	25.5%	27.1%	9.5%	27.7%	27.7%	14.8%	1.2%	7.7%	6.8%	2.3%
APR	17.1%	8.7%	7.0%	13.7%	9.5%	0.3%	1.7%	7.3%	21.5%	24.0%	23.3%	18.7%	12.1%	27.7%	25.0%	19.0%	2.8%	15.0%	10.3%	8.0%
MAY	4.9%	0.0%	0.3%	1.3%	1.5%	0.0%	0.0%	0.0%	12.1%	2.3%	3.5%	7.4%	12.6%	6.8%	10.3%	11.9%	12.7%	33.5%	34.8%	29.4%
JUN	1.0%	0.0%	0.0%	0.0%	0.0%	0.0%	0.0%	0.0%	1.4%	0.0%	0.0%	0.0%	5.7%	2.0%	1.7%	1.3%	25.8%	11.7%	12.7%	20.7%
JUL	0.0%	0.0%	0.0%	0.0%	0.0%	0.0%	0.0%	0.0%	0.0%	0.0%	0.0%	0.0%	0.6%	0.0%	0.0%	0.0%	11.0%	0.0%	0.6%	1.9%
AUG	0.0%	0.0%	0.0%	0.0%	0.0%	0.0%	0.0%	0.0%	0.3%	0.0%	0.0%	0.0%	0.6%	0.0%	0.0%	0.0%	11.4%	0.0%	2.6%	3.2%
SEP	0.3%	0.0%	0.0%	0.0%	0.0%	0.0%	0.0%	0.0%	1.3%	0.0%	0.7%	0.0%	6.8%	1.0%	2.7%	3.7%	18.2%	11.7%	14.3%	18.7%
OCT	6.0%	1.0%	0.0%	3.5%	1.0%	0.0%	0.0%	0.0%	6.8%	1.3%	1.0%	1.0%	14.4%	9.7%	14.8%	25.5%	13.2%	11.0%	15.8%	13.2%
NOV	16.0%	3.7%	5.7%	12.7%	5.1%	0.7%	1.0%	2.7%	13.7%	10.0%	11.3%	8.0%	27.3%	42.0%	36.7%	38.7%	5.1%	12.0%	14.3%	5.0%
	6				7				8				9				10			
	GCM20c	A1FI	A2	B1	GCM20c	A1FI	A2	B1	GCM20c	A1FI	A2	B1	GCM20c	A1FI	A2	B1	GCM20c	A1FI	A2	B1
MAR	9.3%	9.0%	6.8%	11.3%	15.4%	1.0%	4.5%	9.7%	0.0%	1.6%	2.3%	0.6%	0.6%	11.6%	4.5%	1.3%	4.0%	8.1%	5.5%	3.9%
APR	19.8%	8.3%	6.3%	13.0%	9.3%	3.0%	3.0%	6.7%	1.3%	0.3%	2.0%	1.3%	0.8%	6.0%	6.3%	4.0%	5.8%	6.7%	15.0%	8.3%
MAY	30.6%	2.9%	6.8%	9.0%	4.7%	0.0%	0.0%	0.6%	5.6%	11.6%	18.1%	13.9%	6.7%	38.7%	22.3%	19.7%	8.6%	4.2%	3.9%	6.8%
JUN	10.5%	0.0%	0.0%	2.7%	0.0%	0.0%	0.0%	0.0%	17.7%	5.7%	5.0%	17.3%	36.3%	80.7%	80.7%	58.0%	2.8%	0.0%	0.0%	0.0%
JUL	0.8%	0.0%	0.0%	0.0%	0.0%	0.0%	0.0%	0.0%	57.3%	23.2%	21.3%	36.5%	30.6%	76.8%	78.1%	61.6%	0.3%	0.0%	0.0%	0.0%
AUG	0.3%	0.0%	0.0%	0.0%	0.0%	0.0%	0.0%	0.0%	60.8%	23.9%	38.7%	43.2%	27.3%	76.1%	58.7%	53.5%	0.3%	0.0%	0.0%	0.0%
SEP	6.4%	0.0%	0.0%	0.7%	0.3%	0.0%	0.0%	0.3%	39.3%	21.3%	20.3%	35.0%	21.6%	66.0%	61.3%	41.0%	6.2%	0.0%	0.7%	0.7%
OCT	15.6%	1.3%	0.0%	1.9%	1.4%	0.0%	0.0%	0.0%	17.0%	21.0%	24.2%	18.4%	11.5%	50.6%	39.0%	30.6%	13.4%	4.2%	5.2%	5.8%
NOV	12.8%	2.3%	4.7%	6.7%	3.8%	1.7%	2.0%	1.7%	2.4%	5.3%	0.7%	2.7%	3.1%	14.0%	17.0%	8.3%	10.8%	8.3%	6.7%	13.7%

Table B.2 – The mean monthly frequency of the 10 CCSM3 synoptic patterns created at the 700z level. GCM20c percentages are based off of 1960-1999 averages. Future model scenarios are based off of 2050-2059 averages.

CCSM3 - 700mb - 2050s																				
	1				2				3				4				5			
	GCM20c	A1FI	A2	B1	GCM20c	A1FI	A2	B1	GCM20c	A1FI	A2	B1	GCM20c	A1FI	A2	B1	GCM20c	A1FI	A2	B1
MAR	1.0%	5.5%	4.2%	1.6%	10.5%	13.9%	9.4%	10.3%	2.7%	5.8%	2.3%	3.9%	2.1%	16.5%	9.0%	3.2%	6.4%	6.8%	3.9%	6.8%
APR	3.3%	4.3%	7.0%	4.0%	14.8%	13.0%	20.0%	18.3%	6.0%	9.7%	7.7%	6.0%	1.5%	7.7%	6.0%	2.7%	10.3%	6.0%	3.7%	10.0%
MAY	8.1%	20.3%	13.9%	16.8%	23.9%	12.9%	11.0%	11.0%	16.1%	23.5%	32.3%	29.0%	2.8%	33.9%	18.1%	15.5%	17.2%	2.6%	7.4%	9.0%
JUN	22.0%	20.7%	26.7%	26.3%	11.4%	0.3%	1.0%	4.0%	36.3%	9.7%	13.7%	23.3%	13.7%	68.3%	56.7%	39.7%	10.7%	0.3%	0.3%	6.0%
JUL	67.4%	47.1%	48.7%	60.0%	0.4%	0.0%	0.0%	0.0%	15.9%	0.0%	0.0%	2.9%	15.1%	52.9%	51.3%	37.1%	1.9%	0.0%	0.0%	0.0%
AUG	67.8%	59.7%	68.4%	73.9%	1.5%	0.0%	0.0%	0.0%	19.3%	0.3%	2.9%	6.1%	8.9%	40.0%	28.7%	20.0%	2.6%	0.0%	0.0%	0.0%
SEP	36.6%	53.0%	48.3%	56.3%	13.1%	0.3%	2.0%	6.3%	23.5%	12.0%	15.0%	22.0%	2.3%	32.7%	30.0%	8.0%	16.8%	0.0%	2.0%	4.0%
OCT	19.1%	35.5%	37.7%	26.8%	16.2%	8.7%	9.7%	14.5%	15.3%	9.0%	14.2%	16.1%	4.6%	35.5%	24.5%	17.1%	15.9%	3.5%	1.3%	1.9%
NOV	6.2%	11.3%	5.0%	7.7%	14.0%	12.0%	10.3%	15.7%	7.1%	6.7%	9.7%	5.7%	5.3%	19.7%	25.7%	10.7%	7.6%	2.3%	3.0%	4.3%
	6				7				8				9				10			
	GCM20c	A1FI	A2	B1	GCM20c	A1FI	A2	B1	GCM20c	A1FI	A2	B1	GCM20c	A1FI	A2	B1	GCM20c	A1FI	A2	B1
MAR	16.3%	12.9%	21.6%	21.3%	16.6%	4.5%	8.1%	11.6%	10.1%	1.3%	2.3%	3.9%	19.2%	11.0%	9.7%	15.5%	15.1%	21.9%	29.7%	21.9%
APR	14.6%	22.7%	17.3%	11.0%	11.4%	4.0%	5.7%	11.3%	5.4%	0.3%	2.3%	3.7%	14.1%	9.0%	7.3%	11.3%	18.6%	23.3%	23.0%	21.7%
MAY	10.4%	3.2%	7.7%	7.4%	4.2%	0.0%	0.3%	1.0%	1.6%	0.0%	0.0%	0.3%	4.4%	0.0%	1.0%	2.6%	11.4%	3.5%	8.4%	7.4%
JUN	1.7%	0.0%	0.7%	0.0%	0.3%	0.0%	0.0%	0.0%	0.0%	0.0%	0.0%	0.0%	1.0%	0.0%	0.0%	0.0%	3.8%	0.7%	1.0%	0.7%
JUL	0.6%	0.0%	0.0%	0.0%	0.0%	0.0%	0.0%	0.0%	0.0%	0.0%	0.0%	0.0%	0.0%	0.0%	0.0%	0.0%	0.6%	0.0%	0.0%	0.0%
AUG	1.0%	0.0%	0.0%	0.0%	0.0%	0.0%	0.0%	0.0%	0.0%	0.0%	0.0%	0.0%	0.0%	0.0%	0.0%	0.0%	0.3%	0.0%	0.0%	0.0%
SEP	3.0%	1.3%	1.3%	1.0%	0.8%	0.0%	0.0%	0.0%	0.0%	0.0%	0.0%	0.0%	1.0%	0.0%	0.0%	0.0%	3.6%	0.7%	1.3%	2.3%
OCT	7.4%	3.2%	3.5%	3.9%	2.5%	0.3%	0.0%	1.6%	1.4%	0.0%	0.0%	0.0%	6.3%	1.0%	1.0%	4.5%	11.6%	3.2%	8.1%	13.5%
NOV	12.6%	18.3%	18.7%	7.7%	5.8%	1.0%	0.7%	4.0%	3.3%	1.7%	0.7%	1.3%	12.8%	4.7%	7.0%	14.3%	25.3%	22.3%	19.3%	28.7%

Table B.3 – The mean monthly frequency of the 10 CCSM3 synoptic patterns created at the 850t level. GCM20c percentages are based off of 1960-1999 averages. Future model scenarios are based off of 2050-2059 averages.

CCSM3 - 850mb - 2050s																				
	1				2				3				4				5			
	GCM20c	A1FI	A2	B1	GCM20c	A1FI	A2	B1	GCM20c	A1FI	A2	B1	GCM20c	A1FI	A2	B1	GCM20c	A1FI	A2	B1
MAR	10.2%	6.8%	13.5%	16.8%	23.5%	16.1%	29.7%	23.5%	3.0%	17.4%	9.4%	4.8%	0.5%	2.3%	0.3%	0.3%	44.2%	22.9%	26.1%	37.1%
APR	21.8%	17.7%	17.3%	13.3%	19.4%	10.0%	20.7%	16.0%	15.8%	36.7%	18.0%	23.3%	3.8%	8.0%	4.0%	3.7%	24.4%	13.0%	15.0%	25.3%
MAY	13.1%	1.3%	3.5%	3.9%	8.1%	0.0%	2.9%	1.6%	30.8%	31.0%	38.4%	36.5%	16.7%	19.0%	19.7%	14.8%	6.5%	0.0%	0.0%	4.2%
JUN	0.7%	0.0%	0.0%	0.0%	0.7%	0.0%	0.0%	0.0%	26.4%	8.7%	7.7%	9.3%	10.7%	5.3%	3.3%	9.0%	0.0%	0.0%	0.0%	0.0%
JUL	0.0%	0.0%	0.0%	0.0%	0.0%	0.0%	0.0%	0.0%	3.3%	0.0%	0.0%	0.3%	5.7%	0.0%	0.0%	1.6%	0.0%	0.0%	0.0%	0.0%
AUG	0.0%	0.0%	0.0%	0.0%	0.0%	0.0%	0.0%	0.0%	2.7%	0.0%	0.0%	0.0%	9.4%	0.3%	1.0%	3.5%	0.3%	0.0%	0.0%	0.0%
SEP	0.6%	0.0%	0.3%	0.0%	2.0%	0.0%	0.0%	0.3%	12.3%	3.7%	5.0%	5.3%	15.3%	10.7%	13.0%	15.7%	1.1%	0.0%	0.7%	0.7%
OCT	2.6%	0.6%	0.6%	0.3%	10.6%	2.3%	4.8%	8.4%	12.1%	6.8%	9.4%	11.0%	8.0%	9.4%	3.5%	2.6%	11.9%	3.9%	2.6%	9.4%
NOV	3.0%	4.3%	2.0%	0.3%	28.8%	25.3%	26.0%	32.3%	1.7%	12.0%	9.0%	3.0%	0.3%	1.7%	0.0%	0.7%	24.8%	15.3%	17.7%	15.0%
	6				7				8				9				10			
	GCM20c	A1FI	A2	B1	GCM20c	A1FI	A2	B1	GCM20c	A1FI	A2	B1	GCM20c	A1FI	A2	B1	GCM20c	A1FI	A2	B1
MAR	14.8%	4.8%	6.8%	7.1%	0.0%	0.6%	1.0%	0.0%	0.0%	6.5%	0.3%	0.3%	4.2%	22.3%	12.9%	10.0%	0.0%	0.3%	0.0%	0.0%
APR	3.9%	0.7%	2.0%	2.7%	0.6%	1.3%	0.3%	0.3%	0.7%	2.0%	4.0%	1.3%	9.2%	9.0%	17.0%	12.7%	1.1%	1.7%	1.7%	1.3%
MAY	0.3%	0.0%	0.0%	0.0%	2.1%	3.2%	3.9%	0.6%	6.5%	22.9%	16.1%	18.7%	12.1%	2.3%	4.2%	8.4%	4.0%	20.3%	11.3%	11.3%
JUN	0.3%	0.0%	0.0%	0.0%	2.6%	2.0%	2.7%	4.7%	29.9%	44.0%	44.0%	37.0%	4.8%	0.0%	0.3%	1.3%	24.6%	40.0%	42.0%	38.7%
JUL	0.0%	0.0%	0.0%	0.0%	9.4%	12.6%	5.5%	12.6%	28.7%	10.6%	13.9%	20.0%	0.4%	0.0%	0.0%	0.0%	52.6%	76.8%	80.6%	65.5%
AUG	0.0%	0.0%	0.0%	0.0%	14.0%	19.4%	22.3%	18.4%	16.5%	5.5%	7.7%	8.1%	1.9%	0.0%	0.0%	0.0%	55.3%	74.8%	69.0%	70.0%
SEP	0.3%	0.0%	0.0%	0.0%	23.6%	20.0%	10.3%	23.0%	10.7%	13.7%	19.0%	12.7%	13.5%	1.3%	2.0%	4.7%	20.8%	50.7%	49.7%	37.7%
OCT	4.6%	0.3%	0.6%	1.9%	11.2%	16.5%	11.6%	9.0%	4.4%	14.5%	20.6%	11.6%	30.9%	16.1%	29.7%	34.8%	3.7%	29.7%	16.5%	11.0%
NOV	27.4%	10.7%	17.7%	24.3%	2.0%	1.0%	0.0%	0.7%	0.4%	2.7%	1.7%	0.3%	13.3%	26.7%	26.0%	23.3%	0.0%	0.3%	0.0%	0.0%

Table B.4 – The mean monthly frequency of the 10 CCSM3 synoptic patterns created at the 500z level. GCM20c percentages are based off of 1960-1999 averages. Future model scenarios are based off of 2090-2099 averages.

CCSM3 - 500mb - 2090s																				
	1				2				3				4				5			
	GCM20c	A1FI	A2	B1	GCM20c	A1FI	A2	B1	GCM20c	A1FI	A2	B1	GCM20c	A1FI	A2	B1	GCM20c	A1FI	A2	B1
MAR	19.5%	1.9%	4.8%	16.1%	20.3%	0.3%	0.3%	16.1%	20.2%	8.1%	11.3%	17.1%	9.5%	37.1%	34.5%	15.8%	1.2%	16.1%	11.6%	3.9%
APR	17.1%	3.7%	6.0%	10.3%	9.5%	0.7%	0.0%	3.0%	21.5%	9.3%	11.0%	19.7%	12.1%	34.7%	37.0%	21.7%	2.8%	26.0%	20.3%	9.0%
MAY	4.9%	0.0%	0.0%	1.9%	1.5%	0.0%	0.0%	0.3%	12.1%	1.0%	1.3%	7.1%	12.6%	11.0%	7.7%	17.1%	12.7%	35.5%	40.0%	22.3%
JUN	1.0%	0.0%	0.0%	0.0%	0.0%	0.0%	0.0%	0.0%	1.4%	0.0%	0.0%	0.3%	5.7%	0.0%	0.0%	2.0%	25.8%	7.3%	4.7%	10.3%
JUL	0.0%	0.0%	0.0%	0.0%	0.0%	0.0%	0.0%	0.0%	0.0%	0.0%	0.0%	0.0%	0.6%	0.0%	0.0%	0.0%	11.0%	0.0%	0.0%	3.2%
AUG	0.0%	0.0%	0.0%	0.0%	0.0%	0.0%	0.0%	0.0%	0.3%	0.0%	0.0%	0.0%	0.6%	0.0%	0.0%	0.0%	11.4%	0.0%	0.0%	2.3%
SEP	0.3%	0.0%	0.0%	0.0%	0.0%	0.0%	0.0%	0.0%	1.3%	0.0%	0.0%	0.0%	6.8%	0.3%	2.0%	2.7%	18.2%	2.3%	3.7%	16.0%
OCT	6.0%	0.0%	0.0%	1.0%	1.0%	0.0%	0.0%	0.3%	6.8%	0.0%	0.0%	3.2%	14.4%	6.5%	11.3%	19.0%	13.2%	19.7%	13.5%	19.4%
NOV	16.0%	1.7%	0.3%	6.3%	5.1%	0.0%	0.0%	1.3%	13.7%	2.7%	1.7%	11.7%	27.3%	34.0%	41.7%	41.0%	5.1%	16.7%	18.3%	11.7%
	6				7				8				9				10			
	GCM20c	A1FI	A2	B1	GCM20c	A1FI	A2	B1	GCM20c	A1FI	A2	B1	GCM20c	A1FI	A2	B1	GCM20c	A1FI	A2	B1
MAR	9.3%	7.1%	3.5%	9.4%	15.4%	1.3%	0.0%	7.7%	0.0%	4.2%	4.5%	2.9%	0.6%	17.7%	16.5%	1.3%	4.0%	6.1%	12.9%	9.7%
APR	19.8%	3.0%	1.7%	17.7%	9.3%	0.0%	0.7%	2.7%	1.3%	1.3%	3.0%	1.0%	0.8%	16.0%	15.3%	4.7%	5.8%	5.3%	5.0%	10.3%
MAY	30.6%	0.6%	0.3%	9.0%	4.7%	0.0%	0.0%	1.6%	5.6%	4.5%	6.8%	15.2%	6.7%	47.4%	43.9%	18.7%	8.6%	0.0%	0.0%	6.8%
JUN	10.5%	0.0%	0.0%	0.7%	0.0%	0.0%	0.0%	0.0%	17.7%	0.3%	3.0%	24.3%	36.3%	92.3%	92.3%	62.0%	2.8%	0.0%	0.0%	0.3%
JUL	0.8%	0.0%	0.0%	0.0%	0.0%	0.0%	0.0%	0.0%	57.3%	4.8%	7.1%	31.0%	30.6%	95.2%	92.9%	65.8%	0.3%	0.0%	0.0%	0.0%
AUG	0.3%	0.0%	0.0%	0.0%	0.0%	0.0%	0.0%	0.0%	60.8%	7.4%	13.2%	57.4%	27.3%	92.6%	86.8%	40.3%	0.3%	0.0%	0.0%	0.0%
SEP	6.4%	0.0%	0.0%	0.3%	0.3%	0.0%	0.0%	0.0%	39.3%	6.0%	10.3%	41.3%	21.6%	91.3%	84.0%	37.0%	6.2%	0.0%	0.0%	2.7%
OCT	15.6%	0.3%	0.0%	2.6%	1.4%	0.0%	0.0%	0.0%	17.0%	7.7%	11.6%	21.0%	11.5%	65.8%	62.9%	26.1%	13.4%	0.0%	0.6%	7.4%
NOV	12.8%	0.3%	1.3%	6.0%	3.8%	0.3%	0.0%	2.7%	2.4%	2.3%	2.7%	4.7%	3.1%	40.0%	30.0%	7.3%	10.8%	2.0%	4.0%	7.3%

Table B.5 – The mean monthly frequency of the 10 CCSM3 synoptic patterns created at the 700z level. GCM20c percentages are based off of 1960-1999 averages. Future model scenarios are based off of 2090-2099 averages.

CCSM3 - 700mb - 2090s																				
	1				2				3				4				5			
	GCM20c	A1FI	A2	B1	GCM20c	A1FI	A2	B1	GCM20c	A1FI	A2	B1	GCM20c	A1FI	A2	B1	GCM20c	A1FI	A2	B1
MAR	1.0%	10.0%	4.2%	1.6%	10.5%	10.3%	9.4%	10.3%	2.7%	7.1%	2.3%	3.9%	2.1%	28.7%	9.0%	3.2%	6.4%	5.8%	3.9%	6.8%
APR	3.3%	5.3%	7.0%	4.0%	14.8%	9.0%	20.0%	18.3%	6.0%	9.3%	7.7%	6.0%	1.5%	27.0%	6.0%	2.7%	10.3%	4.0%	3.7%	10.0%
MAY	8.1%	13.5%	13.9%	16.8%	23.9%	2.3%	11.0%	11.0%	16.1%	15.2%	32.3%	29.0%	2.8%	55.5%	18.1%	15.5%	17.2%	1.6%	7.4%	9.0%
JUN	22.0%	11.3%	26.7%	26.3%	11.4%	0.0%	1.0%	4.0%	36.3%	2.7%	13.7%	23.3%	13.7%	86.0%	56.7%	39.7%	10.7%	0.0%	0.3%	6.0%
JUL	67.4%	15.8%	48.7%	60.0%	0.4%	0.0%	0.0%	0.0%	15.9%	0.0%	0.0%	2.9%	15.1%	84.2%	51.3%	37.1%	1.9%	0.0%	0.0%	0.0%
AUG	67.8%	27.4%	68.4%	73.9%	1.5%	0.0%	0.0%	0.0%	19.3%	0.0%	2.9%	6.1%	8.9%	72.6%	28.7%	20.0%	2.6%	0.0%	0.0%	0.0%
SEP	36.6%	37.7%	48.3%	56.3%	13.1%	0.0%	2.0%	6.3%	23.5%	0.3%	15.0%	22.0%	2.3%	61.3%	30.0%	8.0%	16.8%	0.0%	2.0%	4.0%
OCT	19.1%	22.6%	37.7%	26.8%	16.2%	2.3%	9.7%	14.5%	15.3%	9.7%	14.2%	16.1%	4.6%	58.1%	24.5%	17.1%	15.9%	0.6%	1.3%	1.9%
NOV	6.2%	9.7%	5.0%	7.7%	14.0%	5.7%	10.3%	15.7%	7.1%	5.3%	9.7%	5.7%	5.3%	54.7%	25.7%	10.7%	7.6%	0.3%	3.0%	4.3%
	6				7				8				9				10			
	GCM20c	A1FI	A2	B1	GCM20c	A1FI	A2	B1	GCM20c	A1FI	A2	B1	GCM20c	A1FI	A2	B1	GCM20c	A1FI	A2	B1
MAR	16.3%	11.9%	21.6%	21.3%	16.6%	0.0%	8.1%	11.6%	10.1%	0.6%	2.3%	3.9%	19.2%	3.9%	9.7%	15.5%	15.1%	21.6%	29.7%	21.9%
APR	14.6%	16.3%	17.3%	11.0%	11.4%	1.3%	5.7%	11.3%	5.4%	0.0%	2.3%	3.7%	14.1%	4.3%	7.3%	11.3%	18.6%	23.3%	23.0%	21.7%
MAY	10.4%	5.8%	7.7%	7.4%	4.2%	0.3%	0.3%	1.0%	1.6%	0.0%	0.0%	0.3%	4.4%	0.0%	1.0%	2.6%	11.4%	5.8%	8.4%	7.4%
JUN	1.7%	0.0%	0.7%	0.0%	0.3%	0.0%	0.0%	0.0%	0.0%	0.0%	0.0%	0.0%	1.0%	0.0%	0.0%	0.0%	3.8%	0.0%	1.0%	0.7%
JUL	0.6%	0.0%	0.0%	0.0%	0.0%	0.0%	0.0%	0.0%	0.0%	0.0%	0.0%	0.0%	0.0%	0.0%	0.0%	0.0%	0.6%	0.0%	0.0%	0.0%
AUG	1.0%	0.0%	0.0%	0.0%	0.0%	0.0%	0.0%	0.0%	0.0%	0.0%	0.0%	0.0%	0.0%	0.0%	0.0%	0.0%	0.3%	0.0%	0.0%	0.0%
SEP	3.0%	0.0%	1.3%	1.0%	0.8%	0.0%	0.0%	0.0%	0.0%	0.0%	0.0%	0.0%	1.0%	0.0%	0.0%	0.0%	3.6%	0.7%	1.3%	2.3%
OCT	7.4%	2.9%	3.5%	3.9%	2.5%	0.0%	0.0%	1.6%	1.4%	0.0%	0.0%	0.0%	6.3%	0.0%	1.0%	4.5%	11.6%	3.9%	8.1%	13.5%
NOV	12.6%	7.3%	18.7%	7.7%	5.8%	0.0%	0.7%	4.0%	3.3%	0.0%	0.7%	1.3%	12.8%	3.3%	7.0%	14.3%	25.3%	13.7%	19.3%	28.7%

Table B.6 – The mean monthly frequency of the 10 CCSM3 synoptic patterns created at the 850t level. GCM20c percentages are based off of 1960-1999 averages. Future model scenarios are based off of 2090-2099 averages.

CCSM3 - 850mb - 2090s																				
	1				2				3				4				5			
	GCM20c	A1FI	A2	B1	GCM20c	A1FI	A2	B1	GCM20c	A1FI	A2	B1	GCM20c	A1FI	A2	B1	GCM20c	A1FI	A2	B1
MAR	10.2%	2.9%	1.6%	7.4%	23.5%	13.5%	19.7%	21.0%	3.0%	26.5%	9.7%	6.8%	0.5%	7.7%	2.3%	0.6%	44.2%	6.1%	16.5%	34.8%
APR	21.8%	6.0%	6.7%	12.7%	19.4%	5.0%	17.7%	24.0%	15.8%	44.0%	31.7%	21.0%	3.8%	9.0%	6.7%	10.0%	24.4%	8.3%	14.3%	14.7%
MAY	13.1%	0.6%	0.6%	3.9%	8.1%	0.0%	0.6%	5.2%	30.8%	31.9%	36.8%	35.5%	16.7%	24.2%	10.3%	15.2%	6.5%	0.0%	0.6%	1.3%
JUN	0.7%	0.0%	0.0%	0.0%	0.7%	0.0%	0.0%	0.0%	26.4%	1.3%	3.0%	5.0%	10.7%	5.3%	0.7%	7.0%	0.0%	0.0%	0.0%	0.0%
JUL	0.0%	0.0%	0.0%	0.0%	0.0%	0.0%	0.0%	0.0%	3.3%	0.0%	0.0%	0.6%	5.7%	0.0%	0.0%	2.3%	0.0%	0.0%	0.0%	0.0%
AUG	0.0%	0.0%	0.0%	0.0%	0.0%	0.0%	0.0%	0.0%	2.7%	0.0%	0.0%	0.0%	9.4%	0.0%	0.0%	2.3%	0.3%	0.0%	0.0%	0.0%
SEP	0.6%	0.0%	0.0%	0.0%	2.0%	0.0%	0.0%	0.0%	12.3%	0.0%	0.3%	5.3%	15.3%	3.7%	4.3%	11.3%	1.1%	0.0%	0.0%	0.0%
OCT	2.6%	0.0%	0.3%	0.6%	10.6%	1.0%	0.6%	8.1%	12.1%	9.7%	8.7%	14.2%	8.0%	14.2%	9.4%	8.7%	11.9%	0.0%	0.3%	6.8%
NOV	3.0%	1.7%	0.0%	2.7%	28.8%	8.7%	20.3%	24.0%	1.7%	8.0%	6.0%	3.3%	0.3%	1.7%	0.7%	0.0%	24.8%	9.0%	3.0%	20.3%
	6				7				8				9				10			
	GCM20c	A1FI	A2	B1	GCM20c	A1FI	A2	B1	GCM20c	A1FI	A2	B1	GCM20c	A1FI	A2	B1	GCM20c	A1FI	A2	B1
MAR	14.8%	1.0%	6.8%	16.1%	0.0%	2.6%	2.3%	0.6%	0.0%	8.4%	4.2%	0.6%	4.2%	26.8%	35.8%	11.9%	0.0%	4.5%	1.3%	0.0%
APR	3.9%	0.0%	0.3%	2.0%	0.6%	1.0%	1.3%	0.7%	0.7%	12.3%	10.3%	1.7%	9.2%	11.0%	10.0%	12.3%	1.1%	3.3%	1.0%	1.0%
MAY	0.3%	0.0%	0.0%	0.0%	2.1%	1.0%	2.3%	4.8%	6.5%	23.2%	31.9%	10.0%	12.1%	1.9%	1.3%	12.6%	4.0%	17.1%	15.5%	11.6%
JUN	0.3%	0.0%	0.0%	0.0%	2.6%	0.7%	0.7%	3.0%	29.9%	46.7%	54.3%	39.7%	4.8%	0.0%	0.0%	2.3%	24.6%	46.0%	41.3%	43.0%
JUL	0.0%	0.0%	0.0%	0.0%	9.4%	5.8%	11.3%	10.0%	28.7%	8.7%	7.7%	24.2%	0.4%	0.0%	0.0%	0.0%	52.6%	85.5%	81.0%	62.9%
AUG	0.0%	0.0%	0.0%	0.0%	14.0%	25.2%	14.8%	17.7%	16.5%	0.3%	1.9%	7.1%	1.9%	0.0%	0.0%	0.0%	55.3%	74.5%	83.2%	72.9%
SEP	0.3%	0.0%	0.0%	0.0%	23.6%	15.7%	14.7%	27.7%	10.7%	11.7%	11.3%	10.3%	13.5%	0.0%	3.0%	6.7%	20.8%	69.0%	66.3%	38.7%
OCT	4.6%	0.0%	0.0%	1.6%	11.2%	10.6%	11.6%	11.6%	4.4%	20.3%	14.2%	7.1%	30.9%	10.3%	27.7%	33.5%	3.7%	33.9%	27.1%	7.7%
NOV	27.4%	3.0%	7.7%	20.7%	2.0%	0.7%	1.7%	0.0%	0.4%	16.0%	17.0%	1.0%	13.3%	47.0%	43.0%	28.0%	0.0%	4.3%	0.7%	0.0%

Table B.7 – The mean monthly frequency of the 10 CGCM3 synoptic patterns created at the 500z level. GCM20c percentages are based off of 1970-1999 averages. Future model scenarios are based off of 2050-2059 averages.

CGCM - 500mb 2050s															
	1			2			3			4			5		
	GCM20c	A2	B1	GCM20c	A2	B1	GCM20c	A2	B1	GCM20c	A2	B1	GCM20c	A2	B1
MAR	5.3%	11.9%	11.6%	5.1%	20.0%	16.8%	21.3%	12.3%	14.8%	2.2%	7.4%	3.5%	1.6%	8.1%	10.6%
APR	7.6%	8.3%	6.7%	10.6%	30.3%	19.7%	13.3%	5.0%	8.3%	6.2%	4.3%	4.3%	3.7%	17.0%	14.0%
MAY	15.2%	2.9%	5.8%	10.3%	12.9%	14.5%	3.3%	0.0%	2.3%	11.5%	8.4%	10.3%	17.1%	47.1%	30.0%
JUN	4.3%	0.3%	0.0%	6.2%	3.7%	4.3%	0.3%	0.0%	0.0%	7.2%	1.0%	2.0%	38.6%	46.3%	49.3%
JUL	0.3%	0.0%	0.0%	0.9%	0.0%	0.0%	0.0%	0.0%	0.0%	5.1%	0.0%	0.6%	23.9%	16.5%	25.8%
AUG	0.0%	0.0%	0.0%	0.6%	0.0%	0.3%	0.0%	0.0%	0.0%	4.8%	0.0%	0.0%	23.0%	17.7%	23.2%
SEP	7.1%	0.0%	0.0%	8.0%	10.0%	7.0%	0.8%	0.0%	0.0%	10.1%	1.0%	0.7%	23.3%	26.0%	18.3%
OCT	15.1%	1.6%	6.1%	18.8%	16.5%	18.7%	1.4%	0.0%	0.3%	13.9%	2.6%	1.0%	16.1%	38.7%	24.2%
NOV	10.7%	10.0%	14.7%	26.2%	48.0%	33.0%	11.1%	3.7%	7.7%	8.3%	1.3%	5.0%	6.9%	16.3%	12.7%
	6			7			8			9			10		
	GCM20c	A2	B1	GCM20c	A2	B1	GCM20c	A2	B1	GCM20c	A2	B1	GCM20c	A2	B1
MAR	0.8%	7.7%	2.6%	10.8%	9.7%	14.2%	14.5%	6.8%	5.2%	16.5%	3.9%	6.1%	22.9%	12.3%	14.5%
APR	1.3%	7.0%	3.3%	9.7%	17.3%	19.3%	11.6%	2.0%	5.7%	13.3%	0.3%	4.3%	22.8%	8.3%	14.3%
MAY	6.1%	14.5%	20.0%	10.5%	8.4%	8.1%	6.9%	1.6%	2.3%	6.2%	0.0%	1.0%	12.8%	4.2%	5.8%
JUN	37.6%	46.7%	42.7%	4.7%	1.3%	1.7%	0.5%	0.7%	0.0%	0.3%	0.0%	0.0%	1.3%	0.0%	0.0%
JUL	70.0%	83.5%	73.5%	0.3%	0.0%	0.0%	0.0%	0.0%	0.0%	0.0%	0.0%	0.0%	0.0%	0.0%	0.0%
AUG	71.7%	82.3%	76.5%	0.0%	0.0%	0.0%	0.0%	0.0%	0.0%	0.0%	0.0%	0.0%	0.0%	0.0%	0.0%
SEP	47.3%	62.0%	74.0%	3.0%	1.0%	0.0%	0.0%	0.0%	0.0%	0.0%	0.0%	0.0%	0.6%	0.0%	0.0%
OCT	22.4%	34.5%	45.8%	5.9%	5.2%	3.2%	1.3%	0.0%	0.0%	1.8%	0.0%	0.0%	4.0%	1.0%	0.6%
NOV	3.7%	9.3%	12.7%	11.8%	6.7%	6.3%	5.8%	2.0%	2.0%	3.3%	0.7%	1.7%	12.2%	2.0%	4.3%

Table B.8 – The mean monthly frequency of the 10 CGCM3 synoptic patterns created at the 700z level. GCM20c percentages are based off of 1970-1999 averages. Future model scenarios are based off of 2050-2059 averages.

CGCM - 700mb 2050s															
	1			2			3			4			5		
	GCM20c	A2	B1	GCM20c	A2	B1	GCM20c	A2	B1	GCM20c	A2	B1	GCM20c	A2	B1
MAR	1.9%	11.0%	6.8%	3.1%	11.6%	7.1%	1.8%	2.6%	3.9%	21.6%	18.4%	17.7%	12.7%	13.9%	11.3%
APR	1.9%	19.3%	7.3%	6.4%	8.3%	5.3%	4.2%	3.7%	6.0%	17.6%	16.0%	18.7%	17.8%	10.7%	17.7%
MAY	6.5%	22.3%	17.4%	12.4%	18.4%	21.6%	9.1%	10.0%	14.8%	14.0%	8.1%	9.7%	20.6%	16.1%	13.5%
JUN	24.4%	59.7%	47.7%	34.4%	19.3%	25.0%	14.2%	11.3%	12.0%	4.4%	0.3%	1.7%	10.1%	2.7%	5.3%
JUL	27.7%	72.3%	60.3%	59.6%	25.8%	33.5%	7.8%	1.9%	5.2%	0.6%	0.0%	0.0%	1.7%	0.0%	0.0%
AUG	23.7%	78.1%	69.0%	61.5%	21.3%	28.1%	7.4%	0.6%	2.9%	0.5%	0.0%	0.0%	2.0%	0.0%	0.0%
SEP	7.1%	35.0%	19.3%	48.4%	43.7%	63.7%	10.0%	8.3%	6.7%	4.1%	2.7%	1.3%	9.4%	2.3%	2.3%
OCT	7.0%	30.3%	16.1%	31.1%	25.5%	41.6%	8.0%	16.5%	10.6%	8.1%	2.9%	11.6%	12.5%	6.5%	9.0%
NOV	5.0%	18.7%	11.3%	9.6%	10.7%	18.3%	4.4%	4.0%	4.7%	17.6%	20.0%	18.3%	11.7%	4.7%	5.3%
	6			7			8			9			10		
	GCM20c	A2	B1	GCM20c	A2	B1	GCM20c	A2	B1	GCM20c	A2	B1	GCM20c	A2	B1
MAR	12.2%	15.2%	20.6%	5.8%	7.1%	4.8%	15.2%	5.8%	9.0%	15.2%	7.1%	5.5%	10.5%	7.4%	13.2%
APR	13.0%	19.0%	15.0%	6.8%	3.3%	4.0%	13.9%	2.7%	6.0%	11.8%	3.3%	8.3%	6.7%	13.7%	11.7%
MAY	5.4%	7.4%	5.8%	10.4%	5.8%	5.5%	9.2%	1.3%	3.2%	7.3%	2.6%	3.5%	5.1%	8.1%	4.8%
JUN	1.3%	1.7%	3.0%	7.7%	1.7%	0.3%	1.2%	0.0%	0.0%	1.3%	0.7%	0.7%	1.7%	2.7%	4.3%
JUL	0.3%	0.0%	0.3%	2.7%	0.0%	0.6%	0.0%	0.0%	0.0%	0.0%	0.0%	0.0%	0.0%	0.0%	0.0%
AUG	0.0%	0.0%	0.0%	4.7%	0.0%	0.0%	0.0%	0.0%	0.0%	0.3%	0.0%	0.0%	0.3%	0.0%	0.0%
SEP	1.3%	3.7%	1.3%	15.3%	1.7%	5.0%	1.4%	0.0%	0.0%	0.7%	0.0%	0.0%	2.1%	2.7%	0.3%
OCT	8.5%	6.1%	3.9%	14.7%	5.2%	2.6%	3.4%	0.0%	1.0%	2.2%	0.6%	1.3%	4.6%	6.5%	2.3%
NOV	22.3%	29.7%	22.7%	7.0%	2.0%	4.3%	5.3%	2.0%	6.0%	7.7%	2.3%	2.3%	9.4%	6.0%	6.7%

Table B.9 – The mean monthly frequency of the 10 CGCM3 synoptic patterns created at the 850t level. GCM20c percentages are based off of 1970-1999 averages. Future model scenarios are based off of 2050-2059 averages.

CGCM - 850mb 2050s															
	1			2			3			4			5		
	GCM20c	A2	B1	GCM20c	A2	B1	GCM20c	A2	B1	GCM20c	A2	B1	GCM20c	A2	B1
MAR	0.0%	1.3%	0.6%	0.3%	0.0%	0.0%	0.0%	0.0%	0.0%	0.3%	1.0%	0.0%	4.6%	24.5%	14.5%
APR	4.2%	11.0%	10.0%	0.8%	6.3%	1.7%	0.0%	0.0%	0.0%	0.8%	1.7%	0.0%	7.0%	18.0%	8.7%
MAY	20.1%	44.8%	24.5%	5.3%	10.3%	16.5%	1.1%	1.9%	1.0%	11.6%	11.9%	15.5%	13.7%	5.5%	10.3%
JUN	38.0%	35.3%	42.3%	35.7%	46.7%	42.7%	3.4%	6.0%	1.7%	12.2%	9.3%	11.3%	3.2%	1.0%	1.3%
JUL	9.8%	2.9%	7.1%	51.2%	69.0%	67.4%	15.6%	15.8%	10.0%	22.8%	12.3%	15.5%	1.0%	0.0%	0.0%
AUG	7.5%	3.5%	5.8%	43.0%	61.0%	58.4%	20.2%	19.4%	18.1%	28.9%	16.1%	17.7%	0.5%	0.0%	0.0%
SEP	8.8%	10.3%	5.3%	19.6%	38.0%	31.0%	22.2%	24.7%	34.7%	27.1%	15.3%	14.0%	13.4%	9.3%	12.3%
OCT	3.3%	11.3%	4.8%	3.4%	21.0%	12.3%	8.4%	10.0%	13.5%	10.2%	14.8%	12.3%	35.7%	23.9%	33.2%
NOV	0.3%	0.3%	0.3%	0.3%	1.0%	0.3%	0.0%	0.0%	0.7%	0.0%	0.3%	0.0%	13.9%	17.7%	20.3%
	6			7			8			9			10		
	GCM20c	A2	B1	GCM20c	A2	B1	GCM20c	A2	B1	GCM20c	A2	B1	GCM20c	A2	B1
MAR	34.9%	18.7%	21.9%	23.3%	14.2%	21.9%	4.7%	8.1%	9.0%	25.6%	28.7%	28.4%	6.5%	3.5%	3.5%
APR	27.9%	9.7%	18.0%	6.7%	2.3%	2.7%	16.2%	17.0%	21.3%	34.2%	33.0%	36.0%	2.4%	1.0%	1.7%
MAY	10.1%	1.9%	7.4%	0.5%	0.0%	0.3%	21.1%	13.5%	15.8%	16.9%	10.0%	8.7%	0.0%	0.0%	0.0%
JUN	0.5%	0.0%	0.0%	0.0%	0.0%	0.0%	5.1%	1.3%	0.0%	2.0%	0.3%	0.7%	0.0%	0.0%	0.0%
JUL	0.0%	0.0%	0.0%	0.0%	0.0%	0.0%	0.6%	0.0%	0.0%	0.3%	0.0%	0.0%	0.0%	0.0%	0.0%
AUG	0.0%	0.0%	0.0%	0.0%	0.0%	0.0%	0.0%	0.0%	0.0%	0.0%	0.0%	0.0%	0.0%	0.0%	0.0%
SEP	0.7%	0.3%	0.0%	0.3%	0.0%	0.0%	3.7%	1.0%	0.7%	4.0%	1.0%	1.7%	0.5%	0.0%	0.3%
OCT	6.2%	2.6%	3.5%	5.6%	0.6%	2.9%	4.7%	4.5%	1.6%	19.7%	9.7%	13.5%	2.7%	1.6%	2.3%
NOV	12.8%	3.7%	5.7%	23.1%	16.7%	28.0%	3.5%	1.7%	0.3%	28.7%	28.3%	27.7%	19.0%	30.3%	16.7%

Table B.10 – The mean monthly frequency of the 10 CGCM3 synoptic patterns created at the 500z level. GCM20c percentages are based off of 1970-1999 averages. Future model scenarios are based off of 2090-2099 averages.

CGCM - 500mb 2090s															
	1			2			3			4			5		
	GCM20c	A2	B1	GCM20c	A2	B1	GCM20c	A2	B1	GCM20c	A2	B1	GCM20c	A2	B1
MAR	5.3%	4.5%	12.3%	5.1%	31.0%	15.8%	21.3%	7.1%	6.5%	2.2%	2.6%	6.1%	1.6%	17.1%	7.7%
APR	7.6%	2.0%	8.0%	10.6%	39.0%	29.0%	13.3%	1.7%	3.7%	6.2%	0.0%	2.3%	3.7%	31.7%	20.0%
MAY	15.2%	1.0%	5.2%	10.3%	15.8%	15.8%	3.3%	0.0%	0.3%	11.5%	0.3%	2.9%	17.1%	60.0%	43.5%
JUN	4.3%	0.0%	0.0%	6.2%	2.0%	6.3%	0.3%	0.0%	0.0%	7.2%	0.0%	0.0%	38.6%	52.7%	52.7%
JUL	0.3%	0.0%	0.0%	0.9%	0.0%	0.0%	0.0%	0.0%	0.0%	5.1%	0.0%	0.0%	23.9%	21.0%	8.4%
AUG	0.0%	0.0%	0.0%	0.6%	0.0%	0.0%	0.0%	0.0%	0.0%	4.8%	0.0%	0.0%	23.0%	10.6%	17.4%
SEP	7.1%	0.0%	0.0%	8.0%	2.3%	9.7%	0.8%	0.0%	0.0%	10.1%	0.0%	0.3%	23.3%	24.3%	39.7%
OCT	15.1%	0.0%	1.6%	18.8%	16.1%	19.0%	1.4%	0.0%	0.3%	13.9%	0.0%	1.9%	16.1%	35.2%	35.5%
NOV	10.7%	2.0%	8.7%	26.2%	41.7%	38.0%	11.1%	0.7%	5.3%	8.3%	0.0%	1.7%	6.9%	25.0%	20.0%
	6			7			8			9			10		
	GCM20c	A2	B1	GCM20c	A2	B1	GCM20c	A2	B1	GCM20c	A2	B1	GCM20c	A2	B1
MAR	0.8%	5.5%	3.2%	10.8%	20.6%	11.6%	14.5%	1.6%	12.6%	16.5%	1.6%	7.7%	22.9%	8.4%	16.5%
APR	1.3%	8.3%	7.3%	9.7%	14.7%	14.0%	11.6%	1.0%	5.3%	13.3%	0.3%	0.0%	22.8%	1.3%	10.3%
MAY	6.1%	18.4%	19.4%	10.5%	3.2%	9.0%	6.9%	1.0%	1.3%	6.2%	0.0%	0.0%	12.8%	0.3%	2.6%
JUN	37.6%	45.3%	41.0%	4.7%	0.0%	0.0%	0.5%	0.0%	0.0%	0.3%	0.0%	0.0%	1.3%	0.0%	0.0%
JUL	70.0%	79.0%	91.6%	0.3%	0.0%	0.0%	0.0%	0.0%	0.0%	0.0%	0.0%	0.0%	0.0%	0.0%	0.0%
AUG	71.7%	89.4%	82.6%	0.0%	0.0%	0.0%	0.0%	0.0%	0.0%	0.0%	0.0%	0.0%	0.0%	0.0%	0.0%
SEP	47.3%	73.3%	49.3%	3.0%	0.0%	1.0%	0.0%	0.0%	0.0%	0.0%	0.0%	0.0%	0.6%	0.0%	0.0%
OCT	22.4%	47.4%	31.6%	5.9%	1.3%	6.8%	1.3%	0.0%	1.9%	1.8%	0.0%	0.0%	4.0%	0.0%	1.3%
NOV	3.7%	28.0%	6.3%	11.8%	2.7%	12.0%	5.8%	0.0%	2.7%	3.3%	0.0%	1.0%	12.2%	0.0%	4.3%

Table B.11 – The mean monthly frequency of the 10 CGCM3 synoptic patterns created at the 700z level. GCM20c percentages are based off of 1970-1999 averages. Future model scenarios are based off of 2090-2099 averages.

CGCM - 700mb 2090s															
	1			2			3			4			5		
	GCM20c	A2	B1	GCM20c	A2	B1	GCM20c	A2	B1	GCM20c	A2	B1	GCM20c	A2	B1
MAR	1.9%	14.5%	9.0%	3.1%	6.8%	7.7%	1.8%	3.2%	4.5%	21.6%	17.4%	17.4%	12.7%	9.7%	15.5%
APR	1.9%	32.3%	17.7%	6.4%	4.3%	9.7%	4.2%	4.7%	6.3%	17.6%	11.0%	17.0%	17.8%	7.3%	10.3%
MAY	6.5%	51.6%	31.6%	12.4%	10.3%	16.5%	9.1%	11.9%	8.4%	14.0%	3.5%	7.7%	20.6%	5.2%	11.0%
JUN	24.4%	86.7%	62.0%	34.4%	6.3%	19.7%	14.2%	6.3%	11.0%	4.4%	0.0%	0.3%	10.1%	0.0%	1.7%
JUL	27.7%	96.8%	67.4%	59.6%	2.6%	32.3%	7.8%	0.6%	0.3%	0.6%	0.0%	0.0%	1.7%	0.0%	0.0%
AUG	23.7%	98.7%	75.8%	61.5%	1.3%	23.5%	7.4%	0.0%	0.6%	0.5%	0.0%	0.0%	2.0%	0.0%	0.0%
SEP	7.1%	78.3%	38.3%	48.4%	19.0%	38.3%	10.0%	2.3%	14.0%	4.1%	0.0%	1.0%	9.4%	0.0%	2.3%
OCT	7.0%	52.6%	27.4%	31.1%	23.9%	25.8%	8.0%	6.5%	12.6%	8.1%	4.8%	3.5%	12.5%	0.3%	7.7%
NOV	5.0%	42.0%	17.3%	9.6%	12.0%	11.0%	4.4%	4.3%	5.0%	17.6%	13.3%	14.0%	11.7%	0.7%	8.7%
	6			7			8			9			10		
	GCM20c	A2	B1	GCM20c	A2	B1	GCM20c	A2	B1	GCM20c	A2	B1	GCM20c	A2	B1
MAR	12.2%	22.6%	11.3%	5.8%	1.6%	5.2%	15.2%	3.9%	6.8%	15.2%	6.1%	13.2%	10.5%	14.2%	9.4%
APR	13.0%	24.7%	15.7%	6.8%	0.3%	0.7%	13.9%	0.7%	3.3%	11.8%	1.0%	8.0%	6.7%	13.7%	11.3%
MAY	5.4%	9.4%	11.9%	10.4%	1.0%	3.2%	9.2%	0.0%	1.6%	7.3%	2.3%	1.9%	5.1%	4.8%	6.1%
JUN	1.3%	0.7%	3.3%	7.7%	0.0%	0.7%	1.2%	0.0%	0.0%	1.3%	0.0%	0.0%	1.7%	0.0%	1.3%
JUL	0.3%	0.0%	0.0%	2.7%	0.0%	0.0%	0.0%	0.0%	0.0%	0.0%	0.0%	0.0%	0.0%	0.0%	0.0%
AUG	0.0%	0.0%	0.0%	4.7%	0.0%	0.0%	0.0%	0.0%	0.0%	0.3%	0.0%	0.0%	0.3%	0.0%	0.0%
SEP	1.3%	0.0%	3.0%	15.3%	0.3%	1.0%	1.4%	0.0%	0.0%	0.7%	0.0%	0.0%	2.1%	0.0%	2.0%
OCT	8.5%	7.1%	11.3%	14.7%	0.0%	3.2%	3.4%	0.0%	0.0%	2.2%	0.0%	3.2%	4.6%	4.8%	5.2%
NOV	22.3%	22.0%	21.0%	7.0%	0.3%	2.3%	5.3%	0.3%	4.7%	7.7%	0.3%	5.0%	9.4%	4.7%	11.0%

Table B.12 – The mean monthly frequency of the 10 CGCM3 synoptic patterns created at the 850t level. GCM20c percentages are based off of 1970-1999 averages. Future model scenarios are based off of 2090-2099 averages.

CGCM - 850mb 2090s															
	1			2			3			4			5		
	GCM20c	A2	B1	GCM20c	A2	B1	GCM20c	A2	B1	GCM20c	A2	B1	GCM20c	A2	B1
MAR	0.0%	5.5%	1.0%	0.3%	1.9%	0.3%	0.0%	0.0%	0.0%	0.3%	1.3%	1.6%	4.6%	19.7%	15.8%
APR	4.2%	32.3%	13.3%	0.8%	11.3%	4.7%	0.0%	0.0%	0.0%	0.8%	1.3%	2.3%	7.0%	9.3%	15.7%
MAY	20.1%	46.8%	43.2%	5.3%	21.9%	18.4%	1.1%	0.6%	2.3%	11.6%	13.5%	8.7%	13.7%	3.5%	4.2%
JUN	38.0%	35.0%	41.3%	35.7%	60.0%	43.3%	3.4%	0.3%	2.3%	12.2%	4.7%	10.7%	3.2%	0.0%	1.0%
JUL	9.8%	3.2%	2.3%	51.2%	75.8%	63.5%	15.6%	11.6%	31.0%	22.8%	9.4%	3.2%	1.0%	0.0%	0.0%
AUG	7.5%	0.3%	1.3%	43.0%	77.1%	60.6%	20.2%	14.8%	25.2%	28.9%	7.7%	12.9%	0.5%	0.0%	0.0%
SEP	8.8%	7.7%	15.0%	19.6%	58.3%	43.7%	22.2%	24.3%	10.3%	27.1%	8.3%	18.7%	13.4%	1.3%	10.3%
OCT	3.3%	13.2%	8.7%	3.4%	37.4%	21.6%	8.4%	12.3%	5.8%	10.2%	8.1%	11.3%	35.7%	21.9%	25.5%
NOV	0.3%	4.0%	1.7%	0.3%	6.3%	1.7%	0.0%	0.3%	0.0%	0.0%	0.7%	0.0%	13.9%	34.3%	14.7%
	6			7			8			9			10		
	GCM20c	A2	B1	GCM20c	A2	B1	GCM20c	A2	B1	GCM20c	A2	B1	GCM20c	A2	B1
MAR	34.9%	13.9%	31.0%	23.3%	6.5%	11.6%	4.7%	9.4%	9.7%	25.6%	39.4%	24.2%	6.5%	2.6%	4.8%
APR	27.9%	5.0%	13.3%	6.7%	1.3%	1.7%	16.2%	9.3%	18.0%	34.2%	29.0%	29.7%	2.4%	1.0%	1.3%
MAY	10.1%	1.6%	1.6%	0.5%	0.0%	0.0%	21.1%	5.5%	13.2%	16.9%	6.5%	8.4%	0.0%	0.0%	0.0%
JUN	0.5%	0.0%	0.0%	0.0%	0.0%	0.0%	5.1%	0.0%	0.7%	2.0%	0.0%	0.7%	0.0%	0.0%	0.0%
JUL	0.0%	0.0%	0.0%	0.0%	0.0%	0.0%	0.6%	0.0%	0.0%	0.3%	0.0%	0.0%	0.0%	0.0%	0.0%
AUG	0.0%	0.0%	0.0%	0.0%	0.0%	0.0%	0.0%	0.0%	0.0%	0.0%	0.0%	0.0%	0.0%	0.0%	0.0%
SEP	0.7%	0.0%	0.0%	0.3%	0.0%	0.0%	3.7%	0.0%	0.7%	4.0%	0.0%	1.3%	0.5%	0.0%	0.0%
OCT	6.2%	0.3%	4.2%	5.6%	0.3%	0.3%	4.7%	0.0%	5.8%	19.7%	4.5%	13.9%	2.7%	1.9%	2.9%
NOV	12.8%	1.3%	8.0%	23.1%	7.0%	15.3%	3.5%	1.3%	2.3%	28.7%	19.7%	31.0%	19.0%	25.0%	25.3%

APPENDIX C

Graphs in Appendix C represent the seasonality of the CCSM3 patterns that did not occur frequently in the summer (and thus were not discussed in section 3.2 above).

Monthly Frequency of CCSM3 500z Non Summer Patterns

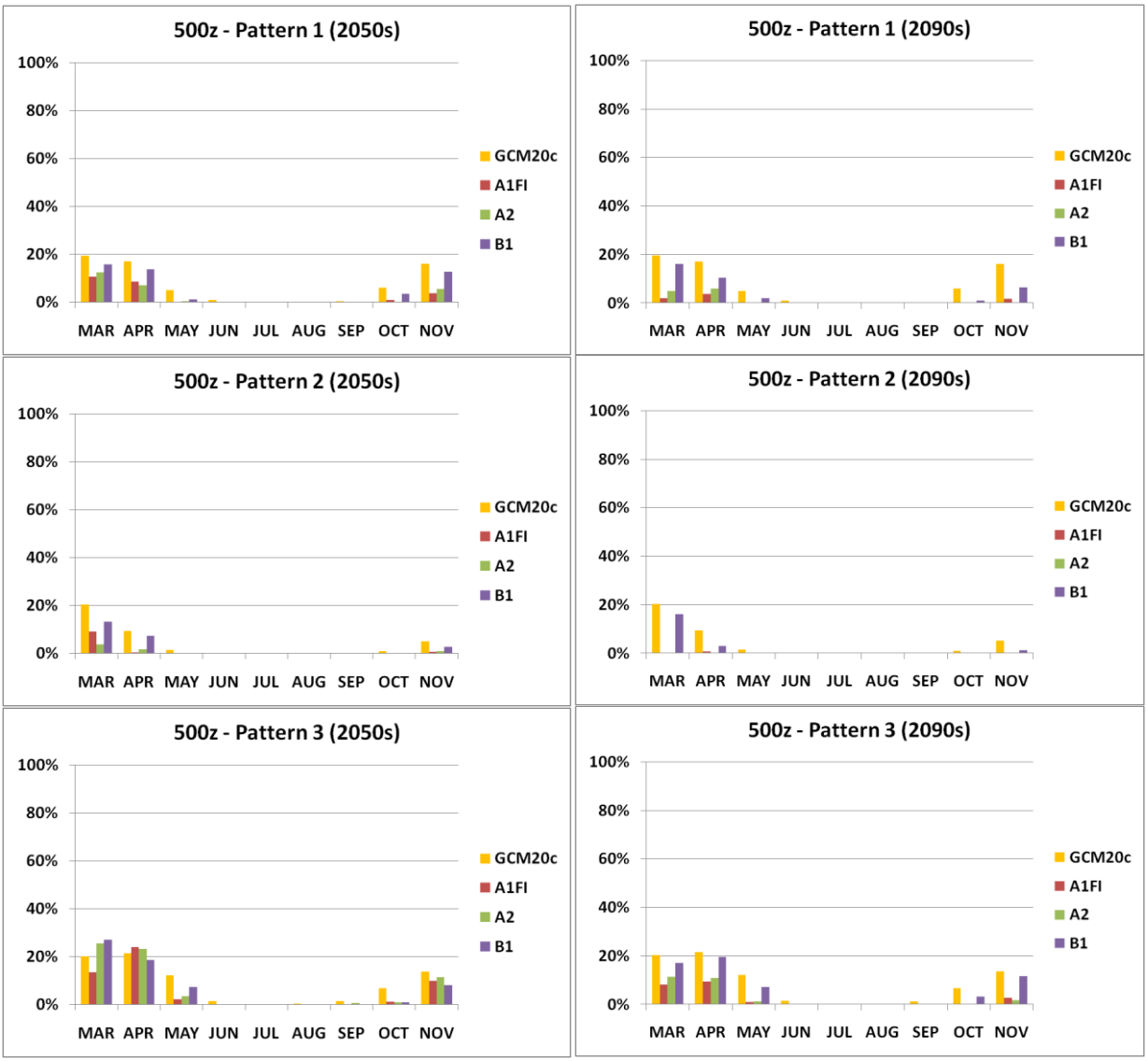

Figure C.1 – The mean monthly frequency of the 7 non-summer CCSM3 synoptic patterns created at the 500z level. GCM20c percentages are based off of 1960-1999 averages. Future model scenarios are based off of 2050-2059 averages (left) and 2090-2099 averages (right). Continued on the next page.

Figure C.1 – Continued

Monthly Frequency of CCSM3 700z Non Summer Patterns

Figure C.2 – The mean monthly frequency of the 7 non-summer CCSM3 synoptic patterns created at the 700z level. GCM20c percentages are based off of 1960-1999 averages. Future model scenarios are based off of 2050-2059 averages (left) and 2090-2099 averages (right). Continued on the next page.

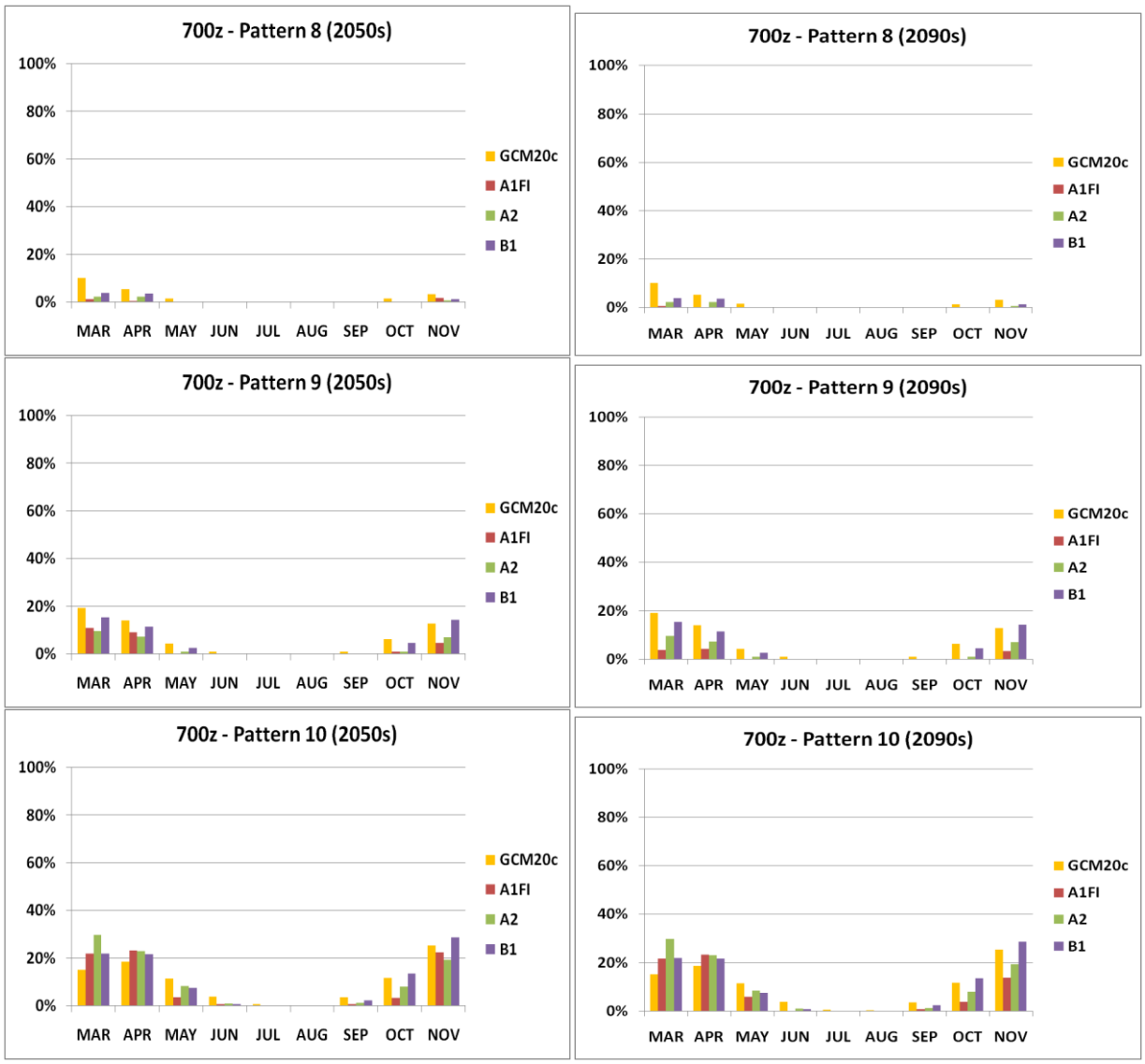

Figure C.2 – Continued

Monthly Frequency of CCSM3 850t Non Summer Patterns

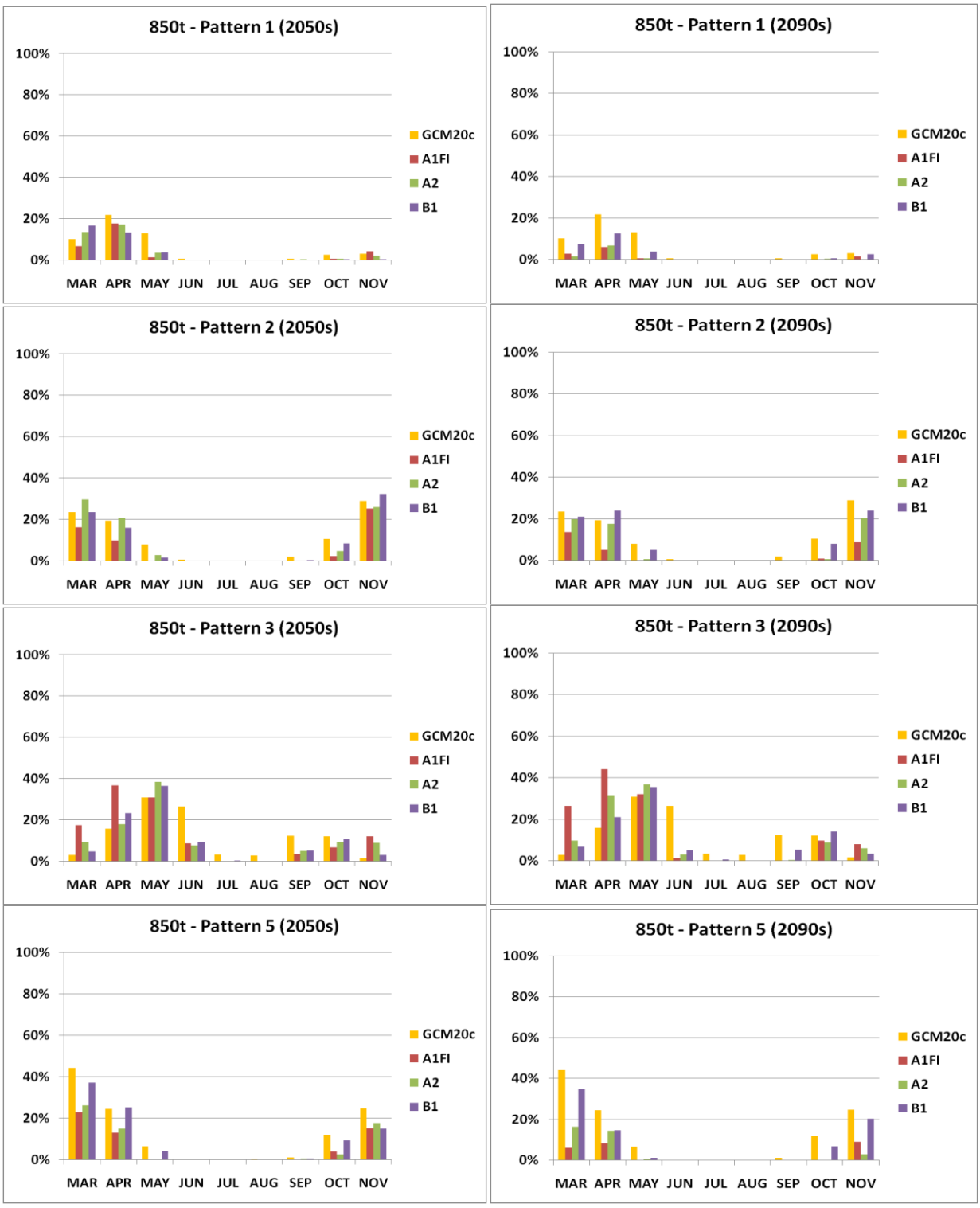

Figure C.3 – The mean monthly frequency of the 6 non-summer CCSM3 synoptic patterns created at the 850t level. GCM20c percentages are based off of 1960-1999 averages. Future model scenarios are based off of 2050-2059 averages (left) and 2090-2099 averages (right). Continued on the next page.

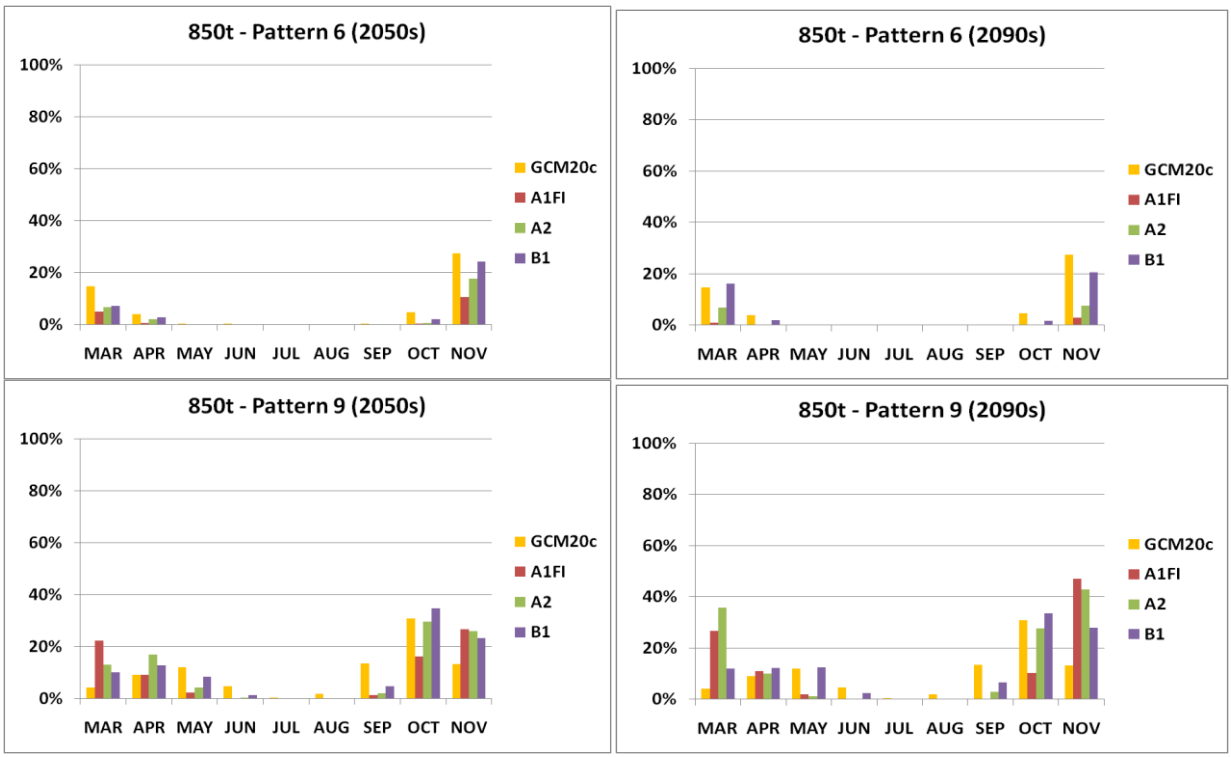

Figure C.3 – Continued